Sami Nyyssönen

Undamped natural frequencies and mode shapes of pre-swirl stator fins in still water in conceptual design

School of Engineering

Thesis submitted for examination for the degree of Master of Science in Technology.

Espoo 30.05.2016

Thesis supervisor:

Prof. Jani Romanoff

Thesis advisors:

M.Sc. (Tech.) Kimmo Kotisalo

M.Sc. (Tech.) Otto Puolakka

Aalto University
School of Engineering

AALTO UNIVERSITY
SCHOOL OF ENGINEERING

ABSTRACT OF THE
MASTER'S THESIS

Author: Sami Nyyssönen

Title: Undamped natural frequencies and mode shapes of pre-swirl stator fins in still water in conceptual design

Date: 30.05.2016 Language: English Number of pages: 59+43

Department of Applied Mechanics

Professorship: Naval Architecture Code: K3005

Supervisor: Prof. Jani Romanoff

Advisors: M.Sc. (Tech.) Kimmo Kotisalo, M.Sc. (Tech.) Otto Puolakka

The current thesis investigates if the simplified two degrees of freedom beam approach is accurate enough to predict the lowest undamped natural frequencies and mode shapes of pre-swirl stator fins in still water. A fast method is needed to estimate the lowest natural frequencies and mode shapes for the risk analysis of vibrations and hydroelastic instabilities in conceptual design.

The fin is simplified as a straight cantilever beam with a solid cross-section. The equations of motion take into account coupled vertical bending and torsion. Structural and fluid-induced damping are neglected. The effect of surrounding water is simplified as the 2D added mass of a flat plate. The cross-section properties are defined with derived approximative formulas based on NACA 4-digit series. The natural frequencies and mode shapes are solved from the eigenvalue problem which is formed with the finite element method.

The approach must take into account the shear deformation, rotary inertia, coupling and added mass terms. The main fin parameters affecting the natural frequencies are the length, chord, thickness, camber, span-wise variation and material. Design graphs to estimate and compare the lowest natural frequency of different designs are generated to assist in conceptual design.

The approach studied is applicable for fins which are solid, made of homogeneous isotropic material and with a cross-section shape close to a NACA 4-digit series or flat plate. It is not applicable for advanced cross-sections and materials. The approach slightly overestimates the frequencies in air but underestimates in water. The added mass effect is overestimated, especially in torsion. The lowest mode type of fins is usually vertical bending.

To predict the natural frequencies in operating conditions, the effects of passing flow and external damping must be studied to determine how much they affect the lowest frequencies.

Keywords: undamped, natural frequency, mode shape, pre-swirl stator fin, NACA 4-digit series, equations of motion, cantilever beam, finite element method, added mass, flat plate

AALTO-YLIOPISTO
INSINÖÖRITIETEIDEN KORKEAKOULU

DIPLOMITYÖN
TIIVISTELMÄ

Tekijä: Sami Nyyssönen

Työn nimi: Staattorin evien vaimentamattomat ominaistaajuudet ja -muodot tyynessä vedessä konseptisuunnittelussa

Päivämäärä: 30.05.2016 Kieli: Englanti Sivumäärä: 59+43

Sovelletun mekaniikan laitos

Professuuri: Meritekniikka Koodi: K3005

Valvoja: Prof. Jani Romanoff

Ohjaajat: DI Kimmo Kotisalo, DI Otto Puolakka

Tässä työssä tutkitaan yksinkertaistetun kahden vapausasteen palkin liikeyhtälöiden soveltuvuutta tyynessä vedessä olevan staattorin evän alimpien vaimentamattomien ominaistaajuuksien ja -muotojen ennustamiseen. Näitä taajuuksia ja muotoja tarvitaan evien hydroelastisten epästabiilius ja värähtely ongelmien arvioimiseksi. Nopeaa alimpien ominaistaajuuksien ja -muotojen ratkaisua tarvitaan näiden ongelmien arvioimiseksi jo evien konseptisuunnitteluvaiheessa.
Evä on yksinkertaistettu suorana ulokepalkkina, jonka poikkileikkaus on umpinainen. Liikeyhtälöt koostuvat kohtisuorasta taivutuksesta ja väännöstä, jotka ovat kytketty. Rakenteen ja veden aiheuttamaa vaimennusta ei ole otettu huomioon. Evää ympäröivän veden vaikutus on yksinkertaistettu ja otettu huomioon tasapaksun levyn lisättynä massana. Poikkileikkauksen ominaisuudet on määritetty tässä työssä johdetuilla likimääräisillä kaavoilla, jotka perustuvat NACA 4-sarjan profiileihin. Ominaistaajuudet ja -muodot on ratkaistu ominaisarvoyhtälöstä elementtimenetelmää hyödyntäen.
Leikkaus muodonmuutos, kierto inertia, kytkentä ja lisätty massa täytyy ottaa huomioon evän liikeyhtälöissä. Evän ominaistaajuuksiin vaikuttavat evän pituus, jänne, paksuus, kaarevuus, jänteen pituussuuntainen vaihtelu ja materiaali. Työssä esitetään näihin parametreihin pohjautuva suunnittelu käyrästö.
Tutkittu menetelmä soveltuu eville, joiden poikkileikkaus on umpinainen, materiaali on homogeeninen ja isotrooppinen ja profiili muistuttaa NACA 4-sarjaa tai tasapaksua levyä. Menetelmä ei sovellu kehittyneille poikkileikkauksille ja materiaaleille. Menetelmä yliarvioi evän ominaistaajuuksia ilmassa mutta aliarvioi niitä vedessä. Menetalmeä yliarvioi lisätyn massan vaikutuksen taajuuksiin, varsinkin väännössä. Evän alin ominaismuoto on yleisesti pystysuuntainen taipuminen.
Ohimenevän virtauksen ja veden vaimennuksen vaikutusta evän ominaistaajuuksiin tulee tutkia, jotta evää voidaan arvioida sen todellisissa käyttöolosuhteissa.

Avainsanat: vaimentamaton, ominaistaajuus, ominaismuoto, staattorin evä, NACA 4-sarjan siipiprofiili, liikeyhtälö, ulokepalkki, elementtimenetelmä, lisätty massa

Preface

This Master's Thesis is written as a part of the Master Degree Program at the Department of Applied Mechanics at Aalto University. The thesis is written in cooperation with the Structural Department of Foreship Ltd.

I would like to express my gratitude to my supervisor, Professor Jani Romanoff, for his guidance and valuable comments throughout the process. The value of his support in the thesis writing process is impossible to overestimate. I am also grateful to my advisors, M.Sc.(Tech.) Kimmo Kotisalo from Foreship Ltd. and M.Sc.(Tech.) Otto Puolakka from Aalto University, for their interest and knowledge.

I would also like to thank all of my colleagues at Foreship, especially the corner room team, for their support and bringing laugh and joy into the daily routine. I owe gratitude for M.Sc.(Tech.) Ville Viitanen from VTT for supporting me throughout the process and being a good friend. I also express my gratefulness to M.Sc.(Tech.) Justin Champion from Foreship Ltd. for proofreading the manuscript of this thesis. I would also like to thank my other study mates for their moral support in the process.

I must present my sincere appreciation to my girlfriend Suvi Takko for her enormous support and encouragement with both the thesis and in my life. I am also thankful to my parents Reijo and Tiina, my grandfather Olli and the rest of my family and friends. A special thanks also to my and Suvi's cats Sira and Susi for their help when working remotely.

Espoo, 30.05.2016

Sami Nyyssönen

Contents

Symbols and abbreviations

Latin symbols

a	Distance between the LE and the pitching axis or SC
A	Cross-sectional area of the fin
A_{root}	Cross-sectional area of the fin at the root
c	Chord length of the fin
c_a	Corrected c
c_{root}	Chord length of the fin at the root
c_{tip}	Chord length of the fin at the tip
C_1	Correction factor for tapered beams
C_{am}	Added mass coefficient
$\{\mathbf{D}\}$	Vector containing the nodal DOFs
e_x	Distance between the COG and SC along the x-axis
e_z	Distance between the COG and SC along the z-axis
E	Young's elastic modulus
EI	Bending stiffness
$E\Gamma$	Warping rigidity in torsion
f	Frequency in Hertz
G	Shear modulus
GJ	Torsional rigidity
$[\mathbf{H_1}]$	Matrix composed of shape functions
$[\mathbf{H_2}]$	Matrix composed of shape functions
$[\mathbf{H_3}]$	Matrix composed of shape functions
I_{xx}	Area moment of inertia about the x-axis with respect to SC
$I_{xx,root}$	I_{xx} at the root
I_{xx}^{COG}	Area moment of inertia about the x-axis with respect to COG
I_{yy}	Polar moment of inertia about the y-axis with respect to SC
I_{yy}^{COG}	Polar moment of inertia about the y-axis with respect to COG
I_{zz}	Area moment of inertia about the z-axis with respect to SC
I_{zz}^{COG}	Area moment of inertia about the z-axis with respect to COG
J	Torsional constant
$[\mathbf{K}]$	Global stiffness matrix
$[\mathbf{K_w}]$	Global stiffness sub-matrix related to bending
$[\mathbf{K_w^e}]$	Local element stiffness matrix related to bending
$\left[\mathbf{K}_{\theta_\mathbf{y}}\right]$	Global stiffness sub-matrix related to torsion
$\left[\mathbf{K}_{\theta_\mathbf{y}}^\mathbf{e}\right]$	Local element stiffness matrix related to torsion
L	Length of the fin
L_s	Distance from the tip of the fin to the centreline of the ship
L'	Added mass part of the lift per unit span
m	Maximum camber of the fin cross-section in per cent of c
M_x	Bending moment about the x-axis
M_y	Torque about the y-axis
M'	Added mass part of the pitching moment

$[\mathbf{M}]$	Global mass matrix
$[\mathbf{M_w}]$	Global mass sub-matrix related to bending
$[\mathbf{M^e_w}]$	Local element mass matrix related to bending
$\left[\mathbf{M}_{\theta_\mathbf{y}}\right]$	Global mass sub-matrix related to torsion
$\left[\mathbf{M}^\mathbf{e}_{\theta_\mathbf{y}}\right]$	Local element mass matrix related to torsion
$\left[\mathbf{M}_{\mathbf{w}\theta_\mathbf{y}}\right]$	Global mass sub-matrix related to inertial coupling
$\left[\mathbf{M}^\mathbf{e}_{\mathbf{w}\theta_\mathbf{y}}\right]$	Local element mass matrix related to inertial coupling
p	Location of the maximum camber as a distance from LE in tenths of c
Q_z	Shear force in the z-direction
S	Surface area of the fin
St	Strouhal number
t	Maximum thickness of the fin cross-section in per cent of c
t_a	Corrected t
u	Deflection due to bending in the x-direction
w	Deflection due to bending in the z-direction
$\overline{x}$	Location of COG along the x-axis as distance from LE
$\tilde{x}$	Location of SC along the x-axis as distance from LE
$\overline{z}$	Location of COG along the z-axis
$\tilde{z}$	Location of SC along the z-axis

Greek symbols

α	Slenderness ratio
β_n	Weighting number for bending related to the nth mode as a fraction of L
Γ	Warping constant
ζ	Aspect ratio
θ_x	Angle of rotation about the x-axis of the cross-section due to bending
θ_y	Angle of twist about the y-axis of the cross-section due to torsion
θ_z	Angle of rotation about the z-axis of the cross-section due to bending
κ^2	Shear coefficient
λ	Eigenvalue
μ	Density ratio between ρ and ρ_w
ν	Poisson's ratio
ξ	Taper ratio between c_{tip} and c_{root}
ρ	Density of fin material
ρ_w	Density of fluid, in this study water
σ_n	Mode shape coefficient related to the nth mode
ϕ	Shear deformation coefficient
ω	Natural frequency in Hertz
ω_n	Natural frequency of the nth mode in Hertz
$\omega_{air,n}$	Natural frequency of the nth mode in air in Hertz
$\omega_{water,n}$	Natural frequency of the nth mode in water in Hertz

Mathematical symbols

$[\ \ ]$	Square matrix
$[\ \ ]^T$	Matrix transpose
$\{\ \ \}$	Column vector
$\dot{w}$	Partial derivative of w with respect to time t, in symbols $\frac{\partial}{\partial t}$
w'	Partial derivative of w with respect to variable y, in symbols $\frac{\partial}{\partial y}$

Abbreviations

BC	Boundary condition
COG	Center of gravity
DOF	Degree of freedom
EOM	Equations of motion
FEM	Finite element method
LE	Leading edge
NACA	National Advisory Committee for Aeronautics
SC	Shear center
TE	Trailing edge

1 Introduction

1.1 Background

A stator fin is a wing-like structure used in ships near the propeller to improve the propulsion efficiency and reduce fuel costs. Fins in front of the propeller are called pre-swirl stator fins. The number of fins can vary depending on the ship. Figure 1.1 shows an example of fins in front of the propeller in single-propeller ships. Their purpose is to pre-rotate the inflow of the propeller, which improves the propeller flow field. The effect of fins on the inflow is illustrated with streamlines in Figure 1.2. The biggest benefits are gained in ships with full hull shapes where the flow comes into the propeller at a higher angle, decreasing the propulsion efficiency. Fins are usually used only in commercial ships with one propeller. According to different suppliers, gains of 3 - 7 percent can be achieved even in ships with an optimized hull form and propeller [21] [44] [15] [16] [46]. Pre-swirl stator fins are used seldomly in multi-propeller ships because the installation is usually more complicated and the propulsion efficiency gains smaller than in single propeller ships. However, multi-propeller pre-swirl stator fin solutions are investigated and developed more and more.

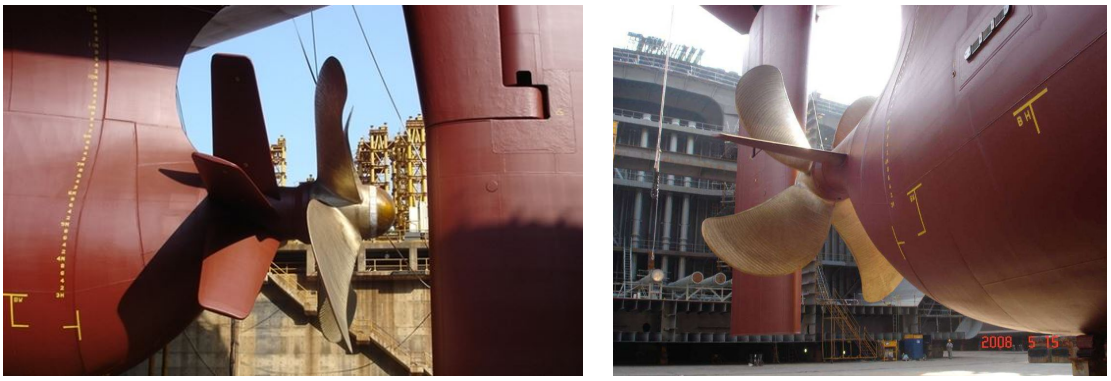

Figure 1.1: Example of pre-swirl stator fins in single-propeller ships. [15] [16]

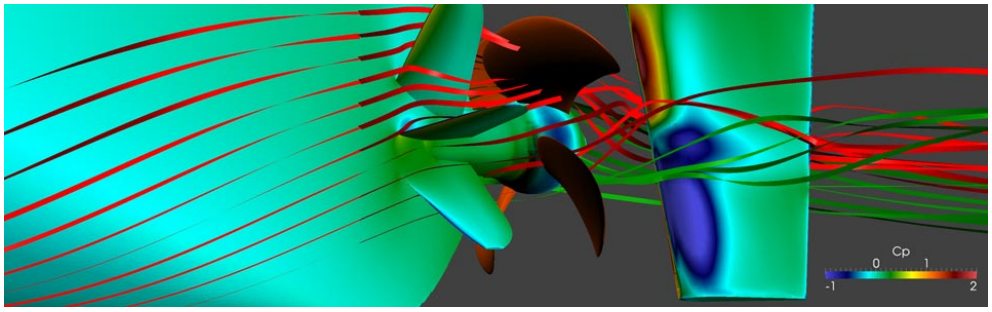

Figure 1.2: Streamlines illustrating how the fins alter the inflow of the propeller. [46]

In the past, fin designs were simple, mostly only a straight rectangular cantilever plate. More advanced cross-section shapes alter the flow more and thus improve the propulsion efficiency more. Even though the design and construction costs are higher, more advanced foil shapes are used in stator fins recently due to high fuel costs. The cross-section can be symmetric or asymmetric. Asymmetric designs have more effect on the flow field and thus the propulsion efficiency gains are again greater. The cross-section shape is usually based on a parametric foil shape which is altered according to the project at hand. One example of parametric foil shapes is sections developed by the National Advisory Committee for Aeronautics (NACA) [1].

Fins are designed to optimally improve the flow field. The length of the fin is usually the same as the length from the propeller tip to the center of the propeller shaft. The length-chord and length-thickness ratios are more or less the same when considering the greatest improvement in the propulsion efficiency. To get the maximum benefit, the fins should be located as close to the propeller as possible. However, the ship hull design and structural arrangement in the aft ship, e.g. bossing, can restrict the positioning and design of the fin. The attachment and construction methods of the fin can also limit the fin design. Thus, the optimum design cannot always be used and different fin dimensions and cross-section shapes must be analysed in the design process.

In addition to the construction-related limitations, it is important to understand and accurately predict the static and dynamic response and stability of a flexible lifting body to ensure its structural safety [13, p. 1]. The stresses and structural stability are very seldom of interest with respect to ultimate limit states because the magnitude of the loads are not great enough to exceed the strength limits [25, p. 965]. The assumption considers conventional designs and materials, meaning solid or thick plated fins made of steel or other metal alloys. Thus, the ultimate limit states might be of interest in case of lightweight fins made of composites or other advanced materials.

Fins are exposed to flow-induced hydrodynamic loads and propulsion machinery-induced excitation loads. Such a dynamic loading causes hydroelastic vibrations which are an issue when the fatigue life of elastic lifting hydrofoils, such as fins, is considered at the design stage [12, p. 402]. In addition, flexible lifting bodies, such as high aspect ratio, highly skewed, or self-adaptive blades, wings and hydrofoils, may be subject to hydroelastic instabilities, such as static divergence or flutter [17, p. 40–41]. Therefore, fatigue issues caused by hydroelastic vibrations and hydroelastic instabilities arising from hydrodynamic loads are of great concern and have to be taken into account in the fin design process.

Moreover, the fins should remain as static as possible. The more the hydroelastic vibration amplitudes or instabilities increase, the further the fin is from the designed optimum position and angle, which decreases the effect to the inflow and the benefits to the propeller efficiency. Therefore, hydroelastic vibrations and instabilities should be minimized.

1.2 Hydroelastic vibrations and instabilities

Hydroelastic vibrations and instabilities are major concerns in the fin design process. Hydroelastic vibrations expose the fin to fatigue issues and hydroelastic instabilities may cause serious damage or even complete destruction of the structure. The issues are caused by external excitation and flow-induced hydrodynamic loads. The hydrodynamic loads cause both vibrations and instabilities, whereas external excitation causes only fin vibrations. Figure 1.3 shows wave slamming which is one cause of hydroelastic vibrations on ships.

Figure 1.3: Example of loads causing hydroelastic vibrations on ships. [45] [47]

The source of external excitation is mainly the propulsion machinery of the ship. The fin is located close to the rotating propeller, which generates pressure pulses. The pressure pulses propagate in water, causing impulse loads to nearby structures. Other parts of the propulsion machinery, such as main engines, may cause structural vibrations spreading to the fins through the hull structures.

Hydrodynamic loads result from water flowing against and around a fin. The flow passing the fin is slowed by viscous forces on and nearby the fin surface. The velocity differences cause pressure differences around the fin which results in lift and drag forces and pitching moment acting on the fin. The viscous forces can also separate the flow from the fin surface, generating eddies and vortices. These flow irregularities induce vibrations on the fin. Moreover, the flow irregularities or the motion of the fin alter the pressures on the fin, causing oscillations of hydrodynamic forces and vibrations of the fin. Figure 1.4 shows flow irregularities around a harmonically plunging NACA0012 foil. Flow irregularities can be seen around the foil and behind the foil in the wake.

The most important hydroelastic instabilities are static and dynamic divergence and flutter [17, p. 40–41]. Static divergence is a linear instability where the deformations induced by the hydrodynamic loads increase with time without oscillations because the loads increase over the effective stiffness of the structure. The deformations may increase until the structure's bending or torsion capacity is exceeded or material failure develops, breaking the structure. Dynamic divergence is similar to static divergence but is nonlinear and dynamic, meaning the structure is oscillating and the amplitude increases with time. The oscillation frequency decays when

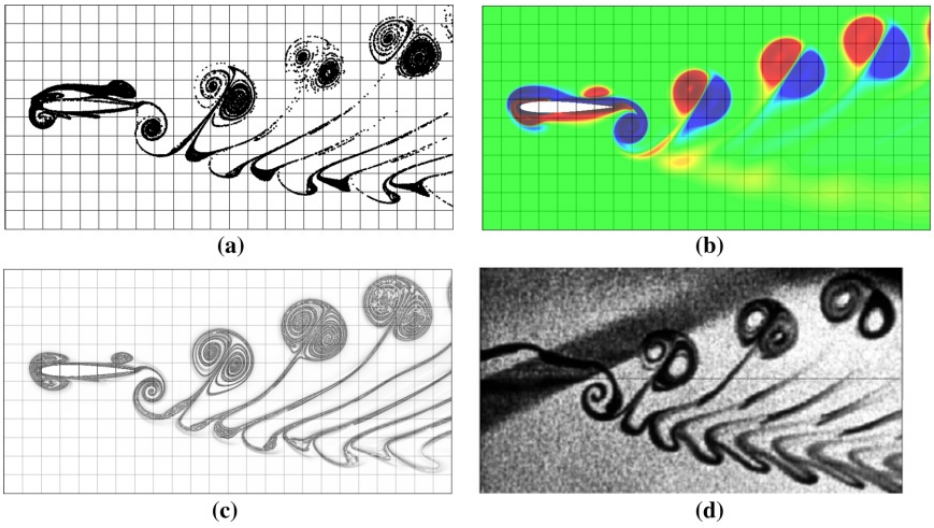

Figure 1.4: Example of pre-swirl stator fins in single-propeller ships. [41]

the amplitude increases. Flutter is a dynamic flow-induced instability in which the structure oscillates with a fixed frequency and the oscillation amplitude increases over time if the net damping decreases. If the net damping decreases to zero, the oscillations increase until the structure breaks. The described instabilities are linked to flow velocities in which the instabilities occur. These critical velocities depend on cross-sectional properties, structural properties, added mass, damping and hydrodynamic forces. The divergence and flutter velocities decrease if the overall density of the fin decreases, meaning the instabilities are an even greater concern in the case of lightweight fins [13, p. 25].

The threat of hydroelastic vibrations can be evaluated by comparing the excitation and load oscillation frequencies to the natural frequencies of the structure. If the external loads oscillate close to the natural frequencies of the structure, resonance may occur. In resonance, the oscillating loads force the structure to vibrate. The amplitude of vibration may increase and break the structure if the net damping decreases to zero. Therefore, the fin vibrations can be reduced by avoiding fin designs with natural frequencies close to the frequencies of the external sources.

The threat of hydroelastic instabilities are evaluated by comparing the critical velocities of the instability to the flow velocities which the structure encounters. Similar to the vibrations, the instabilities can be reduced by avoiding fin designs resulting in critical velocities or by avoiding operation in the critical velocities. The natural frequencies and mode shapes of the structure can be used in solution of critical velocities, meaning they are needed in both resonance and instability analysis. Therefore, modal analysis is important in the estimation of fin response to external excitations and flow-induced hydrodynamic loads.

To avoid resonance and critical velocities, the prediction of the dynamic behaviour of a structure is a key issue. The structures should be designed so that the natural frequencies are higher than the excitation frequencies. Therefore, the lowest natural frequencies are of interest with regard to resonance. The low frequencies

contain more energy than high frequencies and thus are a greater risk. In relation to the solution of critical velocities, only a relatively small number of lower natural modes of a structure are actually needed to describe its deformation in most cases [10, p. 125]. Therefore, the lowest natural frequencies and mode shapes of the fin are the first priorities to estimate.

1.3 Modal analysis in conceptual design

The natural frequencies of a structure are the frequencies at which the structure tends to oscillate in the absence of external excitation. The mode shapes are the shapes of motion in which the structure tends to oscillate in these frequencies. The oscillation of a structure is divided into free and forced vibrations. A free vibration occurs when there is no external excitations but kinetic or potential energy is initially present in the system. A forced vibration occurs when external excitation is applied to the system. Free vibrations occur at the natural frequencies and mode shapes of the structure whereas forced vibrations occur at the excitation frequency. In case excitation frequencies are close to the natural frequencies, resonance occurs as discussed earlier.

The natural frequencies and mode shapes are solved from the equations of motion (EOM) describing the vibrations of the structure. The natural frequencies and normal modes of a structure are dependent only on the stiffness of the structure and the mass which participates in the motion of the structure. The mass includes the mass of the fin and the mass of the fluid moved by the fin, which is also called added mass. However, energy dissipation in motion always exists in any real system, which is called damping. Damping occurs as a result of friction among moving objects or interactions between moving objects and their surrounding environments e.g. in fluids. Damping converts the kinetic energy of a vibrating system to other forms of energy such as heat and acoustic energy. The presence of damping reduces the amplitude of vibrating motion but also decreases the natural frequencies of the system. The damping ratio describes how much the damping affects the vibrations. In case of small damping ratios, such as structural damping, the damping can usually be neglected. The water surrounding the fin causes external damping of the vibrating system due to energy loss due to the movement of water.

The first step in the evaluation of the feasibility of the fin design is to analyse the risk of vibration and instability issues in which the natural frequencies and mode shapes of the fin are needed. Therefore, a fast method is needed for the concept design phase of fins. The aim of the thesis is to study whether the simplified two DOFs beam approach is accurate enough to predict the lowest undamped natural frequencies and mode shapes of pre-swirl stator fins in still water. The significance of shear deformation, rotary inertia, bending-torsion coupling and added mass with respect to the lowest natural frequencies are studied. The natural frequency dependency on the fin design parameters is investigated. The outcomes are used to generate design graphs to estimate and compare the lowest natural frequency of different stator fin designs.

1.4 Limitations and justification

In this study, the stator fin is simplified as a cantilever beam with a solid cross-section. The material of the fin is considered as homogeneous and isotropic. Advanced lightweight designs are not considered. This includes advanced materials such as composites and advanced structures such as hollow cross-sections with stiffened shells and webs. Considering these limitations, the current approach is used to calculate the natural frequencies of composite fins. The material properties of composite fins are applied as isotropic and homogeneous material's properties. The obtained results are compared to measurements and results of advanced methods to study the applicability of the simplified approach to advanced materials and designs. The study doesn't differentiate between different composites and their different behaviour, for example shear vulnerable composites. The fin is assumed to be fixed to the ship hull. The attachment method and its effect on the dynamic behaviour is not studied.

Ships usually have multiple stator fins as shown in Figure 1.1. In this work, the effect of other fins is not taken into account. This means that the distance between fins is assumed to be great enough to neglect the effects or only one stator fin systems is considered.

The fin designs are limited to unswept straight fins, meaning fins with sweep and twist angles are not considered. Fins are not usually skewed and thus not considered. The cross-section shape is constant along the span of the fin but the fin is allowed to taper, meaning the size of the cross-section can vary along the span. The cross-section shape of the fin is modelled as a NACA 4-digit series. This shape is used due to the large amount of studies and measurements but also because the shape is defined with analytical formulas, including symmetric and asymmetric shapes. NACA shapes can also be considered as a good approximation for the shape of stator fins.

The EOM of a cantilever beam in coupled bending and torsion are used with the assumption of small deformation and oscillation theory, meaning vibrations are simplified to be linear. The structural and fluid-induced damping are neglected from the EOM. The effect of water is taken into account only by added mass in still water conditions. The added mass of the fin is approximated with the 2D added mass coefficients of a 2D flat plate.

The EOM are partial differential equations describing the vibrations of a continuous medium. Thus, the stiffness and mass of the structure are introduced in the EOM as a continuous distribution. Since exact solutions of partial differential equations are difficult to obtain, the continuous systems are usually approximated by discrete systems. This means that the stiffness and mass of the structure are introduced as discrete distributions. The EOM can then be described by ordinary differential equations which are easier to solve. In this work, the EOM are discretized via the finite element method (FEM).

To clarify the most significant simplification, the undamped natural frequencies and mode shapes are solved for fins oscillating in still water. The effects of passing flow and external damping due to surrounding water will be left for future work.

2 Methods

The current chapter describes the methods used in the study. The chapter is divided into three parts. The first part presents the governing equations used to describe the motion of the fin. The second part describes the calculation method used to solve the natural frequencies and modes. The third part describes the utilization of the NACA 4-digit series as a fin cross-section in the study and the calculation of the geometric properties of the cross-sections.

2.1 Governing equations and notations

Earlier studies have been done with both beam and plate models. Plate models have been mostly used to calculate simple cantilever plates with rectangular cross-sections and the focus has been on studying the 3D effects and 3D varying loads [39]. In contrast, beam models have been mostly used to calculate cantilevers with more complex cross-section shapes. In these studies, the focus has been on dynamic response, vibrations and natural frequencies [2] [13] [34] [25] [33]. The beam model is chosen for this study due to simpler equations as compared to plate models in case of complex cross-section shapes such as convex foil cross-sections.

The equations of motion (EOM) of a flexural-torsion coupled beam based on Timoshenko beam theory are used as a basis for the study. The beam has three degrees of freedom (DOF) which are transversal bending, vertical bending and torsion. In this work, the equations are simplified to take into account only vertical bending and torsion, meaning the beam used has two DOFs. Both the coupled and uncoupled EOM with and without the shear deformation and rotary inertia terms are used in this study. The effect of surrounding water is simplified to consist only of the 2D added mass term. The added mass of the fin is approximated with the 2D added mass coefficients of a 2D flat plate. The used coordinate systems and notations are described next.

The foil notation is illustrated in Figure 2.1. The leading edge (LE) is the foremost edge and the trailing edge (TE) the rearmost edge of the foil section. The LE and TE are the forward and rearward extremities of both the mean-line and chord-line. The mean-line is a line halfway between the upper and lower surfaces of the section [1, p. 65]. The chord-line is a straight line connecting the LE and the TE. In the case that the foil section is symmetric, the chord-line and the mean-line are coinciding. The flow goes chord-wise from the LE to the TE. [1, p. 112–113]

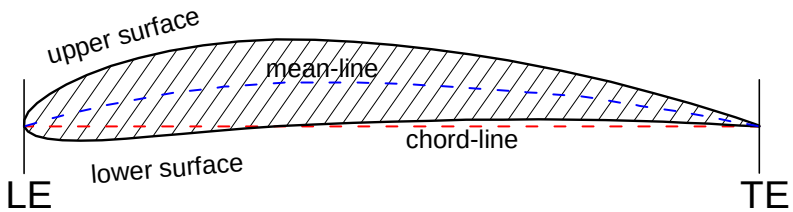

Figure 2.1: The foil cross-section illustrating the mean-line, chord-line and the upper and lower surface of the foil.

The used coordinate system is illustrated in Figure 2.2. The x-axis points from the ship bow to the ship aft meaning the x-axis also shows the flow direction. The y-axis points from the fin root to the fin tip. The y-axis is defined to coincide with the elastic axis. The z-axis points downwards from the fin to the sea bottom. The bending deflection in the z- and x-directions are denoted as w and u, respectively. The cantilever beam in the yz-plane is illustrated in Figure 2.3. The length of the fin is denoted with L and the angle of twist about the y-axis with θ_y.

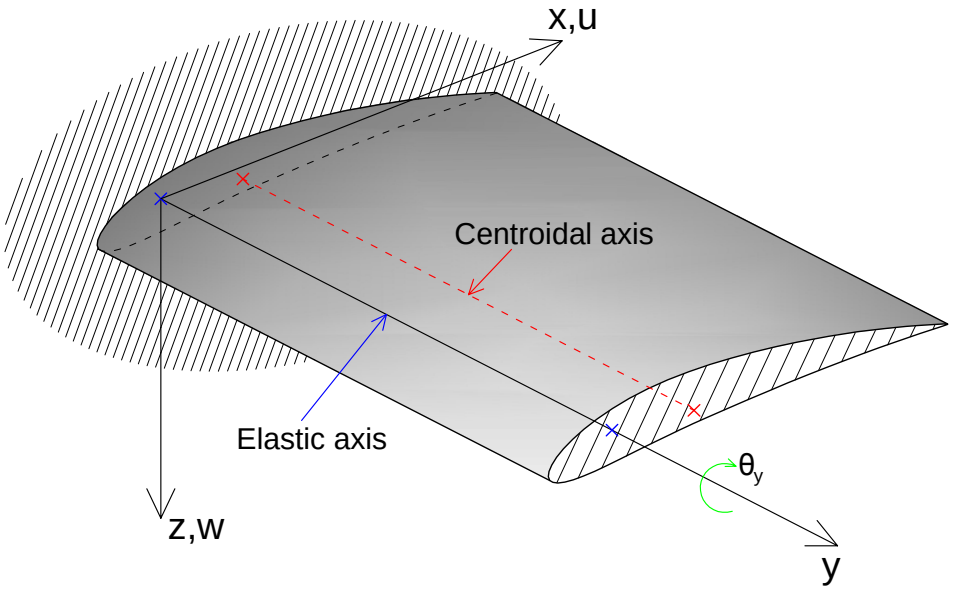

Figure 2.2: The simplified fin illustrating the coordinate system, elastic axis and centroidal axis.

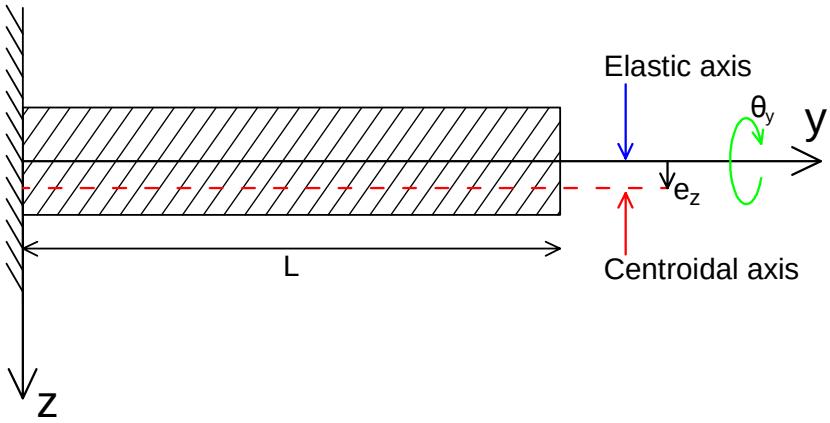

Figure 2.3: The cantilever beam in the yz-plane showing the used notation.

The foil cross-section is illustrated in Figure 2.4. The cross-section is defined in the xz-plane. The chord length, denoted as c, is the distance between the LE and TE, or in other words the length of the chord-line. The center of gravity (COG) of

the cross-section is on the centroidal axis. The shear center (SC) of the cross-section is on the elastic axis. The origin of the plane is located on the elastic axis. The distance between the COG and SC along the x-axis, e_x, is defined as positive when the COG is located between the SC and TE. Similarly, the distance along the z-axis, e_z, is defined as positive when the COG is located between the SC and the lower surface of the foil.

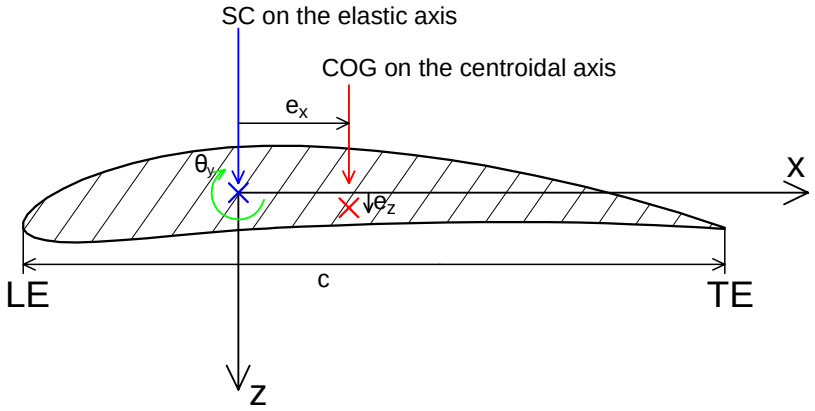

Figure 2.4: The foil cross-section in the xz-plane showing the used notation.

2.1.1 Beam equations of motion

The fin presented in Figure 2.2 can bend about the x- and z-axis and twist about the y-axis. The axial vibrations along the y-axis are neglected. The EOM of composite beams in flexural-torsional vibrations are defined by Sapountzakis [32, p. 1770–1771]. The equations are based on Timoshenko beam theory, which takes into account shear deformations, rotary inertia and coupling of bending and torsion vibrations but neglects rotation around the x- and z-axis (θ_x and θ_z) due to bending. The fourth order inertia terms arising from the coupling of shear deformations and rotary inertia are also neglected. The fin cross-section is assumed to be rigid in the xz-plane and therefore the cross-section twists as a rigid body. The linear small deflection theory is applied in the analysis. The angle of twist about the y-axis is small so that the small angle assumption can be used. Using the coordinate system defined in Figure 2.2 and assuming the fin material to be linear, homogeneous, isotropic and elastic, the EOM are

$$\begin{aligned} &EI_{xx}w'''' + EI_{xz}u'''' + \rho A(\ddot{w} + e_x\ddot{\theta}_y) - \left(\frac{\rho EI_{xx}}{G\kappa^2} + \rho I_{xx}\right)\ddot{w}'' \\ &- \left(\frac{\rho EI_{xz}}{G\kappa^2} + \rho I_{xz}\right)\ddot{u}'' - \left(\frac{\rho EI_{xx}}{G\kappa^2}e_x - \frac{\rho EI_{xz}}{G\kappa^2}e_z\right)\ddot{\theta}_y'' = 0 \end{aligned} \tag{2.1}$$

$$\begin{aligned} &EI_{zz}u'''' + EI_{xz}w'''' + \rho A(\ddot{u} - e_z\ddot{\theta}_y) - \left(\frac{\rho EI_{zz}}{G\kappa^2} + \rho I_{zz}\right)\ddot{u}'' \\ &- \left(\frac{\rho EI_{xz}}{G\kappa^2} + \rho I_{xz}\right)\ddot{w}'' - \left(\frac{\rho EI_{xz}}{G\kappa^2}e_x - \frac{\rho EI_{zz}}{G\kappa^2}e_z\right)\ddot{\theta}_y'' = 0 \end{aligned} \tag{2.2}$$

$$E\Gamma\theta_y'''' - GJ\theta_y'' + \rho I_{yy}\ddot{\theta}_y + \rho A\left(e_x\ddot{w} - e_z\ddot{u}\right) - \rho\Gamma\ddot{\theta}_y'' = 0 \quad . \tag{2.3}$$

The equation (2.1) governs the bending motion about the x-axis, the equation (2.2) the bending motion about the z-axis and the equation (2.3) twisting motion about the y-axis. A dot over a quantity indicates a differentiation with respect to time t and a prime a differentiation with respect to y. ρ is the density of the fin material and A is the cross-sectional area of the fin. e_x and e_z are the distance between the SC and COG along the x-axis and z-axis, respectively. EI is the bending stiffness consisting of Young's elastic modulus E and the cross-sectional area moment of inertia about the x-axis I_{xx} or the z-axis I_{zz}. I_{xx} and I_{zz} are defined about the SC. I_{yy} is the polar moment of inertia with respect to the SC and defined as

$$I_{yy} = I_{xx} + I_{zz} \quad . \tag{2.4}$$

GJ is the torsional rigidity comprising from shear modulus G and torsional constant J. In this study, the shear modulus is calculated with the elastic modulus and Poisson's ratio ν from the formula

$$G = \frac{E}{2\,(1+\nu)} \quad . \tag{2.5}$$

A torsional constant is defined analytically only for elementary shapes [30, p. 472–474]. $E\Gamma$ is the warping rigidity where Γ is the warping constant. κ^2 is the shear coefficient, a dimensionless factor which depends on the shape of the cross-section [22, p. 502]. The shear coefficients are analytically specified only for elementary shapes such as solid rectangles. The fin cross-section is simplified as a solid rectangle in respect to the shear coefficient. The formula for solid rectangular cross-sections is defined in the reference [19, p. 945] as

$$\kappa^2 = \frac{10(1+\nu)}{12+11\nu} \quad . \tag{2.6}$$

The presented EOM can be simplified by taking into account the geometry of the fin. The chord length of the fin is considerably greater than the thickness of the fin cross-section. Thus, the bending stiffness of the fin about the z-axis is considerably greater than that about the x-axis. In fact, the difference between the bending stiffness values is to the power of three compared to the difference between the chord length and thickness. This is due to the definition of the cross-sectional area moment of inertia. In general, an increase in stiffness leads to an increase in vibration frequency. Therefore, the frequency of the bending vibration about the z-axis is higher than that about the x-axis. This can also be seen from the reference [12, p. 425–428] which presents dry mode shapes of the control surface in the high-speed ship. The control surface is a fin with hollow shell structure and two web plates. Figure 2.5 shows the four lowest mode shapes of the control surface. The first and second mode shapes are bending about the x-axis. The third mode shape is torsion about the y-axis and the fourth is bending about the z-axis. The first natural frequency corresponding to bending about the x-axis is approximately 26 Hz and the fourth corresponding to bending about the z-axis is approximately 190 Hz. Thus, the difference is significant. It can also be noted that the torsion DOF

is important because the modes reveal a typical, mixed bending-torsion nature. Since the lower frequencies are of greater interest, the bending about the z-axis is neglected. Accordingly, the equation (2.2) and the terms containing horizontal deflection u are neglected.

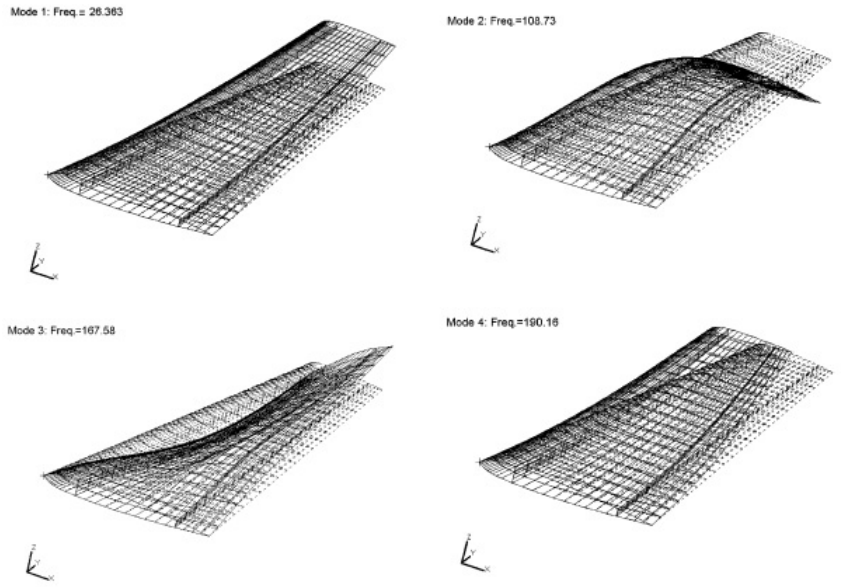

Figure 2.5: The four lowest natural frequencies and mode shapes of the control surface. [12, p. 426–428]

The warping phenomenon related to the twisting of the beam is significant in the analysis of open section, thin-walled section or hollow shell-web cross-section beams [8, p. 47–48] [33, p. 62]. For solid cross-sections, the warping stiffness is negligible and St. Venant's torsion theory, or in other words uniform torsion, is enough to describe the torsion of the beam [34, p. 340] [6, p. 269]. Since the fin is a solid cross-section beam consisting of one material, the warping terms can be neglected. Accordingly, the terms containing Γ are neglected from the equation (2.3).

The elimination of the effect of bending about the z-axis and warping simplifies the EOM presented in the equations (2.1) - (2.3) to

$$\begin{aligned} EI_{xx}w'''' + \rho A(\ddot{w} + e_x\ddot{\theta}_y) - \left(\frac{\rho EI_{xx}}{G\kappa^2} + \rho I_{xx}\right)\ddot{w}'' \\ - \left(\frac{\rho EI_{xx}}{G\kappa^2}e_x - \frac{\rho EI_{xz}}{G\kappa^2}e_z\right)\ddot{\theta}_y'' = 0 \end{aligned} \tag{2.7}$$

$$-GJ\theta_y'' + \rho I_{yy}\ddot{\theta}_y + \rho Ae_x\ddot{w} = 0 \quad . \tag{2.8}$$

Examining the terms of the equation (2.7), the first term is bending deflection, the second term inertia, the third term shear deformation and rotary inertia due to bending and the fourth term shear deformation due to twisting. The first and second term are so-called first order terms whereas shear deformation and rotary inertia are so-called second order terms. The second order terms have greater effect in case of

non-slender or short beams, meaning beams which have cross-section dimensions that are large as compared to the length. Examining the terms of the equation (2.8), the first term is torsional rotation, the second term inertia and the third term the coupling term. In the equation (2.7), the coupling term is the latter half of the inertia term. The fourth term of the equation (2.7) is the so-called second order coupling term related to shear deformation. Coupling of the bending and torsion vibration is caused by the offset between the SC and COG. The coupling terms are related to the inertial terms which means that the EOM are inertially coupled [34]. If the second order terms are neglected from the bending, the EOM simplify to

$$EI_{xx}w'''' + \rho A\left(\ddot{w} + e_x\ddot{\theta}_y\right) = 0 \tag{2.9}$$

$$-GJ\theta_y'' + \rho I_{yy}\ddot{\theta}_y + \rho A e_x\ddot{w} = 0 \quad , \tag{2.10}$$

which are based on Euler-Bernoulli beam theory and are in accordance with the literature [34, p. 340] [33, p. 59].

2.1.2 Assumptions in practice

The second order terms, shear deformation and rotary inertia in bending, come from the fact that the beam element rotates about the x-axis due to shear in addition to a deflection due to bending. Therefore, the total deflection of the beam element is the sum of bending and shear deflections, which is illustrated in Figure 2.6. The Euler-Bernoulli beam theory assumes that this rotation due to shear is not happening, meaning plane sections remain perpendicular to the bending line. In the Timoshenko beam theory, however, beam sections are allowed to rotate due to shear, meaning plane sections do not remain normal to the bending line. Due to this difference the beam stiffness is overestimated with the Euler-Bernoulli beam theory. However, this starts to cause significant error only when the slenderness ratio decreases and when the higher natural frequencies are of interest. Due to the fact that pre-swirl stator fin designs can be non-slender, the Timoshenko beam theory cannot be neglected in the study but the effect on the results is studied. [35, p. 337–338] In this study, the shear deformation term due to twisting, meaning the fourth term, is neglected from the EOM presented in the equation (2.7).

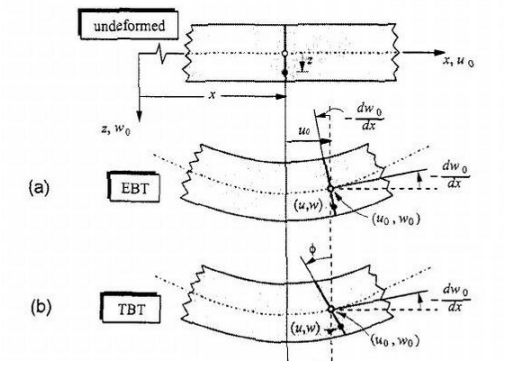

Figure 2.6: The transversal deformation of Euler-Bernoulli and Timoshenko beams. [31, p. 12]

The importance of the shear deformation term is related to the slenderness of the beam. The term can be neglected in case of slender beams, meaning the length of the beam is large compared to the thickness and width of the beam. The beam is considered slender when the slenderness ratio is larger than ten and when the beam length is at least ten times the beam thickness. The slenderness ratio α is defined as

$$\alpha = \frac{L}{c} \quad . \tag{2.11}$$

If beam thickness is defined in per cent of beam width, the beam is slender when $\alpha > 10$ and $t < \frac{\alpha}{10}$ or $\frac{\alpha}{t} > 10$. In case of fins, the thickness is usually less than half of the chord and at least less than the chord. Thus, fins can be considered slender if $\alpha > 10$. Therefore, the shear term has to be taken into account when the slenderness ratio is lower than ten. [19, p. 973–975]

The importance of the rotary inertia can be evaluated through that of the shear deformation. The shear deformation term is always γ^2 times larger than the rotary inertia term. The ratio γ^2 is defined as

$$\gamma^2 = \frac{2(1+\nu)}{\kappa^2} \quad . \tag{2.12}$$

This can be derived from the rotary inertia and the shear deformation terms of the non-dimensional EOM of the Timoshenko beam theory presented in [19, p. 949]. The ratio depends on the Poisson's ratio ν, a physical property depending on the material, and the shear coefficient κ^2, a dimensionless factor depending on the Poisson ratio and the cross-section geometry. Considering the Poisson ratio of typical metal to be about 0.3, the shear coefficient gets a value of about 0.85 according to the equation (2.6). With these values, the ratio γ^2 is about three, meaning the shear term is roughly three times larger than the rotary term in case of a solid rectangular cantilever beam. Generally, the ratio γ^2 ranges from 3 to 6 for a typical metal and cross-section. [19, p. 973–975] Therefore, the shear deformation term is always more important to take into account than the rotary inertia term. However, if the shear term is highly important, the rotary term can be relatively important too. Thus, the importance of these terms are studied shortly with respect to fins.

Before evaluating the importance of the bending-torsion coupling terms, the cause of the coupling has to be discussed. The bending-torsion coupling is dependent on the location of the SC and the COG of the beam cross-section. The shear center (SC) is the point on a cross-section in which a shear force can be applied without any torsion occurring. If the SC and COG are not coinciding in free vibration conditions, inertial forces acting on the COG are not applied in the SC, meaning they create additional torsion. [38, p. 474–476] The locations of the SC and COG are related to the symmetry of the cross-section. There are three kinds of cross-sectional symmetry: double symmetry, single symmetry and asymmetry. [34, p. 339–340]

In double symmetry, the beam cross-section is symmetric about both the x-axis and z-axis as shown in Figure 2.7. The SC and COG are coinciding, meaning the bending and torsion are uncoupled. [34, p. 339–340] As an example, a rectangle is the

cross-section with double symmetry and it is used in simple stator fins constructed only from plates.

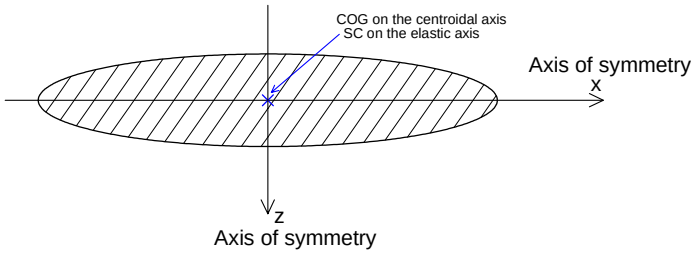

Figure 2.7: An example of doubly symmetric cross-section: elliptical cross-section.

In single symmetry, the beam cross-section is symmetric about only one of the x- or z-axis as shown in Figure 2.8. The SC and COG are not coinciding but both are located on the axis of symmetry. In this case, the EOM must be coupled when the transverse vibration is occurring in the direction perpendicular to the axis of symmetry. [34, p. 339–340] As an example, a symmetric NACA 4-digit cross-section is symmetric parallel to the x-axis but not in the perpendicular direction and thus the coupling must be considered in the bending about the x-axis.

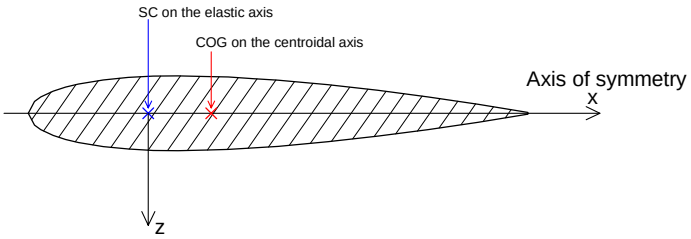

Figure 2.8: An example of single symmetric cross-section: symmetric NACA 4-digit cross-section.

An asymmetric cross-section is the most general case in which the SC and COG are not coinciding in either direction as shown in Figure 2.9. Therefore, the EOM must be coupled when the transverse vibration is occurring in both perpendicular directions. [34, p. 339–340] As an example, in case of an asymmetric NACA 4-digit section, the coupled EOM must be used.

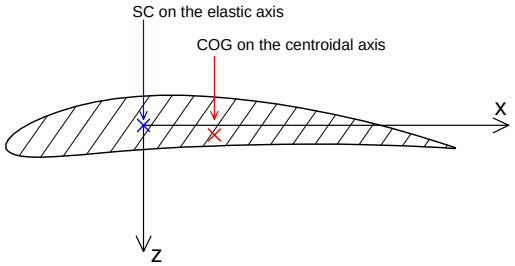

Figure 2.9: An example of asymmetric cross-section: asymmetric NACA 4-digit cross-section.

Recalling the simplification of the vibrations to 2D, the cross-sectional symmetry in the z-direction is not relevant from the point of view of the EOM because it has an effect only in transverse vibration in the x-direction. However, the distance of the SC and COG in the z-direction affects the area moment of inertia about the z-axis and the polar moment of inertia, meaning that the symmetry in the z-direction cannot be neglected in the calculation of cross-sectional properties. Regardless, the NACA 4-digit series is either single symmetric or asymmetric, meaning the bending about the x-axis and torsion about the y-axis are coupled. Noting that the coupling is dependent on the e_x and e_z of the fin cross-section, the importance of the coupling terms with respect to the natural frequencies are studied in this work.

2.1.3 Submerged beam equations of motion

In the previous section, the EOM of the beam were presented. The presented equations, however, describe only the dynamic behaviour of the beam in a vacuum. In this section, the effects of the hydrodynamic forces due to the water surrounding the fin are discussed from the view point of the natural frequency calculation. The effects of interest for this work are narrowed to consist only of the added mass effect, neglecting the effect of the chord-wise flow. The added mass of the fin is approximated with the 2D added mass coefficient of a flat plate. The derived added mass terms are introduced to the EOM of the beam presented in the previous section.

Free surface significantly influences the dynamic characteristics of the submerged cantilever plate but the effect decreases with an increase in the depth of the plate. Moreover, when the submerged depth is up to one half the length of the plate the free surface is negligible. [26, p. 1227] The stator fins are located on the level of the propeller, meaning that the submerged depth is more than the propeller radius. The length of a fin is usually a little bit more than the propeller radius. Therefore, the free surface effects can be neglected in this study.

The fin is submerged in water and it undergoes a chord-wise flow due to the forward motion of the ship. The chord-wise flow over the fin generates hydrodynamic forces to the fin. In addition, the fin moves perpendicularly to the chord-wise flow due to the heaving and rolling motions of the ship. This transverse motion of the fin also generate hydrodynamic loads on the fin due to momentum transfer to the water at the water-fin interface. The generated hydrodynamic forces are lift, pitching moment and drag. Lift is the component of load perpendicular to the oncoming flow. Pitching moment is the component causing a moment about the y-axis. Drag is the component parallel to the oncoming flow. Drag is relevant when the resistance is of interest. In this study, the chord-wise response of the fin is neglected and only the lift and pitching moment are of interest.

The lift and pitching moment can be decomposed into added mass and hydrodynamic damping components and their cross-terms. The added mass corresponds to the amount of fluid which moves with a body while this body is accelerating. The added mass component acts in-phase with the fin acceleration, causing the reduction of the vibration frequency. Damping causes the attenuation of the vibration amplitude. The hydrodynamic damping component acts in-phase with the fin velocity but

on opposite phase with respect to the fin acceleration. [18, p. 207] Damping affects the amplitude and phase of the body's motion. Added mass affects the frequency of the body's motion. The damping is neglected in this study. However, it should be noted that damping also decreases the natural frequencies of the system. [23, p. 453–457]

The importance of the other hydrodynamic effects can be evaluated with the Strouhal number. The Strouhal number St is a dimensionless number describing the mechanisms of the oscillating flow. In case of the hydrofoil, the characteristic length related to the St is defined as the chord length c when the St is defined as

$$St = \frac{c}{U} f \quad . \tag{2.13}$$

According to [4, p. 73–78], the three prevailing mechanisms related to lift are leading edge vortex, added mass reaction and leading edge vortex convection and interaction with the wing. The latter mechanism captures the effect of the wake. The relative effects of these mechanisms were compared in three regimes in [4, p. 73–78]. In the first regime of $St < 0.1$, only the leading edge vortex has a significant effect. In the second regime of $0.05 < St < 0.5$, the all three have an effect. In the third regime of $St > 0.5$, the added mass becomes dominant. Therefore, the added mass effect becomes more dominant as the St increases. [24, p. 589] In general, the ship operation speeds are at least 10 kn and the chord length of stator fins can be considered to be more than 0.5 meters. To reach an St larger than 0.5 with these values, the oscillating frequency of the fin should be higher than 5.2 Hz. As such, the St regime can be assumed to be larger than 0.5 in this study.

In summary, only the added mass components of the lift and pitching moment need to be taken into account in this work. The added mass has a significant role when defining the natural frequencies and modes of the body due to the fact that the movement of the surrounding fluid requires an additional force that is necessary to accelerate the body itself. [24, p. 579] The added mass is easy to evaluate in steady motion because it depends only on the fluid density and the body shape. However, in the situations when the body is in unsteady motion, local fluid accelerations may happen due to other effects than the body's motion, making the evaluation of the added mass more complex. [23, p. 441] [24, p. 582] The fin is in unsteady motion due to the ship motions. In this study, the fin is assumed to be in steady motion. The nonlinear effects are primarily related to hydrodynamic damping and not to the added mass according to [5] and [18]. Therefore, the added mass related to the vibrating fin can be taken as linear.

Cavitation affects the added mass and hydrodynamic loads and therefore affects the natural frequencies and critical velocities [3, p. 170]. Cavitation is the formation of vapour cavities in a liquid usually occurring when a liquid is subjected to rapid changes of pressure. The effect of cavitation on the natural frequency of the lowest bending mode is found to increase the frequency by about three per cent for a cavity length of about 40 per cent of the chord length [7, p. 47]. The cavitation can be neglected in the conceptual design phase because the effect to the lowest frequency is relatively small and especially because the data related to the cavitation is not usually available at this stage.

In this study, the added mass is calculated from a 2D cross-section model and thus the span-wise or 3D effects are not taken into account. The reference [18, p. 218] observed a generally good agreement in the added mass component of lift between the results of 2D and 3D cantilever plate models. Noticeable differences arise only as the tip of the plate is approached. The differences can be ascribed to the formation of tip vortices which are not captured by 2D models because the flow is assumed to be in the xz-plane. This discrepancy becomes more prominent for low aspect ratio plates. For plates with aspect ratio larger than three, the results can be considered to be accurate.

The aspect ratio ζ is defined as

$$\zeta = \frac{(2L_s)^2}{S} \quad , \tag{2.14}$$

where S is the surface area and L_s is the distance from the tip of the wing to the centreline of the airplane [10, p. 234]. In case of the stator fin, L_s is defined from the tip to the centreline of the ship, which is the same as the centreline of the propeller axis in single propeller ships. Noting that the fin is close to the propeller where the width of the bossing is not large, L_s can be simplified as L. Thus, for a uniform stator fin, the ζ can be simplified to

$$\zeta = \frac{2L}{c} \quad , \tag{2.15}$$

which is two times the slenderness ratio defined in the equation (2.11). In other words, the high aspect ratio means that the fin is slender. Therefore, the added mass of fins with a slenderness ratio larger than 1.5 can be approximated accurately with the 2D model.

However, the 2D models seem to overestimate rather than underestimate the added mass effect due to the reduced order of the model according to the reference [18, p. 218]. Thus, 2D models may tend to underestimate the natural frequency of vibrating submerged cantilever plates. The same conclusion is made in the reference [5], where the experimentally measured resonance frequencies of compliant beams vibrating underwater were found to exceed theoretical predictions. In addition, the same conclusion is made by Yadykin et al. [39, p. 122] by studying the flexible plate oscillating in a fluid. Yadykin et al. [39, p. 122] concluded that the added mass tends to overestimate the results for aspect ratios higher than ≈ 1.4, and underestimates these values for lower aspect ratio plates vibrating in the fundamental mode. Therefore, the added mass of the fins with a slenderness ratio smaller than 0.7 is underestimated while one greater than 0.7 is overestimated. In conclusion, the added mass obtained with the 2D model is conservative from the point of view of the natural frequency analysis due to the fact that, generally, lower natural frequencies are considered as worse designs.

The 2D unsteady thin airfoil theory has been shown to be sufficiently accurate for the oscillating 2D airfoils in a multitude of experimental investigations [10, p. 280] [27]. In this theory, the foil is simplified as a flat plate in a small-amplitude unsteady motion. This is illustrated in Figure 2.10, where a is a distance between

the LE and the pitching axis. The pitching axis is the axis about which the pitching motion of the foil occurs. The EOM are defined about the SC and thus the pitching axis coincides with the elastic axis. The motion consists of an oscillatory heaving and pitching motion which generates lift and a pitching moment to the foil. The foil is moving with constant velocity U in an otherwise stationary fluid. Despite the simplifications of the theory, this model is said to be useful in estimating the unsteady loads in cases such as wing flutter or propulsion [23, p. 453–457].

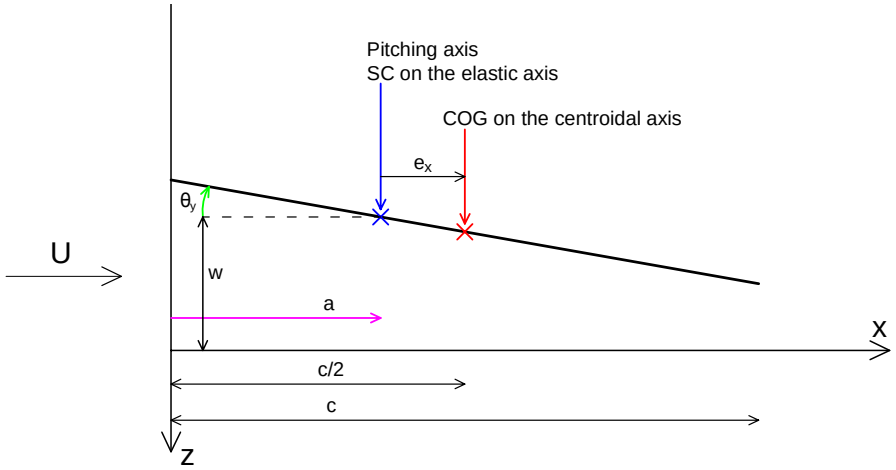

Figure 2.10: The illustration of a 2D flat plate in the oscillatory pitching and heaving motion. Modified from [23, p. 454]

Newman [28, p. 145] has presented the 2D added mass coefficients for an oscillating flat plate without a chord-wise flow. He states that the added mass of a flat plate for heave motion is $\frac{1}{4}\pi\rho_w c^2$ and for a pitching motion $\frac{1}{128}\pi\rho_w c^4$. ρ_w is the density of the fluid which is in this case water. The coupling of the heave and pitching motions is not taken into account. The values are given for the case where the COG and the pitching axis are located in the middle of the plate.

The reference [23, p. 453–457] introduces the lift and pitching moment equations for an oscillating flat plate moving with constant velocity U in an otherwise stationary fluid. The equations include the damping and the added mass parts and also cross-terms containing the velocity U which take the passing flow into account. Roughly, the damping parts are dependent on velocities and the added mass parts on accelerations. The equations are defined about the pitching axis. The COG is located in the middle of the plate and thus the following relation between the a and the e_x can be written

$$e_x = \frac{c}{2} - a \quad . \tag{2.16}$$

By considering only the terms related to acceleration and introducing the relation (2.16), the added mass parts of the lift per unit span L' and the pitching moment

M' are obtained as

$$L' = \frac{\pi\rho_w c^2}{4}\left(\ddot{w} - e_x\ddot{\theta}_y\right) \tag{2.17}$$

$$M' = \frac{\pi\rho_w c^2}{4}\left[-e_x\ddot{w} + \left(\frac{1}{8} + \frac{4e_x^2}{c^2}\right)\frac{c^2}{4}\ddot{\theta}_y\right] \quad , \tag{2.18}$$

where ρ_w is the density of the fluid which is in this case water. The equations are defined about the SC, as are the EOM. It can be seen that these equations are also inertially coupled, as are the EOM. The equations are same as Newman's but in addition taking into account the coupling. This can be seen in case of $e_x = 0$.

In the article [24, p. 585], the panel method is used to calculate the added mass of NACA0012 section. The results can be compared to the equations (2.17) and (2.18) when $e_x = \frac{c}{6}$. The differences are between one and three per cent. Therefore, the flat plate simplification is accurate enough to approximate the 2D added mass effect of the NACA 4-digit sections.

The added mass terms of lift and pitching moment are inertial forces similar to the inertia terms of the EOM in Section 2.1.1. Thus, the equations (2.17) and (2.18) can be added into the EOM in Section 2.1.1. Including the 2D added mass terms, the EOM of the submerged fin are

$$EI_{xx}w'''' + \rho A(\ddot{w} + e_x\ddot{\theta}_y) + \frac{\pi\rho_w c^2}{4}\left(\ddot{w} - e_x\ddot{\theta}_y\right) - \left(\frac{\rho EI_{xx}}{G\kappa^2} + \rho I_{xx}\right)\ddot{w}'' = 0 \tag{2.19}$$

$$-GJ\theta_y'' + \rho I_{yy}\ddot{\theta}_y + \rho A e_x\ddot{w} + \frac{\pi\rho_w c^2}{4}\left[-e_x\ddot{w} + \left(\frac{1}{8} + \frac{4e_x^2}{c^2}\right)\frac{c^2}{4}\ddot{\theta}_y\right] = 0 \quad . \tag{2.20}$$

As the added mass term is dependent on the density of the surrounding fluid, its significance to the EOM can be evaluated with the density ratio. The density ratio is defined as the ratio between the fin and the surrounded fluid densities as

$$\mu = \frac{\rho}{\rho_w} \quad . \tag{2.21}$$

As the density ratio increases, the contribution of the added mass decreases. [24, p. 589] Thus, the added mass terms can be omitted when the density ratio is very large. [10, p. 279] [24, p. 582] As a matter of fact, the density ratio is very large only in case of air and thus the added mass must be taken into account in water, regardless of the fin density. In this study, the fin density is same as the fin material density because a solid fin cross-section is considered.

2.2 Calculation method

In this section, the procedure for the solving of the natural frequencies and mode shapes from the EOM is presented. The EOM are describing the dynamic behaviour of the system but they are infinite dimensional partial differential equations and are therefore complicated to solve exactly. Different numerical methods can be used to solve the structural response and natural frequencies of the cantilever beams or

plates. The finite element method (FEM) is used to solve the natural frequencies and mode shapes, for example in [42] [40] [26] [17]. The boundary element method is also used, but to solve the structural responses, for example in [25] [32].

In this study, the FEM is used to discretize the EOM to ordinary differential equations and solve them in an approximative manner. The natural frequencies and modes of the fin can be solved from the eigenvalue problem which is formed from the discretized EOM.

First, the FEM is presented shortly in general. Second, the EOM are discretized via the FEM. Boundary conditions (BC) are required to define the cantilever beam model as the calculation model. Third, the solution of the natural frequencies and modes from the eigenvalue problem is presented.

2.2.1 Finite Element Method

The finite element method (FEM) is a numerical method used to solve field problems in an approximative manner. A field problem is described by a differential equation or by an integral expression. The fundamental idea of the FEM is to divide the calculation domain into discrete sub-domains, so-called finite elements, in which the equations are calculated. Elements have an finite number of nodes defining the points where the variables are solved. The variation of the variables over each element is approximated between the nodes of the element with shape functions that are usually polynomials. Once the variable values are known at the nodes, the approximate distribution of the variable over each element is known. Solving the behaviour of all elements one by one, the behaviour of the whole domain can be formed by patching the elements together. Thus, instead of solving the differential equations at every infinite number of points over a continuum, the equations need to be solved only at a finite number of points. With the FEM, various physical phenomena can be treated numerically inside the continuum under investigation and good approximate solutions can be obtained for the entire continuum. The idealization steps related to the procedure are illustrated in Figure 2.11. [29, p. 1 – 4] [14, p. 1 – 2]

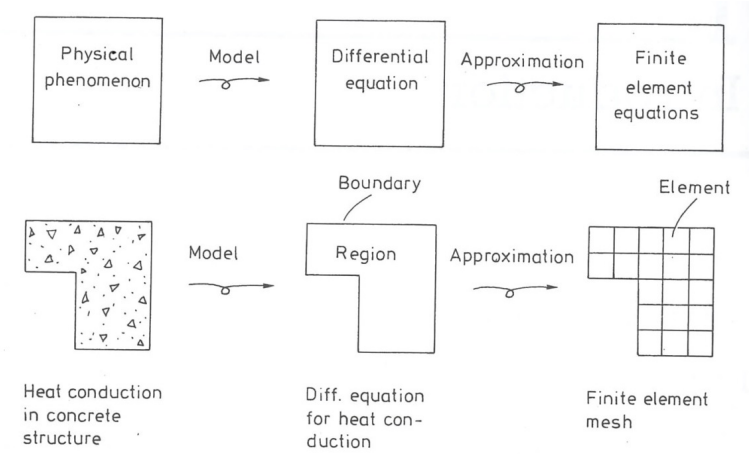

Figure 2.11: The idealization steps related to the FEM. [29, p. 2]

The behaviour of an element is defined with local system matrices. The local matrices define the system parameters for the element at the nodes according to the governing equations and shape functions. Elements are connected through coincident nodes at the boundaries of the elements. By knowing the particular arrangement of elements called mesh, the entire domain can be assembled from elements. The local matrices are assembled to the global system matrices which define the system parameters of all the nodes in the domain. The global matrices are needed to solve the differential equations at each node concurrently. [29, p. 1 – 4] [14, p. 1 – 2]

In this study, the problem is treated as a linear boundary value problem of an elastic continuum. The boundary value problem is a differential equation in which certain information is known *a priori* for the unknown variables at the boundary nodes of the domain [29, p. 1]. The BCs are described either by static conditions or by kinematic conditions. In the problem at hand, the static conditions are related to the moments and forces and the kinematic conditions to the deflections and slopes at the boundary nodes. [29, p. 311–331]

2.2.2 Finite Element Method implementation

In this study, a uniform 2D beam element with a node at each end, shown in Figure 2.12, is used. Each node has four DOFs consisting of flexural translation in the z-direction w, slope of flexural translation θ_x, torsional rotation around y-axis θ_y and slope of torsional rotation θ'_y. The slopes are defined as

$$\theta_x \qquad \text{and} \qquad \theta'_y = \frac{\partial \theta_y}{\partial y} \tag{2.22}$$

in case of Timoshenko beam theory and

$$\theta_x = w' = \frac{\partial w}{\partial y} \qquad \text{and} \qquad \theta'_y = \frac{\partial \theta_y}{\partial y} \tag{2.23}$$

in case of Euler-Bernoulli beam theory. Beam behaviour can be defined by shear forces, bending and twisting moments, and corresponding displacements. There are three reactions at each node consisting of shear force in the z-direction Q_z, bending moment about the x-axis M_x and torque about the y-axis M_y. The length of the beam element is h.

In the EOM, all material and geometrical parameters of the beam element dy are assumed to be constant along an element. In reality, the fin has a variable cross-section. The tapering is taken into account by using a number of stepped uniform beam elements along the domain. The results converge to the solutions of smoothly tapered beams as the number of the stepped elements increases [36, p. 834]. Thus, the calculation procedure becomes simpler.

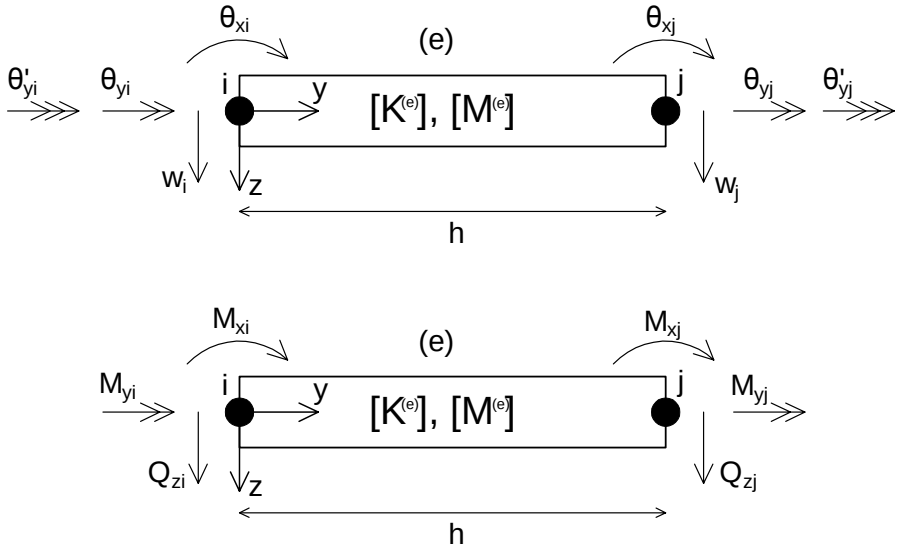

Figure 2.12: The nodal DOFs and nodal forces of a 2D beam element with two nodes i and j.

The global form of the beam EOM for a multi-element structure [14, p. 376] is

$$[\mathbf{M}]\left\{\ddot{\mathbf{D}}\right\} + [\mathbf{K}]\{\mathbf{D}\} = 0 \qquad , \tag{2.24}$$

where $\{\mathbf{D}\}$ is a vector containing the nodal DOFs to be solved, $[\mathbf{K}]$ is the global stiffness matrix and $[\mathbf{M}]$ the global mass matrix. For the chosen beam element, the vector $\{\mathbf{D}\}$ is defined as

$$\{\mathbf{D}\} = \begin{bmatrix} w \\ \theta_x \\ \theta_y \\ \theta'_y \end{bmatrix} \qquad . \tag{2.25}$$

The EOM consist of transverse (2.19) and torsion equations (2.20). Thus, the global stiffness matrix $[\mathbf{K}]$ is composed with global sub-matrices $[\mathbf{K_w}]$ and $\left[\mathbf{K}_{\theta_\mathbf{y}}\right]$ related to translational and torsional stiffness, respectively. The global mass matrix $[\mathbf{M}]$ is composed with global sub-matrices $[\mathbf{M_w}]$, $\left[\mathbf{M}_{\theta_\mathbf{y}}\right]$ and $\left[\mathbf{M}_{\mathbf{w}\theta_\mathbf{y}}\right]$ related to translational, torsional and coupling, respectively. The global matrices [34, p. 342] are composed as

$$[\mathbf{K}] = \begin{bmatrix} [\mathbf{K_w}] & 0 \\ 0 & \left[\mathbf{K}_{\theta_\mathbf{y}}\right] \end{bmatrix} \qquad \text{and} \qquad [\mathbf{M}] = \begin{bmatrix} [\mathbf{M_w}] & \left[\mathbf{M}_{\mathbf{w}\theta_\mathbf{y}}\right] \\ \left[\mathbf{M}_{\mathbf{w}\theta_\mathbf{y}}\right]^T & \left[\mathbf{M}_{\theta_\mathbf{y}}\right] \end{bmatrix} \qquad . \tag{2.26}$$

The inertial coupling of the EOM can be seen from the off-diagonal terms $\left[\mathbf{M}_{\mathbf{w}\theta_\mathbf{y}}\right]$ and $\left[\mathbf{M}_{\mathbf{w}\theta_\mathbf{y}}\right]^T$ in the global mass matrix in contrast to the diagonal global stiffness matrix.

The global sub-matrices are assembled from local element matrices. Using cubic Hermite polynomials [43, p. 36] as shape functions, the local element matrices can

be written in the form [14, p. 26–27] [34, p. 342]

$$[\mathbf{K_w^e}] = \frac{EI_{xx}}{h^3}\frac{1}{1+\phi}\begin{bmatrix} 12 & 6h & -12 & 6h \\ 6h & (4+\phi)h^2 & -6h & (2-\phi)h^2 \\ -12 & -6h & 12 & -6h \\ 6h & (2-\phi)h^2 & -6h & (4+\phi)h^2 \end{bmatrix} \tag{2.27}$$

$$\left[\mathbf{K_{\theta_y}^e}\right] = \frac{GJ}{30h}[\mathbf{H_2}] \tag{2.28}$$

$$[\mathbf{M_w^e}] = \frac{\rho Ah}{420}[\mathbf{H_1}] + \frac{\rho I_{xx}}{30h}[\mathbf{H_2}] + \frac{\pi\rho_w c^2 h}{1680}[\mathbf{H_1}] \tag{2.29}$$

$$\left[\mathbf{M_{\theta_y}^e}\right] = \frac{\rho I_{yy}h}{420}[\mathbf{H_1}] + \left(\frac{1}{8} + \frac{4e_x^2}{c^2}\right)\frac{\pi\rho_w c^4 h}{6720}[\mathbf{H_1}] \tag{2.30}$$

$$\left[\mathbf{M_{w\theta_y}^e}\right] = \frac{e_x\rho Ah}{420}[\mathbf{H_1}] - \frac{\pi\rho_w c^2 e_x h}{1680}[\mathbf{H_1}] \quad , \tag{2.31}$$

where h is the length of the beam element and ϕ is defined as [14, p. 27]

$$\phi = \frac{12EI_{xx}}{\kappa^2 AGh^2} \quad . \tag{2.32}$$

The matrices $[\mathbf{H_1}]$, $[\mathbf{H_2}]$ and $[\mathbf{H_3}]$ are composed of the shape functions. They are defined as

$$[\mathbf{H_1}] = \begin{bmatrix} 156 & 22h & 54 & -13h \\ 22h & 4h^2 & 13h & -3h^2 \\ 54 & 13h & 156 & -22h \\ -13h & -3h^2 & -22h & 4h^2 \end{bmatrix} \tag{2.33}$$

$$[\mathbf{H_2}] = \begin{bmatrix} 36 & 3h & -36 & 3h \\ 3h & 4h^2 & -3h & -h^2 \\ -36 & -3h & 36 & -3h \\ 3h & -h^2 & -3h & 4h^2 \end{bmatrix} \tag{2.34}$$

$$[\mathbf{H_3}] = \begin{bmatrix} 12 & 6h & -12 & 6h \\ 6h & 4h^2 & -6h & 2h^2 \\ -12 & -6h & 12 & -6h \\ 6h & 2h^2 & -6h & 4h^2 \end{bmatrix} \quad . \tag{2.35}$$

The local bending stiffness matrix $[\mathbf{K_w^e}]$ includes the shear deformation term in the form of ϕ. When a beam element becomes more and more slender, ϕ approaches zero. Therefore, the matrix $[\mathbf{K_w^e}]$ can be written as [34, p. 342]

$$[\mathbf{K_w^e}] = \frac{EI_{xx}}{h^3}[\mathbf{H_3}] \quad , \tag{2.36}$$

when the shear deformation is neglected from the EOM, meaning the EOM given in (2.9) and (2.10) are used. The rotary inertia term is the second part of the local mass matrix $[\mathbf{M_w^e}]$. The added mass terms are the last parts of the local mass matrices $[\mathbf{M_w^e}]$, $\left[\mathbf{M_{\theta_y}^e}\right]$ and $\left[\mathbf{M_{w\theta_y}}\right]$.

The EOM contain eight spatial derivatives requiring eight BCs and four time derivatives requiring four initial conditions. However, only spatial BCs are required because only the natural frequencies and modes are to be solved. In the cantilever beam model, one end of the beam is free and another is fixed. The deflections and slopes at the free end are unrestricted but the bending moment, shear force and torque must vanish. This gives the following BCs for the free end:

$$M_x = -EI_{xx}w'' = 0 \tag{2.37}$$
$$Q_z = -EI_{xx}w''' = 0 \tag{2.38}$$
$$M_y = GJ\theta_y' = 0 \quad . \tag{2.39}$$

At the fixed end, the bending moment, shear force and torque are unrestricted but the deflections and slopes must vanish. This gives the following BCs for the fixed end:

$$w = 0 \tag{2.40}$$
$$\theta_x = -w' - \frac{EI_{xx}}{GA\kappa^2}w''' = 0 \quad \text{in case of Timoshenko beam theory} \tag{2.41}$$
$$\theta_x = w' = 0 \quad \text{in case of Euler-Bernoulli beam theory} \tag{2.42}$$
$$\theta_y = 0 \tag{2.43}$$
$$\theta_y' = 0 \quad . \tag{2.44}$$

The BCs at the free end are static and the conditions at the fixed end kinematic. [22, p. 495–503] [32, p. 1771 – 1772]

2.2.3 Solution of natural frequencies and modes

In this section, the procedure to solve the natural frequencies and mode shapes from the discretized EOM is presented. The natural frequencies and mode shapes of the system are related to the eigenvalues and eigenvectors of the equations defining the behaviour of the system. Eigenvalues and eigenvectors can be solved from the eigenvalue problem. [22, p. 279]

In this study, the eigenvalues and eigenvectors are solved computationally from the generalized eigenvalue problem. For the studied undamped vibration, the problem is formulated as

$$\lambda \left[\mathbf{M}\right] \left\{\overline{\mathbf{D}}\right\} = \left[\mathbf{K}\right] \left\{\overline{\mathbf{D}}\right\} \quad , \tag{2.45}$$

where λ is an eigenvalue and $\left\{\overline{\mathbf{D}}\right\}$ is an eigenvector associated with the eigenvalue [22, p. 294].

The natural frequencies ω in Hertz are obtained from the eigenvalues with the formula

$$\omega = \frac{\sqrt{\lambda}}{2\pi} \quad . \tag{2.46}$$

The eigenvectors define only the relative values for the nodes, meaning that the mode shapes describe only the shape of the oscillation related to the natural frequency and not the absolute deflections [22, p. 279].

2.3 Case study: NACA 4-digit series

In this work, the NACA 4-digit series is used to describe the fin cross-section. This series is commonly used in measurements and simulations as a foil cross-section model both in air and water. Thus, the used calculation method can be validated with the NACA 4-digit cross-section beam by comparing the obtained results to the literature results. The aim is to study the natural frequency dependency on the fin parameters and to produce design graphs for the conceptual design phase. Although the camber and asymmetric shape of the cross-section probably have more effect on the hydrodynamics and thereby on the flutter cases, the effect on the natural frequencies is studied.

The NACA cross-section shapes are easy to vary for the parameter study because the cross-section shapes are defined with analytical formulas consisting of three parameters. The parameters are the maximum thickness of the section t, the maximum camber m and the location of the maximum camber as a distance from the LE p. The numbering system of NACA 4-digit series is based on these three parameters. The first integer indicates the value of m in per cent of the chord. The second integer indicates the value of p in tenths of the chord. The last two integers indicate the value of t in per cent of the chord. [1, p. 114]

The NACA 4-digit cross-section is defined by a thickness distribution and a mean line equation. The thickness distribution is symmetric and defines the location of the upper and lower surface of a symmetrical wing section along the chord line as a function of t. The mean line equation takes into account asymmetry of the wing section with the camber and the shape of the mean line. It is a function of m and p. The symmetric cross-section is defined with the thickness distribution and thus m and p equal 0. The asymmetric distribution is defined by a combination of the thickness distribution and the mean line equation. [1, p. 113–114]

The parameters c, t, m and p describe the fin cross-section satisfyingly from the fin design point of view but geometrical properties are needed to describe the structural response. The cross-sectional area A, the area moments of inertia I_{xx} and I_{zz} and the polar moment of inertia I_{yy} can be calculated with analytical formulas [30, p. 687–689]. The torsion constant J and the distance between the SC and COG e_x and e_z have analytical formulas only for elementary cross-sections such as a circle and rectangle. A good option is to calculate all geometrical properties with FE-software. This would be time consuming for the used cross-sections with varying parameters and therefore the approximative formulas are developed to define all the geometrical properties as a function of the parameters c, t, m and p. Thus, only the four cross-section parameters c, t, m and p are required to calculate the geometrical properties. Moreover, these parameters are used as variables in the fin design graphs and other cross-sectional parameters can be omitted. In addition, the simplicity of the approximative formulas can help to outline the effect of the four parameters to the cross-sectional properties and the fin stiffness and moreover helps to underline the parameters having the greatest effect on the natural frequencies.

The regression analysis is used to develop the approximative formulas. The geometrical properties of symmetric cross-sections NACA0009 and NACA0012 and

asymmetric NACA2412, NACA5412 and NACA9412 are calculated with the FE-software FEMAP and utilized in the regression analysis. The rectangle from the elementary shapes is found to be a relatively good approximation for the NACA 4-digit series and is therefore used in the development of the approximative formulas for the cross-sectional area A, the area moment of inertia about the x-axis at the SC I_{xx}, the polar moment of inertia about the y-axis at the SC I_{yy}, the distance between the COG and SC parallel to x-axis e_x and the torsion constant J.

The cross-sectional area is found to match the value of the rectangle when the chord length c and the thickness t are corrected by multiplying them with the factor of 0.825. A similar match is found for the area moments of inertia and therefore the corrected chord length c_a and corrected thickness t_a are utilized and defined as

$$c_a = 0.825c \tag{2.47}$$
$$t_a = 0.825t \quad . \tag{2.48}$$

The other two parameters, m and p, are not affecting the cross-sectional area and the area moment of inertia about the z-axis at the COG I_{zz}^{COG} but both are found to affect the area moment of inertia about the x-axis at the COG I_{xx}^{COG}.

The e_x and e_z values are defined with the locations of the COG and the SC as

$$e_x = \overline{x} - \tilde{x} \quad \text{positive when COG is on the TE side of SC} \tag{2.49}$$
$$e_z = \overline{z} - \tilde{z} \quad \text{positive when COG is on the lower surface side of SC,} \tag{2.50}$$

where $\overline{x}$ and $\overline{z}$ are the location of the COG and $\tilde{x}$ and $\tilde{z}$ the location of the SC. The e_x value is defined as positive when the COG is on the TE side of the SC and the e_z when the COG is on the lower surface side of the SC. This is illustrated previously in Figure 2.4. The value of $\overline{x}$ is found to depend only on the chord length and $\overline{z}$ on the parameters m and p. The values of $\tilde{x}$ and $\tilde{z}$ are found to depend on all the three parameters c, m and p.

The good approximation for the torsion constant J is found to be based on the analytical equation of a torsion member having a narrow rectangular cross-section. The analytical equation is obtained by using the membrane analogy by assuming $t << c$. [30, p. 472–474]

The developed approximative formulas of the geometrical properties are listed below:

$$
\begin{aligned}
A &= c_a t_a && (2.51)\\
\overline{x} &= 0.42c && (2.52)\\
\overline{z} &= 0.85m - 0.2mp \quad (= 0 \text{ if } p = 0) && (2.53)\\
\tilde{x} &= ((1 + 0.6m)0.34 + 0.1mp)\, c && (2.54)\\
\tilde{z} &= (1.2m - 0.2mp)\, c && (2.55)\\
I_{xx}^{COG} &= \left(1 + 4.5m + 30m^2 p\right) \frac{c_a t_a^3}{12} && (2.56)\\
I_{zz}^{COG} &= \frac{t_a c_a^3}{12} && (2.57)\\
I_{yy}^{COG} &= I_{xx}^{COG} + I_{zz}^{COG} && (2.58)\\
I_{xx} &= I_{xx}^{COG} + e_z^2 A && (2.59)\\
I_{zz} &= I_{zz}^{COG} + e_x^2 A && (2.60)\\
I_{yy} &= I_{xx} + I_{zz} && (2.61)\\
J &= \frac{c_a t_a^3}{3} \quad . && (2.62)
\end{aligned}
$$

The applicability of the derived formulas is justified by comparing the geometric property values calculated with both the FE-software and the approximative formulas in Table 2.1. The geometric property values of NACA0009, NACA0012, NACA2412, NACA5412 and NACA9412 are compared. The relative difference in per cent is used to compare results.

To summarize, the relative differences are less than five per cent in general. For symmetric cross-sections, the differences are less than three per cent. In case of asymmetric cross-sections, the difference increases if the camber ratio m increases. The difference of the area moment of inertia about the x-axis at the SC I_{xx} increases the most, gaining the greatest difference of eight per cent in the NACA9412. Since other properties are differing less than five per cent, the derived approximative formulas can be used to define the geometric properties of the studied cross-sections.

Table 2.1: The list of the cross-sectional properties calculated with the commercial FE-software FEMAP and with the approximative formulas (2.51) - (2.62). The relative difference is calculated with respect to FEMAP values and is given in per cent. A negative relative difference means that the approximated value is smaller than the FEMAP value. The cross-sectional properties are calculated for the cross-sections NACA0009, NACA0012, NACA2412, NACA5412 and NACA9412.

Cross-sectional	NACA0009			NACA0012			NACA2412			NACA5412			NACA9412		
properties	FEMAP	Approx.	RD [%]	FEMAP	Approx.	RD [%]	FEMAP	Approx.	RD [%]	FEMAP	Approx.	RD [%]	FEMAP	Approx.	RD [%]
correction factor		0.825			0.825			0.825			0.825			0.825	
c [m]	1	0.825		1	0.825		1	0.825		1	0.825		1	0.825	
t [m]	0.09	0.07425		0.12	0.099		0.12	0.099		0.12	0.099		0.12	0.099	
m	0	0		0	0		0.02	0.02		0.05	0.05		0.09	0.09	
p	0	0		0	0		0.4	0.4		0.4	0.4		0.4	0.4	
A [m^2]	6.17E-02	6.13E-02	-1	8.22E-02	8.17E-02	-1	8.23E-02	8.17E-02	-1	8.26E-02	8.17E-02	-1	8.36E-02	8.17E-02	-2
$\bar{x}$	4.20E-01	4.20E-01	0	4.20E-01	4.20E-01	0	4.20E-01	4.20E-01	0	4.20E-01	4.20E-01	0	4.18E-01	4.20E-01	1
$\bar{z}$	0.00E+00	0.00E+00	0	0.00E+00	0.00E+00	0	1.56E-02	1.54E-02	-1	3.89E-02	3.85E-02	-1	6.97E-02	6.93E-02	-1
$\tilde{x}$	3.42E-01	3.40E-01	-1	3.43E-01	3.40E-01	-1	3.44E-01	3.45E-01	0	3.51E-01	3.52E-01	0	3.62E-01	3.62E-01	0
$\tilde{z}$	1.18E-06	0.00E+00	-100	4.64E-06	0.00E+00	-100	2.27E-02	2.24E-02	-1	5.67E-02	5.60E-02	-1	1.02E-01	1.01E-01	-1
e_x [m]	7.87E-02	8.05E-02	2	7.79E-02	8.05E-02	3	7.63E-02	7.56E-02	-1	6.91E-02	6.83E-02	-1	5.61E-02	5.85E-02	4
e_z [m]	-1.18E-06	0.00E+00	-100	-4.64E-06	0.00E+00	-100	-7.09E-03	-7.00E-03	-1	-1.78E-02	-1.75E-02	-2	-3.26E-02	-3.15E-02	-3
I_{xx}^{COG} [m4	2.87E-05	2.81E-05	-2	6.81E-05	6.67E-05	-2	6.99E-05	7.30E-05	4	7.98E-05	8.37E-05	5	1.07E-04	1.00E-04	-7
I_{zz}^{COG} [m4	3.40E-03	3.47E-03	2	4.54E-03	4.63E-03	2	4.55E-03	4.63E-03	2	4.59E-03	4.63E-03	1	4.69E-03	4.63E-03	-1
I_{yy}^{COG} [m4	3.43E-03	3.50E-03	2	4.61E-03	4.70E-03	2	4.62E-03	4.71E-03	2	4.67E-03	4.72E-03	1	4.80E-03	4.73E-03	-1
I_{xx} [m4]	2.87E-05	2.81E-05	-2	6.81E-05	6.67E-05	-2	7.41E-05	7.70E-05	4	1.06E-04	1.09E-04	3	1.96E-04	1.81E-04	-8
I_{zz} [m4]	3.78E-03	3.87E-03	2	5.04E-03	5.16E-03	2	5.02E-03	5.10E-03	1	4.98E-03	5.01E-03	1	4.96E-03	4.91E-03	-1
I_{yy} [m4]	3.81E-03	3.90E-03	2	5.10E-03	5.23E-03	2	5.10E-03	5.18E-03	2	5.09E-03	5.12E-03	1	5.15E-03	5.09E-03	-1
J [m^4]	1.14E-04	1.13E-04	-1	2.67E-04	2.67E-04	0	2.67E-04	2.67E-04	0	2.68E-04	2.67E-04	-1	2.71E-04	2.67E-04	-2

3 Results

The current chapter is divided into four parts. In the first part, the calculation method is verified against analytical results and the calculated results are validated against experimental results of NACA 4-digit section beams. The second part studies the significance of the shear deformation, rotary inertia, coupling and added mass terms with respect to natural frequencies. The purpose is to check when the terms can be neglected in calculations and when not. The third part defines natural frequency dependencies on the calculation parameters. The parameters are length, chord length, thickness, camber, location of maximum camber, span-wise variation and material. The purpose is to give guidelines for the designer on how the change in parameter affects the frequencies. The fourth part presents the idea to utilize design graphs in the selection of fin parameters. The purpose is to give the lowest frequencies in the graphs so that the designer can check the predicted frequency with different sets of parameters.

3.1 Verification and validation

In this section, the calculation method to predict the natural frequencies and modes is verified against analytical results and the results are validated against experimental results of NACA 4-digit series. First, the method is verified by comparing results to analytical formulas of the most simple case of uniform and linearly tapered cantilever beams with solid rectangular cross-sections in a vacuum, meaning without coupling and added mass. In addition, the method is verified by comparing natural frequencies of bending to numerical results of cantilever beams with NACA 4-digit cross-sections in a vacuum and water without coupling. Second, the results are validated against experimental studies of NACA 4-digit cross-section wings in a vacuum, air and water. The vacuum and air cases are used to validate if the simplified approach and the approximative cross-section properties are capable of predicting such a fin structure. The water and air cases are used to validate if the simplification can take the fin-fluid interaction into account in order to predict natural frequencies and mode shapes at a reasonable level also for submerged fins. Since only the lowest natural frequencies and modes are of interest, the accuracy in low frequencies is priority in evaluation. The results should be inside the margin of five or ten per cent in case of the lowest natural frequencies.

3.1.1 Verification of the calculation method

In this section, the analytical formulas for different cantilever beams are used to verify the calculation method for the dry uncoupled EOM. The method is verified by comparing the lowest natural frequencies of bending and torsion. The analytical formulas are based on Euler-Bernoulli beam theory. The cantilever beams are consisting of both uniform and linearly tapered beams with solid rectangular cross-sections. In addition, the numerical results of NACA0012 cross-section beams are used to verify the calculation method for the submerged uncoupled bending EOM.

The analytical formula to calculate the natural frequencies of a slender and uniform cantilever beam in transverse vibration is given as

$$\omega_n = \frac{\beta_n^2}{2\pi}\sqrt{\frac{EI}{\rho A}} \quad , \tag{3.1}$$

where the natural frequency ω is in Hertz. The analytical formula for the corresponding mode shapes is given as

$$X_n(x) = \cosh \beta_n x - \cos \beta_n x - \sigma_n(\sinh \beta_n x - \sin \beta_n x) \quad . \tag{3.2}$$

The symbol n is the ordinal number of the natural frequency and the corresponding mode shape. The symbol β_n is a weighting number for bending as a fraction of a length of the beam L. The symbol σ_n is a mode shape coefficient. The coefficient values for the five lowest natural frequencies and modes are given in Table 3.1. [22, p. 500]

The results of the five lowest natural bending frequencies and mode shapes for the uniform cantilever beam calculated without shear deformation, rotary inertia, coupling and added mass terms are presented in Table 3.1 and Figures A.1 and A.2 in comparison to the analytical results. The results are obtained with property values of $A = 1$, $E = 1$, $L = 1$, $I = 1$ and $\rho = 1$. Both the natural frequency values and the natural mode shapes are matching perfectly with each other.

Table 3.1: The comparison of analytical and calculated natural frequencies in bending for uniform cantilever beams without the shear deformation, rotary inertia, coupling and added mass terms.

n	β_n	σ_n	analytical ω_n	calculated ω_n	relative difference [%]
1	1.875	0.734	0.56	0.56	0.1
2	4.694	1.019	3.51	3.51	0.1
3	7.855	0.999	9.82	9.82	0.0
4	10.996	1.000	19.24	19.24	0.0
5	14.137	1.000	31.81	31.81	0.0

The analytical formula for natural frequencies of a uniform cantilever beam in torsional vibration is given as

$$\omega_n = \frac{(2n-1)}{4L}\frac{GJ}{\rho I_{yy}} \quad , \tag{3.3}$$

where the natural frequency ω is in Hertz. The analytical formula for the corresponding mode shapes is given as

$$X_n(x) = \sin \frac{(2n-1)\pi x}{2L} \quad . \tag{3.4}$$

[22, p. 493]

The results of the five lowest natural torsional frequencies and mode shapes for the uniform cantilever beam calculated without shear deformation, rotary inertia,

coupling and added mass terms are presented in Table 3.2 and Figures A.3 and A.4 in comparison to the analytical results. The results are obtained with property values of $G = 1$, $J = 1$, $L = 1$, $I_{yy} = 1$ and $\rho = 1$. Again, both the natural frequency values and mode shapes are matching perfectly with each other.

Table 3.2: The comparison of analytical and calculated natural frequencies in torsion for uniform cantilever beams without shear deformation, rotary inertia, coupling and added mass terms.

n	analytical ω_n	calculated ω_n	relative difference [%]
1	0.25	0.25	0.0
2	0.75	0.75	0.0
3	1.25	1.25	0.0
4	1.75	1.75	0.0
5	2.25	2.25	0.0

The analytical formula for the first natural frequency of a linearly tapered cantilever beam in bending vibration is approximated as

$$\omega_1 = \frac{C_1}{L^2}\sqrt{\frac{EI_{xx,root}}{\rho A_{root}}} \quad , \tag{3.5}$$

where the parameters $I_{xx,root}$ and A_{root} are the cross-section values at the root. The formula is based on the analytical formula presented in the equation (3.1) but is modified with the correction factor C_1, which takes the linear truncation into account. The truncation is assumed to be so that the width tapers and the height does not. The correction factor for a solid rectangular cross-section is defined as

$$C_1 = 1.14 - 1.95\xi + 3.35\xi^2 - 3.08\xi^3 + 1.10\xi^4 \quad , \tag{3.6}$$

where ξ is a taper ratio defined as

$$\xi = \frac{c_{tip}}{c_{root}} \quad , \tag{3.7}$$

where c_{tip} and c_{root} are the width of the beam at the tip and at the root, respectively. [20]

The results of the first natural frequency for the linearly tapered cantilever beams calculated without shear deformation, rotary inertia, coupling and added mass terms are presented in Table 3.3 and Figures A.5, A.6, A.7, A.8 and A.9 in comparison to the analytical results. The results are obtained with property values of $A_{root} = 1$, $E = 1$, $L = 1$, $I_{xx,root} = 1$ and $\rho = 1$. Five different beam designs are investigated with taper ratios of 0, 0.2, 0.4, 0.6 and 0.8. Again, the natural frequency values of both beam designs are matching perfectly with each other.

Table 3.3: The comparison of analytical and calculated natural frequencies in bending for linearly tapered cantilever beams without shear deformation, rotary inertia, coupling and added mass terms.

span-wise variation	c_{root}	c_{tip}	analytical ω_n	calculated ω_n	relative difference [%]
linear	1	0	1.14	1.14	0.0
linear	1	0.2	0.86	0.86	0.0
linear	1	0.4	0.73	0.73	0.0
linear	1	0.6	0.65	0.65	0.0
linear	1	0.8	0.6	0.6	0.0

The natural frequencies of the cantilever beam with NACA0012 cross-section are numerically solved in the article [25]. In the article, the governing equations are based on Euler-Bernoulli beam theory and the coupling is disregarded. The added mass of the cross-section is solved numerically. The results of the four lowest bending frequencies in a vacuum and water are compared in Table 3.4. The bending frequencies are calculated with both uncoupled and coupled equations taking into account shear deformation and rotary inertia terms. Figure 3.1 shows the calculated results of the beam in air with coupled EOM. The six lowest natural frequencies and modes shapes are shown in six separate graphs. The graphs show the bending shape with a dotted line and the torsion shape with a dashed line. The rest of the calculated results are shown in Figures A.10, A.11, A.12 and A.13. The material properties and cantilever dimensions are taken from the article [25] but the cross-section properties are calculated with the approximative formulas presented in Section 2.3. The deviation between numerical and calculated results is less than 2 per cent. In case of uncoupled results in vacuum, the relative difference decreases when the frequency increases. In water, however, the difference increases when the frequency increases. The current method slightly overestimates the frequency in a vacuum and underestimates in water. In case of coupled results in water, the difference increases when the frequency increases and the frequencies are slightly underestimated.

Table 3.4: The comparison of numerical and calculated natural frequencies in bending for a uniform NACA0012 cross-section beam.

	La Mantia (2013) ω_n	calculated ω_n (uncoupled)	relative difference [%]	calculated ω_n (coupled)	relative difference [%]
Mode 1					
in vacuum [Hz]	22.2	22.5	1.3	22.5	1.3
in water [Hz]	10.5	10.5	-0.2	10.5	-0.5
C_{am}	3.46	3.59	3.9	3.62	4.7
Mode 2					
in vacuum [Hz]	139.2	140.5	0.9	140.2	0.7
in water [Hz]	65.9	65.8	-0.2	65.7	-0.3
C_{am}	3.46	3.56	2.8	3.55	2.7
Mode 3					
in vacuum [Hz]	389.8	392.6	0.7	391.0	0.3
in water [Hz]	184.6	184.0	-0.3	183.3	-0.7
C_{am}	3.46	3.55	2.7	3.55	2.6
Mode 4					
in vacuum [Hz]	763.8	767.1	0.4	760.0	-0.5
in water [Hz]	361.8	359.6	-0.6	356.4	-1.5
C_{am}	3.46	3.55	2.7	3.55	2.6

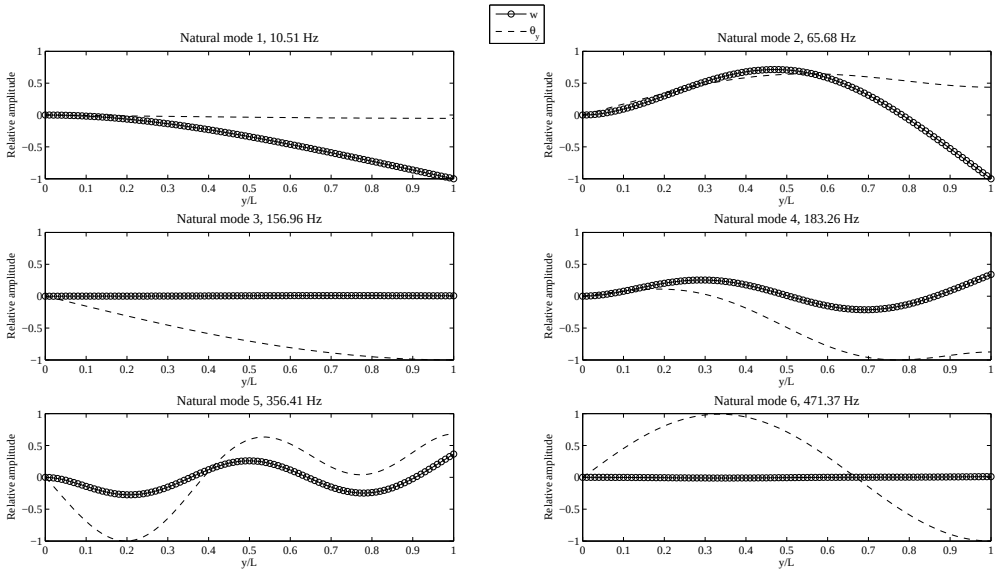

Figure 3.1: Verification against numerical results: NACA0012 cantilever in water with the coupling term

In summary, the calculation method gives exact results for uniform and linearly tapered cantilever beams when compared to simplified analytical solutions. In addition, the calculated results are very close to the numerical results of [25]. The natural bending frequencies of the NACA0012 cross-section beam with and without added mass are deviating less than 2 per cent.

3.1.2 Validation of the NACA 4-digit cross-section beam results

In this section, the partly experimental results are used to validate the applicability of the simplified approach to the prediction of the lowest natural frequencies and mode shapes of the NACA 4-digit cross-section beams. In addition, the added mass effect is compared between the current approach and the literature.

The results are validated with three experimental studies made for symmetric NACA 4-digit cross-section cantilevers and one experimental study made for NACA16-022 cross-section cantilever. All of the experiments were measured in both air and still water conditions. The latter study has more extensive experiments than in the other three studies and thus it is used for validation, although NACA 4-digit series cross-section was not used. The four validation cases are described below. In the first validation case, the natural frequencies of a uniform NACA16-022 cross-section cantilever beam were measured experimentally in air and water by [9]. In addition, theoretical calculations were done with analytical formulas. In the second case, the three lowest natural frequencies of a uniform NACA0009 cross-section cantilever beam were measured numerically and experimentally in air and water by [40]. The numerical solution of the frequencies were executed in FEM sofware with a 3D model consisting of solid elements. In the third case, the three lowest natural frequencies of a uniform NACA0009 cross-section cantilever beam were measured

numerically and experimentally in air and water by [37]. The numerical solution of frequencies was executed in FEM sofware with a 3D model consisting of solid elements. The TE of the used cross-section is truncated whereas in Case 2 the TE is sharp according to the Donaldson shape. In the fourth validation case, the lowest natural bending frequencies of tapered NACA0009 cross-section cantilever beams were measured numerically and experimentally in air and water by [42]. The beam is linearly tapered so that the tip chord is half of the root chord. The measurements were conducted for beams made of steel, aluminium and two different composites. Thus, the validation case is divided into four sub-cases respective to the beam material. For the steel and aluminium beams, impact test were executed only in air and the values in water were obtained by estimating the added mass according to Blevins [11]. For the composite beams, impact test were conducted in both air and water. In addition, the natural frequencies and mode shapes of the two composite beams were calculated numerically in FEM sofware with a 3D model consisting of plate elements.

Table 3.5 presents the calculation parameters used in the four validation cases. The material properties and the length of the cantilever are taken from the articles but the cross-section properties are calculated with the approximative formulas presented in Section 2.3. Validation Case 1 is calculated without shear deformation and rotary inertia terms because the information given in the article is insufficient. The value of the cross-sectional area moment of inertia about the x-axis calculated with the approximative formulas is underestimated by two per cent in Validation Cases 4.1 and 4.2 and by five per cent in Cases 4.3 and 4.4. The polar moment of inertia about the y-axis is underestimated by six per cent in Validation Case 4. Validation Cases 4.3 and 4.4 are calculated with estimated Poisson's ratio values due to insufficient information. In addition, it should be noted that the cantilever is simplified as an isotropic solid although it is a composite.

Table 3.5: The calculation parameters used in the validation cases.

Calculation parameters	Case 1	Case 2	Case 3	Case 4.1	Case 4.2	Case 4.3	Case 4.4
material	73 % lead, 27 % tin	aluminium	aluminium	steel	aluminium	composite CFRP00	composite CFRP30
cross-section design	solid with steel spar	solid	solid	solid	solid	layered	layered
L	0.381	0.15	0.15	0.3	0.3	0.3	0.3
c_{root} [m] & c_{tip} [m]	0.152 & 0.152	0.1 & 0.1	0.1 & 0.1	0.12 & 0.06	0.12 & 0.06	0.12 & 0.06	0.12 & 0.06
α	2.5	1.5	1.5	2.5 & 5.0	2.5 & 5.0	2.5 & 5.0	2.5 & 5.0
t_{max}		0.01	0.01	0.0108	0.0108	0.0108	0.0108
mass per length [kg/m]	17.5						
e_x [per cent of c/2]	0.0133						
radius of gyration [per cent of c/2]	0.00586						
ρ [kg/m^3]		2700	2700	7900	2700	1600	1600
EI_{xx}	163.3						
E [Pa]		6.90E+10	6.90E+10	1.93E+11	7.10E+10	6.50E+10	2.60E+10
GJ	55.1						
G [Pa]		2.59E+10	2.59E+10	7.42E+10	2.66E+10	2.50E+10	1.00E+10
ν		0.334	0.334	0.3	0.334	0.3 (guessed)	0.3 (guessed)

The experimental and numerical results of the validation cases are presented in Tables 3.6 and 3.7. The lowest natural frequencies of bending and torsion are given in Hertz. The effect of added mass is studied with the added mass coefficient C_{am}. The coefficient is defined as

$$C_{am} = \left(\frac{\omega_{air,n}}{\omega_{water,n}} \right)^2 - 1 \quad , \tag{3.8}$$

where $\omega_{air,n}$ and $\omega_{water,n}$ are the corresponding natural frequencies of nth mode in air and water, respectively [37, p. 175]. The definition comes from the approximative relation between the natural frequency and the mass in the most simplified EOM in bending [7, p. 46–47]. The experimental and numerical values are compared in Table 3.8 The relative difference is calculated with respect to experimental values and given in per cent. A negative relative difference means that numerical results are smaller than experimental.

Table 3.6: The experimental results of the validation cases in air and water. The lowest bending and torsion frequencies are given in Hertz. The added mass coefficient C_{am} is defined in Equation (3.8).

Experimental results	Case 1	Case 2	Case 3	Case 4.1	Case 4.2	Case 4.3	Case 4.4
ω in bending in air [Hz]	11.0	288.2	270.2	100	100	112	72
ω in torsion in air [Hz]	33.0	1027.6	1018.6	-	-	-	-
ω in bending in water [Hz]	8.4	123.8	130.2	62	42	41	26
ω in torsion in water [Hz]	27.0	621.3	614.8	-	-	-	-
C_{am} in bending	0.71	4.42	3.31	1.60	4.67	6.46	6.67
C_{am} in torsion	0.49	1.74	1.74	-	-	-	-

Table 3.7: The numerical results of the validation cases in air and water. The lowest bending and torsion frequencies are given in Hertz. The added mass coefficient C_{am} is defined in Equation (3.8).

Numerical results	Case 1	Case 2	Case 3	Case 4.1	Case 4.2	Case 4.3	Case 4.4
ω in bending in air [Hz]	10.78	283	274.9	-	-	104	76
ω in torsion in air [Hz]	31.83	1044	1024.0	-	-	415	304
ω in bending in water [Hz]	8.19	132	125.3	-	-	-	-
ω in torsion in water [Hz]	24.12	637	630.0	-	-	-	-
C_{am} in bending	0.73	3.60	3.81	-	-	-	-
C_{am} in torsion	0.74	1.69	1.64	-	-	-	-

Table 3.8: The relative differences of experimental and numerical natural frequencies of the validation cases in air and water. The relative difference is calculated with respect to experimental results shown in Table 3.6 and is given in per cent. A negative relative difference means that numerical results are smaller than experimental.

Relative difference [%]	Case 1	Case 2	Case 3	Case 4.1	Case 4.2	Case 4.3	Case 4.4
ω in bending in air [Hz]	-2.0	-1.8	1.7	-	-	-7.1	5.6
ω in torsion in air [Hz]	-3.5	1.6	0.5	-	-	-	-
ω in bending in water [Hz]	-2.5	6.6	-3.8	-	-	-	-
ω in torsion in water [Hz]	-10.7	2.5	2.5	-	-	-	-
C_{am} in bending	2.5	-18.6	15.3	-	-	-	-
C_{am} in torsion	50.1	-2.8	-5.9	-	-	-	-

The numerical results obtained with finite element software in Validation Cases 2, 3 and 4 match the experimental results with good accuracy. In general, the difference between the results stay below seven per cent. The finite element calculations with a solid 3D model used in Cases 2 and 3 show good correspondence to the experiments in air, deviating less than two per cent. Greater deviance can be seen in frequencies in water, but mostly in the bending in water. The lowest bending frequency in water is overestimated in case of a sharp TE and underestimated in case of a truncated TE. The finite element calculations with a plate element model used in Cases 4.3 and 4.4 show greater difference to the experiments than with the solid element model. However, the beam in Cases 4.3 and 4.4 is composite and its modelling layer by layer may lead to extra deviations when compared to experiments. Numerical results match well with the experiments except in case of the lowest torsion frequency in water, which deviates 11 per cent. In summary, the results calculated with 3D models are deviating 7 per cent at maximum. This must be noted when comparing the experiments to the results calculated in this work.

The natural frequencies calculated with the current approach are presented in Table 3.9. The lowest natural frequencies of bending and torsion are given in Hertz. The calculated values are compared to both experimental and numerical values with the relative difference, which is calculated in respect to experimental or numerical values and given in per cent. The calculated values are compared to experimental values in Table 3.10 and to numerical values in Table 3.11. The relative difference is calculated with respect to experimental values or to numerical values and is given in per cent. A negative relative difference means that calculated results are smaller than experimental or numerical results.

Table 3.9: The natural frequencies of the validation cases in air and water calculated by the current approach. The lowest bending and torsion frequencies are given in Hertz. The added mass coefficient C_{am} is defined in Equation (3.8).

Calculated results	Case 1	Case 2	Case 3	Case 4.1	Case 4.2	Case 4.3	Case 4.4
ω in bending in air [Hz]	11.8	296.5	296.5	103.7	107.4	133.2	84.2
ω in torsion in air [Hz]	36.8	1023.6	1023.6	739.5	756.3	950.4	352.6
ω in bending in water [Hz]	8.3	129.5	129.5	64.1	44.9	44.6	28.2
ω in torsion in water [Hz]	15.2	486.6	486.6	487.2	345.2	349.5	118.2
C_{am} in bending	1.05	4.24	4.24	1.62	4.72	7.92	7.92
C_{am} in torsion	4.86	3.43	3.43	1.30	3.80	6.39	7.90

Table 3.10: The natural frequencies calculated by the current approach are compared to experimental natural frequencies shown in Table 3.6. The relative difference is calculated with respect to experimental results and is given in per cent. A negative relative difference means that calculated results are smaller than experimental.

Relative difference [%]	Case 1	Case 2	Case 3	Case 4.1	Case 4.2	Case 4.3	Case 4.4
ω in bending in air [Hz]	7.3	2.9	9.7	3.7	7.4	18.9	16.9
ω in torsion in air [Hz]	11.5	-0.4	0.5	-	-	-	-
ω in bending in water [Hz]	-1.8	4.6	-0.5	3.4	6.9	8.8	8.5
ω in torsion in water [Hz]	-43.7	-21.7	-20.9	-	-	-	-
C_{am} in bending	46.3	-4.1	28.2	1.0	1.1	22.6	18.7
C_{am} in torsion	884.5	97.4	96.3	-	-	-	-

Table 3.11: The natural frequencies calculated by the current approach are compared to numerical natural frequencies shown in Table 3.7. The relative difference is calculated with respect to numerical results and is given in per cent. A negative relative difference means that calculated results are smaller than numerical.

Relative difference [%]	Case 1	Case 2	Case 3	Case 4.1	Case 4.2	Case 4.3	Case 4.4
ω in bending in air [Hz]	9.5	4.8	7.8	-	-	28.1	10.8
ω in torsion in air [Hz]	15.6	-2.0	0.0	-	-	129.0	16.0
ω in bending in water [Hz]	0.7	-1.9	3.4	-	-	-	-
ω in torsion in water [Hz]	-37.0	-23.6	-22.8	-	-	-	-
C_{am} in bending	42.8	17.9	11.2	-	-	-	-
C_{am} in torsion	555.6	103.1	108.6	-	-	-	-

First, the calculated results are compared to the experimental results. The calculated bending frequencies in both air and water are deviating less than ten per cent when Validation Cases 4.3 and 4.4 are not considered. The calculated torsion frequencies in water are deviating more than 20 per cent but matching well in air. The torsion frequencies in water are small compared to experimental values. Thus, the added mass effect is highly overestimated in torsion.

When the torsion in water is not considered, the results are deviating less than five per cent in Cases 2 and 4.1. The NACA0009 cross-section was used in these cases. The deviation in bending frequencies and added mass coefficient are greater in Case 3 than in Case 2. Thus, the truncated TE in Case 3 seems to have a greater effect on the bending behaviour than the torsion. It must be noted that the truncated TE was not taken into account in the calculation model. The results of Validation Case 1 are deviating more than in Cases 2, 3, 4.1 and 4.2 but the calculated results are still matching reasonably well. The added mass coefficient deviates highly in both in air and water and thus the flat plate simplification is not working for this cross-section profile. It must also be noted that the tested beam was constructed by cementing segments to steel spars and segments were ballasted to produce desired characteristics. The segments were made of lead and tin. This might be the reason for such large differences in bending and torsion behaviour due to neglected chord-wise response.

Although the beam cross-section is the same as in Cases 4.1 and 4.2, the bending frequencies in air deviate almost 20 per cent. The difference between beams is the used material, which is composite in these cases compared to steel and aluminium in Cases 4.1 and 4.2. The simplified approach is not able to represent a composite consisting of different layers and varying material properties. The added mass coefficient also deviates by 20 per cent compared to four per cent in Case 2. It seems that the flat plate simplification overestimates the added mass effect in bending more when the density ratio decreases.

Second, the calculated results are compared to the numerical results. The focus is to compare the 3D finite element calculations to the used beam approach. In Validation Cases 2 and 3, the bending frequencies in air and water and the torsion frequencies in air are matching well. The 3D finite element model seems to provide no significant advantages over the beam approach when comparing the lowest natural frequencies of solid cross-section fins made of isotropic materials. When comparing the results of solid or hollow fins made of composite material, the benefits of more accurate 3D modelling are significant. Liang et al. compared numerical results to experimental results which gave the error of five per cent in air and ten per cent in water in case of submerged cantilever plate natural frequencies [26, p. 1241]. Therefore, the simplified approach used is accurate enough to approximate the lowest natural frequencies and faster in comparison to more thorough 3D modelling.

In summary, the trend is that the calculated natural frequencies are overestimated in bending and torsion in air but underestimated in water. The added mass effect seems to be overestimated in both bending and torsion as predicted in Section 2.1.3. Validation Case 2 showed exception by slightly underestimating the added mass effect in bending. In case of fins, the low values of natural frequencies are considered worse than the high values. Thus, the underestimation of values is considered conservative from the designing point of view. The lowest bending frequency seems to be much lower than the lowest torsion frequency and thus the better accuracy in the bending frequency calculation is more important. Taking into account the good accuracy in bending frequencies and the underestimation of frequencies in water, the current approach is applicable to estimate the lowest natural frequencies

of fins similar to NACA 4-digit series in still water.

3.2 The significance of terms

In this section, the relative significance of shear deformation, rotary inertia, coupling and added mass terms is studied. The goal is to point out the parameter ranges in which the terms have a significant effect. This is studied for four cases. The first case studies the shear deformation term, the second the rotary inertia term, the third the coupling term and the fourth the added mass term. The relative significance is studied by comparing the five lowest natural frequencies calculated with and without a term studied at a time. The frequencies are compared with the relative difference with respect to results without a term studied. The results used as a reference value are calculated with the EOM without shear deformation, rotary inertia, coupling and added mass terms. The cross-sectional properties are calculated with the approximative formulas given in Section 2.3. The cross-section used is NACA0012 except in Cases 1 and 2, in which the thickness relative is varying. The beam is uniform and made of steel except in Case 4, in which the density ratio is varying.

In Cases 1 and 2, the significance of shear deformation and rotary inertia terms are studied by varying the dimensions of the beam. In case of NACA 4-digit series, the thickness is defined in per cent of the chord length c and thus the ratio $\frac{\alpha}{t}$ can be used to describe the ratio between the length and thickness as mentioned in Section 2.1.2. The cases can be studied by varying the slenderness ratio α and the ratio $\frac{\alpha}{t}$. The values of α are chosen so that one value is clearly over the slenderness limit, one at the limit and one clearly below the limit. The values for α are 50, 10 and 2. The values for $\frac{\alpha}{t}$ are 1, 0.5 and 0.1 and are chosen to describe very thick, thick and thin foil sections, respectively.

In Case 3, the significance of the coupling term is studied by varying the slenderness ratio and the distance between the SC and COG e_x. The value of e_x is defined in per cent of the chord length, as with the thickness value. The same α values of 50, 10 and 2 are used. The values of e_x are 0.01, 0.05 and 0.25 and are chosen to describe an almost double symmetric foil section, a generally average NACA 4-digit section and a very LE weighted foil section.

In Case 4, the significance of the added mass term is studied by varying the slenderness ratio α and the density ratio μ. The same α values of 50, 10 and 2 are used. The density ratio μ is the ratio between the density of the beam and the fluid. The values of μ are 7.8, 2.7 and 1.0. The first and second values are chosen to describe a solid beam made of steel and aluminium, respectively. The third value is describing a lightweight beam made of composites.

The case results are presented in graphs in Appendix C. In the graphs, the number in the legend indicates the type of the mode shape. The bending mode is indicated with number 1, torsion with number 2 and mixed mode with number 3. The type is defined as bending or torsion if the maximum relative amplitude of the respective mode shape is more than five times larger than another. Otherwise, the type is defined as a combination. Hyphens separate the results with and without

term studied, respectively. Commas separate the modes 1st, 2nd, 3rd, 4th and 5th, respectively. The relative differences are summarized in Table 3.12, in which the relative differences in first bending and torsion modes are shown in per cent separately for the four cases.

Table 3.12 shows that the shear deformation and rotary inertia affect only the bending frequencies, which can be seen already from the EOM. The results show that the shear deformation has an effect of about three times more on the bending frequencies than on the rotary inertia. This is in accordance with the assumption related the ratio γ^2 in Section 2.1.2. Both of the ratios affect the significance of the terms. However, the slenderness ratio can be the considered the more important factor due to the fact that the length and the chord varies more than the thickness in the fin designs. Figures C.1 and C.2 show that the terms are more significant for higher bending frequencies. In the graph showing the relative differences in Case 1 with parameters $\alpha = 1$ and $\frac{\alpha}{t}$, the shear deformation seems to affect the higher torsion frequencies. The difference, however, results from the changed cross-sectional properties which increased the torsion frequencies so that the fourth mode is changed from torsion to bending and the fifth mode from the third torsional mode to second. A similar change in mode type can be seen in the graph of case 2 with parameters $\alpha = 1$ and $\frac{\alpha}{t}$. Based on the study, the shear deformation term affects the results if the fin is slender. Even if only the first bending frequency is of interest, the shear deformation can be neglected if the fin section is thin. The rotary inertia term can be neglected only if the first bending frequency is of interest.

In Case 3, Table 3.12 shows that the coupling has more effect on the first torsion frequency than on the first bending frequency. Figure C.3 show that the coupling term changes many of the higher bending modes to mixed modes, even in case of slender beams. Although the frequencies deviate more when α decreases and e_x increases, the coupling term seems to have a greater effect on the mode shapes than on the frequencies due to the mixing of bending and torsion modes. Based on the study, the coupling term can be neglected if the fin is slender, the cross-section is almost double symmetric and only the lowest frequency is of interest. However, the term has significant effect in case of short and wide fins with a very LE weighted section.

Figure C.4 shows that the added mass term has greater effect on the torsion frequencies than on the bending frequencies. This follows from the fact that the terms are different for torsion and bending in the EOM. Table 3.12 shows that the added mass is always a significant term in this study. The density of water is large enough even when compared to the steel, so that the added mass cannot be neglected. The significance increases when the density ratio decreases. This is in line with the assumption in Section 2.1.3. Based on the study and previous assumptions, the added mass term needs to be taken into account regardless of the fin design. In addition, the term decreases the natural frequencies, which is considered worse trend. This study considers only solid fin designs but the added mass effect is even greater in case of lightweight fin designs that decrease the natural frequencies even more.

In summary, if only the lowest natural frequency is of interest, the shear defor-

mation, rotary inertia and coupling terms can be neglected in case of slender fins. However, in case of short and wide fins with asymmetric cross-sections, the terms should be taken into account. The added mass must always be taken into account if the fin is submerged in water.

Table 3.12: The summary of term significance study. The relative difference in first bending and torsion modes is shown in per cent separately for the shear deformation, rotary inertia, coupling and added mass cases.

Case 1: shear deformation term

Relative difference [%] in first bending mode

α \ α/t	1	0.5	0.1
50	0	0	0
10	0	0	0
2	10	2.5	0

Relative difference [%] in first torsion mode

α \ α/t	1	0.5	0.1
50	-	-	-
10	0	0	0
2	0	0	0

Case 2: rotary inertia term

Relative difference [%] in first bending mode

α \ α/t	1	0.5	0.1
50	0	0	0
10	0	0	0
2	3	1	0

Relative difference [%] in first torsion mode

α \ α/t	1	0.5	0.1
50	-	-	-
10	0	0	0
2	0	0	0

Case 3: coupling term

Relative difference [%] in first bending mode

α \ e_x	0.01	0.05	0.25
50	0	0	0
10	0	0	0
2	0	0	2.5

Relative difference [%] in first torsion mode

α \ e_x	0.01	0.05	0.25
50	-	-	-
10	0	2	8
2	0	2	35

Case 4: added mass term

Relative difference [%] in first bending mode

α \ μ	7.8	2.7	1
50	32	52	69
10	32	52	69
2	32	52	69

Relative difference [%] in first torsion mode

α \ μ	7.8	2.7	1
50	-	-	-
10	46	63	78
2	46	63	78

3.3 Calculation parameter dependencies

In this section, the effect of the calculation parameters on the natural frequencies and mode shapes are studied. The goal is to find trends which can be taken into account in design graph production and in the fin design process itself.

The parameters can be divided into material and geometric properties. The material properties are E, ν, G, ρ and ρ_w. The fluid density is taken as constant although the water density varies a bit across the globe. The other properties are dependent on the fin material and thus the fin material can be the only material-

related parameter used in the parameter study. Three different materials are used and presented with the material property values in Table 3.13. Steel is a good guess for the material in the marine field as it is commonly used. Steel is a relatively heavy material and thus lighter materials are chosen for comparison. Aluminium is also commonly used in the marine field and is almost three times lighter than steel. One material representing composites is used to include a more lightweight design into the study. Since the fin cross-sectional design is limited to only a solid cross-section made of one material, the results cannot be taken as an accurate representation of composite fins, but rather only to evaluate trends. This can be concluded from the results presented in Section 3.1.2.

Table 3.13: The material properties used in the parameter dependency study.

Material	Name	E [GPa]	**ρ** [kg/m^3]	**ν**	G [GPa]	E/**ρ** [Pa*kg/m^3]	G/**ρ** [Pa*kg/m^3]
1	Steel	200	7800	0.3	77	2.56E+07	9.86E+06
2	Aluminium	69	2700	0.334	26	2.56E+07	9.58E+06
3	Composite	26	1000	0.3	10	2.60E+07	1.00E+07

The geometric properties can be divided into cross-sectional and span-wise properties. The cross-sectional properties are A, c, e_x, I_{xx}, I_{yy} and J. In case of NACA 4-digit sections, these properties can be defined by approximative formulas presented in Section 2.3. Therefore, all cross-sectional properties can be defined with the chord length c, the maximum thickness as a fraction of chord t, the maximum camber as a fraction of chord m and the location of the maximum camber as a fraction of a chord from LE p. The amount of parameters decreased from six to four but moreover now the parameters used can be related easily to the actual cross-section design. The span-wise properties are length L and beam cross-sectional variation along the span. The variation of a cross-section is simplified to consist only of the variation of chord length c. This means that the shape remains constant but the size is scaled by a varying chord. The three span-wise variations chosen are uniform, linearly tapered and polynomially tapered. Table 3.14 shows the variation type and taper ratio. The taper ratio ξ is the ratio of chord length at the tip to the chord length at the root. Five different taper ratios are chosen for the linearly tapered beam and one for the polynomially tapered. The polynomially tapered beam tapers by the second order polynomial as $c(y) = \left(1 - 0.8\frac{y^2}{L^2}\right) c_{root}$. A uniform beam is basically the extreme of a linearly tapered beam with taper ratio value of 1.

Table 3.14: The span-wise variations used in the parameter dependency study.

Span-wise variation	chord length	taper ratio
1	uniform	1
2	linearly tapered	0.8
3	linearly tapered	0.6
4	linearly tapered	0.4
5	linearly tapered	0.2
6	linearly tapered	0
7	polynomially tapered	0.2

The number of parameters is seven, consisting of four cross-sectional parameters, two span-wise parameters and one material parameter. The effect of parameters is studied by varying one parameter at a time. The effect of one parameter is studied also by varying other parameters to study if the effect changes, increases or decreases. Therefore, each parameter is studied in ten different as cases listed in Table 3.15. Three parameters are chosen to vary in these cases. The parameters m and p are chosen to study if the effects are different in asymmetric fins in comparison to symmetric fins. The combination of $m = 0$ and $p = 0$ indicates a symmetric section. The other two combinations of $m = 0.05$, $m = 0.09$ and $p = 0.4$ are chosen to represent asymmetric sections. The parameter c is chosen to study how slenderness affects the parameter effects. The chord lengths of 1 and 0.2 meters are represent slender and non-slender beams, respectively. Other parameters are constant in these cases. The length is two meters, the thickness 0.12 of the chord length, the beam is uniform and the material is steel. The cases from 1 to 6 are calculated with coupled EOM and the cases from 7 to 10 with uncoupled EOM. The uncoupled cases are used to study the parameter dependencies separately in bending and torsion because the coupling may mix the dependencies. Otherwise, the EOM include all other terms: shear deformation, rotary inertia and added mass.

Table 3.15: The ten cases of parameter dependency study.

Case	c [m]	m	p	equations of motion
1	1	0	0	coupled
2	0.2	0	0	coupled
3	1	0.05	0.4	coupled
4	0.2	0.05	0.4	coupled
5	1	0.09	0.4	coupled
6	0.2	0.09	0.4	coupled
7	1	0	0	uncoupled
8	0.2	0	0	uncoupled
9	1	0.05	0.4	uncoupled
10	0.2	0.05	0.4	uncoupled

The parameter values are limited to vary inside case-relevant values. The parameter ranges are listed in Table 3.16. The length is somewhat dependent on the propeller diameter and thus the length range is chosen based on propeller sizes of

relevant ships. Relevant ships are commercial ships with one propeller, thus mainly bulk carriers, tankers and container ships. The propeller sizes for these ships are mainly ranging from one meter to seven meters but the biggest ones can be up to nine meters. The length of fin should be approximately the same as the propeller radius. Thus, the length range is chosen to be from 0.5 meters to 4.5 meters. The chord length is chosen to range from 0.1 meters to 2.5 meters. Hence, the aspect ratio of the fin is reasonable both with minimum length and chord length and maximum length and chord length. Reasonable thickness values for the NACA 4-digit series are considered to be from 0.06 to 0.30. The NACA 4-digit series is limiting values of m to a range of 0 to 0.09 and values of p to a range of 0 to 0.9. However, the range of p is chosen to be from 0.1 to 0.9 because it is reasonable only if $m = 0$.

Table 3.16: The parameter ranges used in the parameter dependency study.

Parameter varied	number of values	minimum value	maximum value	step size
L [m]	9	0.5	4.5	0.5
c [m]	9	0.1	2.5	0.3
t [per cent of c]	9	0.06	0.3	0.03
m	10	0	0.09	0.01
p	9	0.1	0.9	0.1
span-wise variation	7	1	7	1
material	3	1	3	1

The relation between the parameters and results are studied by analytical and numerical means. First, the dependency of each parameter is approximated analytically from the uncoupled EOM. Then, it can be seen whether the relations in bending and torsion EOM are the same or different. Second, the dependencies are evaluated from the calculation results of coupled EOM. Then, it can be seen how the coupled EOM are behaving in comparison to the uncoupled EOM and how the relations work in the combination modes. Finally, guidelines can be given for the designers on how the parameter selections or modifications affect the natural frequencies and modes.

The relation of parameters and natural frequencies are first estimated analytically from the uncoupled EOM without shear deformation, rotary inertia and added mass. These are later compared to the calculated relations. In bending, the effect of the parameters can be estimated from the formula [22, p. 590]

$$\omega = \sqrt{\frac{\frac{EI_{xx}}{L^3}}{\rho AL}} \quad , \tag{3.9}$$

which comes from the eigenvalue problem with the approximative formulas from Section 2.3. The estimated relations between the parameters and natural frequencies in bending are listed in Table 3.17. Similarly, the effects in torsion can be estimated

from the formula [22, p. 8]

$$\omega = \sqrt{\frac{\frac{GJ}{L}}{\rho I_{yy} L}} \quad , \tag{3.10}$$

which comes from the eigenvalue problem with the approximative formulas from Section 2.3. The estimated relations between the parameters and natural frequencies in torsion are listed in Table 3.18.

Table 3.17: The relation between the parameters and natural frequencies in bending estimated from Equation (3.9).

Parameter	Analytical dependency	Approx. dependency
L	$\omega \sim \sqrt{\frac{1}{L^4}}$	$\omega \sim \frac{1}{L^2}$
c	$\omega \sim \sqrt{\frac{c^3}{c}}$	$\omega \sim c$
t	$\omega \sim \sqrt{\frac{t^3+t}{t}}$	$\omega \sim t$
m	$\omega \sim \sqrt{m+2m^2}$	$\omega \sim m$
p	$\omega \sim \sqrt{p+(1+p)^2}$	$\omega \sim p$
material	$\omega \sim \sqrt{\frac{E}{\rho}}$	$\omega \sim \sqrt{\frac{E}{\rho}}$

Table 3.18: The relation between the parameters and natural frequencies in torsion estimated from Equation (3.10).

Parameter	Analytical dependency	Approx. dependency
L	$\omega \sim \sqrt{\frac{1}{L^2}}$	$\omega \sim \frac{1}{L}$
c	$\omega \sim \sqrt{\frac{c}{3c^3}}$	$\omega \sim \frac{1}{c}$
t	$\omega \sim \sqrt{\frac{t^3}{t^3+3t}}$	$\omega \sim 1$
m	$\omega \sim \sqrt{\frac{1}{1-m+3m^2}}$	$\omega \sim \frac{1}{m}$
p	$\omega \sim \sqrt{\frac{1}{2+p+2p^2}}$	$\omega \sim \frac{1}{p}$
material	$\omega \sim \sqrt{\frac{G}{\rho}}$	$\omega \sim \sqrt{\frac{G}{\rho}}$

The case results are presented in graphs in Appendix D. The results of Case 3 are shown in Figure 3.2 for an example. One graph shows one parameter varied. One figure includes all seven parameter graphs of the case. In the graphs, the five lowest natural frequencies are shown with different marker lines as defined in the legend. The numbers inside brackets indicate the type of the mode shape. The bending mode is indicated with the number 1, the torsion with number 2 and the mixed mode with number 3. The type is defined as bending or torsion if the maximum relative amplitude of the respective mode shape is more than five times larger than

another. Otherwise, the type is defined as a combination. The dependencies are summarized in Table 3.19. One remarkable observation is that the mode type of the lowest natural frequency is pure bending in most cases within the parameter ranges studied. Torsion and mixed mode types can be seen only with extreme parameter values.

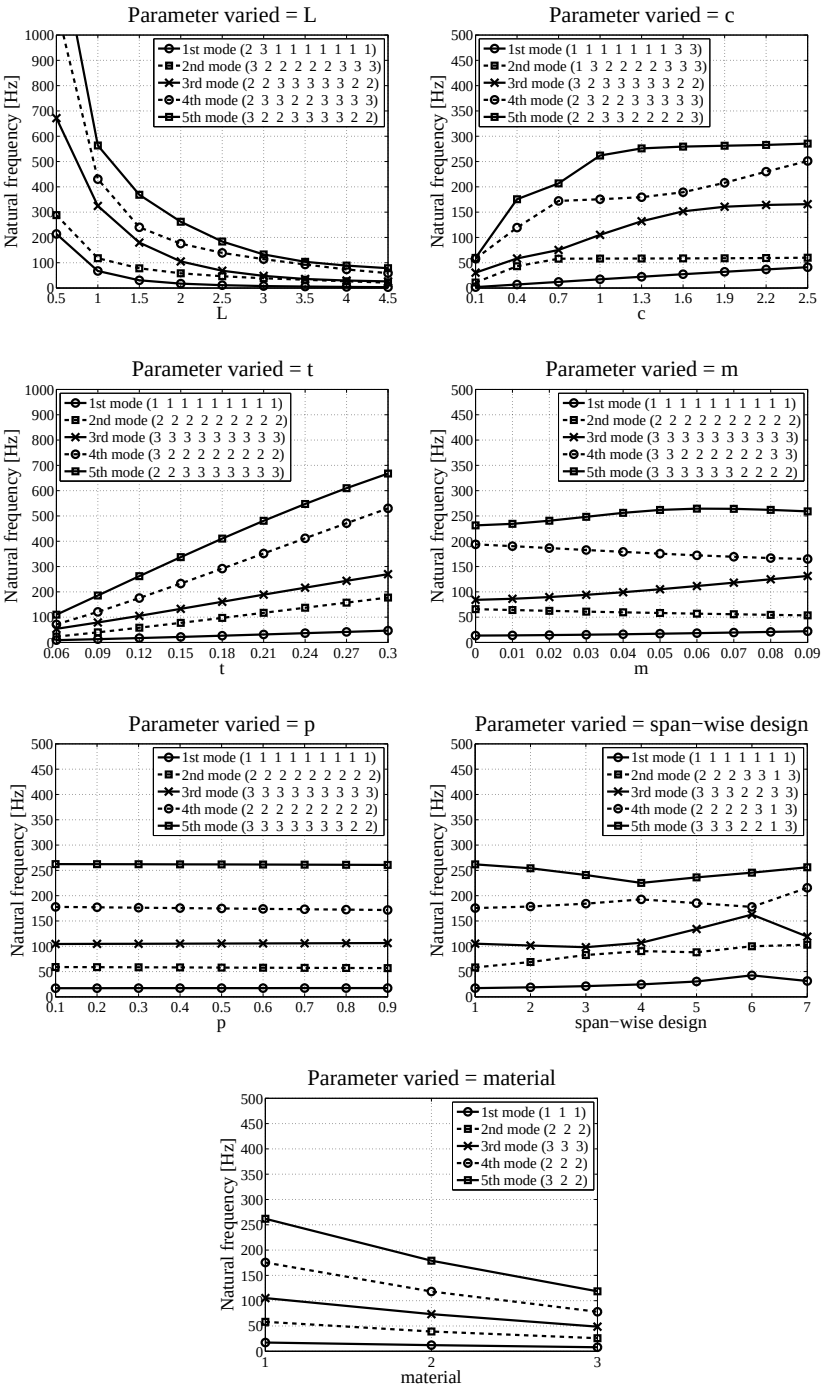

Figure 3.2: Case 3 with coupled EOM and parameters $L = 2$ m, $c = 1$ m, $m = 0.05$ and $p = 0.4$.

Table 3.19: The summary of the parameter dependency study.

parameter increased	effect on bending frequency	effect on torsion frequency
L	decreased exponentially	decreased exponentially
c	increased linearly	negligible
t	increased linearly	increased linearly
m	increased linearly	negligible
p	negligible	negligible
span-wise variation	effect on bending frequency	effect on torsion frequency
linearly tapered, taper ratio decreased	decreased	increased
from linearly to polynomially tapered, taper ratio 0.2	increased	increased
material	effect on bending frequency	effect on torsion frequency
E, G, ρ decreased	decreased	decreased

The natural frequency seems to have a second order (polynomial) dependency on the length, in other words $\sim \frac{1}{L^2}$. The dependency seems to be the same for both bending and torsion frequencies whereas, according to the analytical estimation, the dependency should be linear in torsion, in other words $\sim \frac{1}{L}$. In Case 6, the dependency seems to be steeper and even exponential. The effect is greater in case of higher frequencies than lower frequencies.

The natural frequency seems to have clearly different dependency on the chord length in the bending and torsion mode types. In bending, the dependency seems to be $\sim c$ as estimated analytically. In torsion, there seems to be no dependency at all, which is not in accordance with the analytical estimation of $\sim \frac{1}{c}$. The difference can be seen best in Case 10, which is calculated with uncoupled EOM. In the combination type, the bending dependency seems to dominate.

The natural frequency seems to have clearly linear dependency on the thickness, in other words $\sim t$. The same dependency was obtained analytically for the bending type. According to the analytical estimation, there should be no dependency in the torsion type. The dependency seems to be steeper on the higher modes than on the lowest modes. Comparing the 3rd and 4th mode in Case 6, it can be seen that the thickness may have greater effect on torsion than on bending.

The effect of camber cannot be checked from cases 1, 2, 7 and 8 because they have symmetric sections. Some effects can be seen, however, because the approximative formulas are not neglecting the combination of $m \neq 0$ and $p = 0$ which is basically an impossible design. The natural frequency seems to have clearly different dependency on the camber in the bending and torsion mode types. The dependency seems to be $\sim m$ in bending and $\sim \frac{1}{m}$ in the torsion case, which would be in accordance with the analytical estimations. The effect seems to be greater in bending than in torsion meaning that the frequencies increase more in bending than they decrease in torsion when camber is increased. Similarly, as for the chord length, the bending dependency seems to be dominant in combination cases.

The natural frequency seems to have minor dependency on the location of the maximum camber. The dependency seems to be $\sim p$ in bending and $\sim \frac{1}{p}$ in the torsion case, which would be in accordance with the analytical estimations. The

effect seems to be greater in torsion and in higher frequencies. The significance of the effect seems to only be a few per cent and thus can be neglected in the prediction of lowest natural frequencies.

The natural frequency seems to have varying dependency on the span-wise beam design. Studying the linearly tapered beam in the uncoupled cases, it can be concluded that the bending frequency decreases and the torsion frequency increases when the taper ratio decreases. Comparing span-wise variations 5 and 7, which are linearly and polynomially tapered with taper ratios of 0.2 respectively, it can be seen that both the bending and torsion frequencies are higher with a polynomially tapered beam.

The natural frequency seems to have clear dependency on the material. Both the bending and torsion frequencies decrease when the material properties decrease. This is in line with the analytical estimations.

3.4 Design graphs and procedures

In this section, the lowest natural frequency of different fin designs are presented in design graphs. The design graphs can be used to check the prediction for the lowest natural frequency with the main fin parameters. The main parameters are length, chord length, thickness, maximum camber, location of maximum camber, span-wise variation and material. The design graphs show the lowest natural frequency as a function of two variables, one on each axis. Thus, two parameters must be selected as variables inside the graph and other parameters must be varied between graphs.

The principle in utilization of design graphs is to identify which parameters are or can be varied most and which can be varied less or not at all for the fin project at hand. The most varying parameters are used as variables in design graphs and others as variables between graphs.

Usually, projects have fixed parameters because of different limitations and requirements. The length of the fin is usually selected based on the propeller diameter and thus can be defined as constant for the project. The construction costs, material costs, construction method, attachment method and ship material affect the selection of the fin material. The number of potential materials is also small, at least when composites are neglected. Thus, the material selection is usually quite limited and there can only be a few alternatives. The chord length, thickness, camber and location of maximum camber are more or less decided based on hydrodynamic calculations. These parameters mostly affect the efficiency of a fin and hence the improvement in propeller efficiency. The span-wise variation of the cross-section also affects the fin efficiency and it can basically be of arbitrary shape. In this level of calculation, the variation is, and in most cases can be, simplified to basic shapes which are represented by linear and polynomial shapes in this study. Thus, the span-wise variation is considered as the less varying parameter. Table 3.19 concluded that the natural frequency dependency on the location of the maximum camber is negligible and thus it can be neglected in this level of calculation. Therefore, the most varied parameters are chord length, thickness and camber. Among these, the two parameters varying the most should be chosen as the two variables used in the design

graphs. The other one that is varying less is then used as a variable between graphs. With this method, the amount of design graphs needed is minimized.

A fewer number of varying parameters results in a faster use of design graphs. By giving fixed values for some of the parameters, the needed design graphs can be limited to the graph group consisting only of the graphs with the needed varying parameters and correct constant parameters having fixed values. For example, if material, span-wise variation, length and chord are fixed to steel, uniform, one meter and three meters, then the graph group consist only of the graphs in which the fin has the listed parameter values and the varying parameters are thickness, camber and location of maximum camber. The two of these having the most freedom in selection are taken as the variables inside graphs and the one having fewer alternatives is taken as the variable between graphs.

As an example, one design graph group is presented in Figure 3.3 and the parameters used in Table 3.20. The calculations are executed with the EOM, including shear deformation, rotary inertia, coupling and added mass terms. The water density of 1000 kg/m^3 is used. The variables inside the graphs are chosen to be chord length and camber because they are the only parameters having different effects on bending and torsion frequencies according to Table 3.19. The location of the maximum camber is defined as constant with a value of 0.4. Steel is used as the fin material and length is chosen to be 2.7 meters. The span-wise variations of linearly and polynomially tapered chord length with taper ratio 0.2 are chosen to represent different fin designs. Three thickness values are checked. Chord length is chosen to vary between 1.2 and 2 meters with step size 0.1 meters. Camber can have values between 0.01 and 0.09. This leads to a design graph group of six graphs which consist of 81 chord and camber combinations. The lowest natural frequency value for the total of 486 different fin designs is shown in Figure 3.3. The parameter values used are shown above each of the graphs. Linear indicates option 1 in Table 3.20 and poly indicates option 2. S indicates steel. The first natural frequencies are shown in contours with a step size of five Hertz. The colorbar on the right side of each graph shows the contour levels of the frequency in Hertz.

More design graphs are shown in Appendix E, which shows a larger graph group. The larger group is used to describe the use of design graphs in situations having more freedom in parameter selection. The chord length and camber are used again as the variables inside graphs. The parameters used and their ranges are shown in Table 3.21. The location of maximum camber is defined again as constant with a value of 0.4. Three different materials were considered in the parameter dependency study in Section 3.3. Steel and aluminium are used in the design graphs. Composite materials are neglected because the results in Section 3.1.2 showed that the current approach used is not accurate for lightweight fins made of composites. The span-wise variations of uniform, linearly tapered with taper ratio 0.2 and polynomially tapered with taper ratio 0.2 are chosen to represent different fin designs. Three thickness and length values are checked. Chord length is chosen to vary between 0.5 and 1.5 meters with step size 0.1 meters. Camber can have values between 0.01 and 0.09. This leads to a design graph group of 54 graphs which consists of 81 chord and camber combinations. The lowest natural frequency value for the total of 4374

different fin designs is shown Appendix E. The calculations are executed with the EOM, including shear deformation, rotary inertia, coupling and added mass terms. The water density of 1000 kg/m^3 is used.

The graphs are divided into one page groups with four different ways to illustrate how the comparison of parameter values can be made easier depending on the project. The presentation alternative 1 shows nine graphs with all the length and thickness combinations on one page. The second presentation alternative shows six graphs with all span-wise variation and material combinations on one page. The third and fourth alternatives show nine graphs with all span-wise and length or thickness combinations on one page. The alternatives are shown in Figures E.1, E.2, E.3 and E.4, respectively. The second alternative is best when the length and thickness choices are narrowed to a few combinations, for example $L = 2.4$ m and $t = 0.08$ or $L = 2.6$ m and $t = 0.12$. The same principal works for the other alternatives as well. Figures E.5 - E.10 show the whole design group defined in Table 3.21 in 54 graphs and 6 figures in total. The length and thickness are varied between the 9 graphs in the same figure, meaning the first presentation alternative is used. The span-wise variation and material are varied between the 6 figures.

Table 3.20: The parameter values used in the example shown in Figure 3.3

Parameters varied inside graphs	number of values	minimum value	maximum value	step size
c [m]	9	1.2	2	0.1
m	9	0.01	0.09	0.01

Parameters varied between graphs	number of values	minimum value	maximum value	step size
t [per cent of chord]	3	0.12	0.14	0.01
span-wise variation	2	option 1: linearly tapered with taper ratio 0.2 option 2: polynomially tapered with taper ratio 0.2		

Constant parameters	value
material	steel
p	0.4
L [m]	2.7

Table 3.21: The parameter values used in the graph group shown in Appendix E.

Parameters varied inside graphs	number of values	minimum value	maximum value	step size
c [m]	9	0.8	1.6	0.1
m	10	0	0.09	0.01

Parameters varied between graphs	number of values	minimum value	maximum value	step size
L [m]	3	2.4	2.8	0.2
t [per cent of chord]	3	0.08	0.16	0.04
span-wise variation	3	option 1: uniform option 2: linearly tapered with taper ratio 0.2 option 3: polynomially tapered with taper ratio 0.2		
material	2	option 1: steel option 2: aluminium		

Constant parameters	value
p	0.4

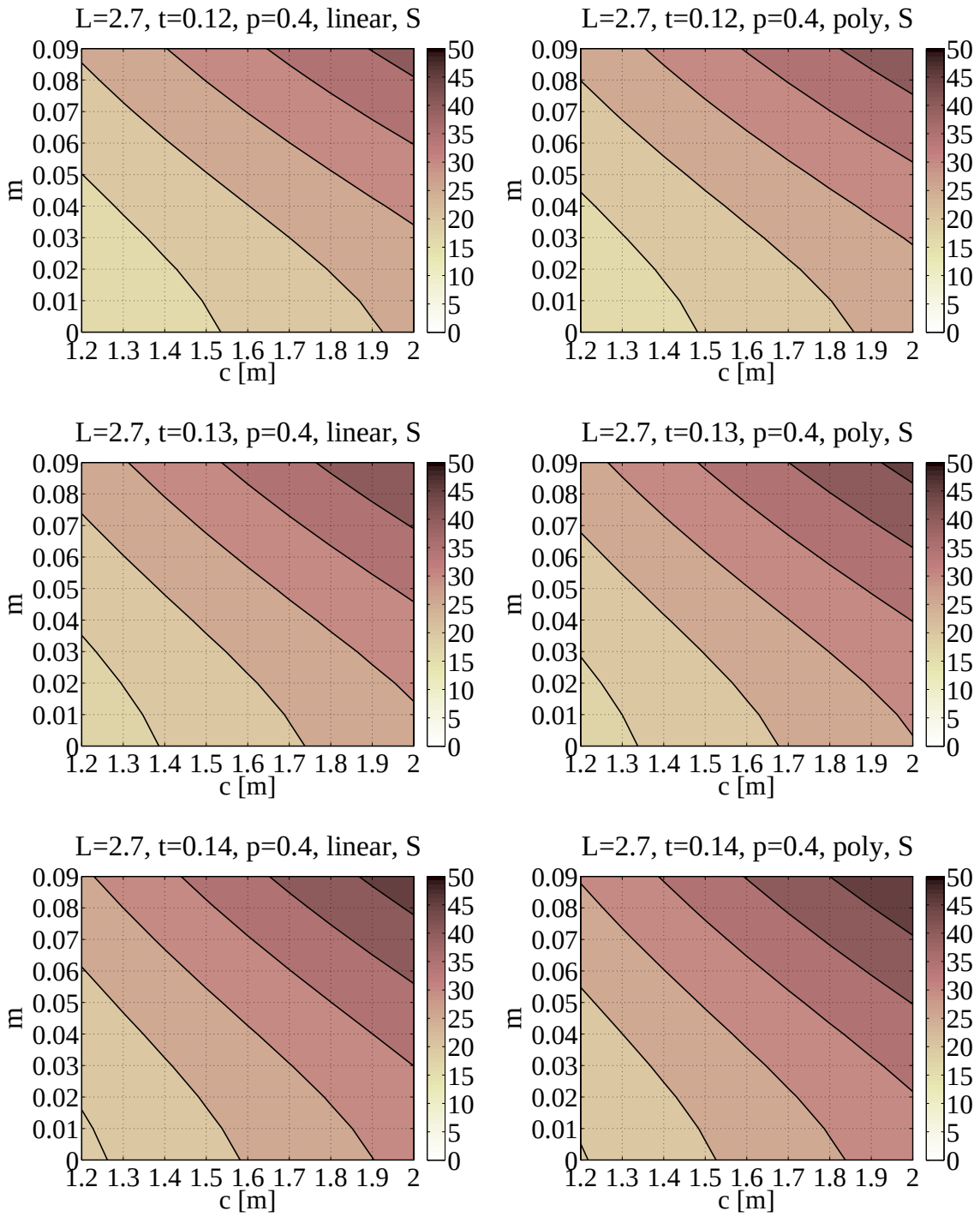

Figure 3.3: The example of one design graph group which shows 6 graphs in total. The thickness and span-wise variation are varied between the 6 graphs.

4 Conclusions

4.1 Summary of findings and their meaning

The aim of the thesis was to investigate if the simplified two DOFs beam approach is accurate enough to predict the lowest natural frequencies and mode shapes of stator fins in still water. The significance of shear deformation, rotary inertia, bending-torsion coupling and added mass with respect to the lowest natural frequencies were studied. The natural frequency dependency on the fin design parameters was investigated. The outcomes were used to generate design graphs to estimate and compare the lowest natural frequency of different stator fin designs.

The simplified beam approach seems to overestimate bending and torsion frequencies in air but underestimate in water. The lowest bending frequencies deviate less than ten per cent in both air and water. The lowest torsion frequencies deviate roughly 20 per cent in water but less than eight per cent in air. The added mass of the fin was estimated with a 2D flat plate model. The added mass effect of fins is overestimated in both bending and torsion as predicted, based on [18], [5] and [39]. The added mass effect is overestimated more in torsion than in bending. When considering Validation Case 1, with a cross-section not from NACA 4-digit series, the added mass effects are overestimated significantly more than in the other cases. One reason is that the cross-section of NACA16-022 is more elliptical than NACA 4-digit shapes, thus differing more from the flat plate. One reason for the extremely overestimated added mass effect in torsion might be that the torsion equations are not enough to describe the torsional motion. The greater difference of the torsion frequency in air supports this conclusion. In case of thicker and more elliptical NACA cross-sections, the added mass of the ellipse could provide a better approximation. This could be investigated in the future. However, since the added mass effect is overestimated, the natural frequencies in water are underestimated. In this case, the underestimation of natural frequencies is better than overestimation because lower frequency values are avoided. This means that the obtained frequency predictions are conservative with respect to design criteria. Therefore, the used approach works for the stator fins which have a cross-section shape close to NACA 4-digit shapes. However, designs might end up to be too safe or conservative because of the underestimation of torsion frequencies in water.

Based on the results of the validation case, term significance and parameter dependency studies presented in Appendices B, C and D, the lowest natural frequency seems to always be the bending mode or at least the bending-dominated mixed mode. The mode type of the second lowest frequency varies between the bending, torsion and mixed modes. Therefore, the natural frequencies in bending are important to predict accurately. Based on the validation cases, the current approach predicts bending frequencies accurately in both air and water.

The validation cases included only single symmetric NACA profiles and thus the natural frequencies of asymmetric fins are not compared to the experimental results.

This is a shortage for this study but the significance of asymmetricity is considered by using the calculated results. According to the parameter dependency study, the camber affects linearly to bending but negligibly to torsion frequencies. The location of the maximum camber affects negligibly to both frequencies. In this aspect, the asymmetricalness seems to only affect bending frequencies. The effect seems to be greater in non-slender fins and higher frequencies. Therefore, the used approach should also be applicable for asymmetric fins. The greatest differences might come from the fact that the flat plate is not accurate enough to estimate the added mass.

The approach overestimates the natural frequencies of composite fins in bending by almost 20 per cent, which is significantly more than in case of solid steel or aluminium fins. The results also deviate from those obtained with the quadrilateral shell element model. This means that the beam model taking into account only bending about the x-axis and torsion about the y-axis is not enough to describe the behaviour of composite fins. In contrast, when comparing the results to those obtained with the solid element model in case of solid aluminium fins, the deviations are less than eight per cent in air. This means that 3D modelling gives benefits only in case of advanced material which are homogeneous and isotropic or in case of hollow cross-sections with a stiffened shell and inside webs. The results might differ because warping in torsion can be significant factor in these hollow cross-sections [8] [33]. In this study, warping is neglected because the current approach assumes a solid cross-section. The cross-section of the fin is also assumed to rotate as a rigid body in torsional motion about the y-axis, which may cause error in case of hollow cross-sections.

In summary of the term significance study, the shear deformation, rotary inertia, coupling and added mass terms must be included in the simplified beam approach. The shear deformation, rotary inertia and coupling terms can be neglected in case of slender fins, which is in accordance with theory [19]. The added mass term must always be taken into account if a fin is submerged in water, regardless of the fin material. This is also in accordance with theory [10] [24].

In summary of the parameter dependency study, the length, chord-length, thickness, camber, span-wise variation and material affect the natural frequencies. The location of maximum camber seems to have negligible effect. The increase in the length of the fin exponentially decreases both bending and torsion frequencies. The increase in the chord length and camber increases bending frequencies linearly but has negligible effect on torsion frequencies. The increase in the thickness increases both bending and torsion frequencies linearly. The use of lighter material with smaller elastic and shear modulus decreases both frequencies. Considering linearly tapered fins, the decrease in taper ratio decreases bending frequencies but increases torsion frequencies. When using polynomially tapered fins instead of linearly tapered, both bending and torsion frequencies increase. These results can be used to understand whether the main parameters should be modified to obtain a desired change in the bending or torsion frequency of the stator fin. The dependencies are a good supplement for the presented design graph procedure proposed for the concept design phase.

The presented design graphs show the lowest natural frequency when the main

parameters are varied. The graphs can be used to compare natural frequencies with excitation frequencies and thus to evaluate resonance risk. The graphs can be modified to also show other frequencies. However, to evaluate hydroelastic instability risks, the mode shape must be given along with the natural frequency. Therefore, the graphs are not suitable for instability evaluations but natural frequencies and mode shapes must be solved for different fin designs separately. This is because natural frequencies and mode shapes are needed to solve the critical velocities of fin designs which are used to evaluate instability risk.

4.2 Future work

The current fin model assumes that the fin is attached to the ship hull rigidly. This assumption basically idealizes that the fin is welded perfectly to the rigid foundation. In reality, the ship hull deforms, which also might affect the behaviour of the fin. In addition, other attachment methods, such as bolting, might be used in fin installation to reduce installation costs and to enable a more optimum positioning of fins. Therefore, the effect of the attachment method should be studied for example by altering BC.

The linear small deflection theory is applied in this study, meaning the vibration amplitudes of the fin are considered small. Moreover, this means that either the resonance is not occurring or the excitation amplitudes are small. This assumption might cause error if the current approach is modified and used to calculate forced vibrations.

In this study, the cross-section shape of fins is constant along the span of fins but fins are allowed to taper, meaning the size of the cross-section can vary along the span. Fin designs with sweep and twist angles are not considered. However, in reality, to obtain the optimum design, stator fins most probably have small sweep and twist angles. In addition, ships usually have multiple stator fins as shown in Figure 1.1. In this work, the distance between fins is assumed to be great enough to neglect the effects of other fins. Therefore, the effect of sweep and twist angles and also the effect of other fins should be studied in the future.

The cross-section shape of the stator fin is optimized separately for every ship. The search of the optimum shape usually starts with parametric cross-section shapes like NACA series, which are used generally. Shapes can be modified by varying parameters but the chosen optimum shape is usually close to NACA profiles. Therefore, NACA series can be considered as a realistic shape to be used in concept design phase calculations. The approximative formulas to calculate the cross-sectional properties are developed for fins with solid NACA 4-digit shaped cross-sections. In case of other NACA section families being used, the formulas for the cross-sectional parameters must be modified for the new NACA family. However, if the new cross-section shapes are not differing much from the used NACA 4-digit series the current approximative formulas can be used.

Traditionally, marine propulsion and control equipment have been manufactured from metal, particularly with nickel-aluminium, bronze or stainless steel which are homogeneous and isotropic. Therefore, the current approach was developed for

solid cross-sections made of homogeneous and isotropic material. Advanced materials, such as composites, and lightweight designs, such as hollow cross-sections with stiffened shell and inside webs, are not studied in this work. However, composite materials are continuously developed and are gradually used more in ship applications because they offer advantages over traditional materials, including reduced weight, corrosion resistance and the potential for hydrodynamic performance improvement through hydroelastic tailoring [42, p. 327]. On the other hand, in case of the lightweight fin designs, the low density ratio increases the risk of vibrations and instabilities due to lower natural frequencies and critical velocities [42, p. 331] [25, p. 965]. Since the current approach is not accurate for orthotropic and heterogeneous designs, it must be further developed.

In this study, the stator fin is simplified to oscillate in still water, meaning both the ship and water are still. In reality, both the ship and water are moving. The passing flow and ship motions affect the oscillations of the fin. But only the passing flow affects the natural frequencies of the fin because it affects added mass and damping. In the future, the effect of the passing flow and ship or flow velocity on the natural frequencies should be studied and taken into account in predictions if having significant effect. The current approach neglects damping, thus solving the undamped natural frequencies of fins. The structural damping is negligible in most cases but the external damping due to water can be significant. The damping decreases the undamped natural frequencies which usually means that the risk of resonance and hydroelastic instabilities increases. Therefore, damping should be added to the current approach in the future.

In this work, the natural frequencies and mode shapes are solved from the generalized eigenvalue problem as presented in Section 2.2.3. The form of the problem is lacking in terms of computational effort [22, p. 294–295]. The computation of one case in this work took only a few seconds. However, when more terms, such as damping, are added, the computation time may increase depending how the damping is introduced [22, p. 322–323]. Therefore, a more computationally efficient form of the problem should be considered in future.

In summary, the simplified two DOFs beam approach presented is applicable to predict the lowest natural frequencies of stator fins if fins are solid and made of a homogeneous isotropic material. The cross-section of fins should be close to NACA 4-digit shapes or closer to a flat plate shape than an elliptical shape. The approach is tested only for straight fins and the applicability in case of fins with sweep angle and skewness must be studied after this work. In case of fins made of advanced materials, the approach must be further developed. The current approach predicts the undamped natural frequencies only in still water conditions. To predict the natural frequencies of stator fins in operating conditions, the effects of passing flow and external damping must be included and studied to determine how much they affect the lowest frequencies.

References

[1] ABBOTT, I.H. & VON DOENHOFF, A.E. *Theory of Wing Sections - Including a Summary of Airfoil Data.* Dover Publications, New York, 1959. ISBN 978-0-486-60586-9.

[2] AKCABAY, D.T. et al. *Cavity Induced Vibration of Flexible Hydrofoils.* Journal of Fluids & Structures, 2014. pp. 463-484. ISSN 08899746.

[3] AKCABAY, D.T. & YOUNG Y.L. *Influence of Cavitation on the Hydroelastic Stability of Hydrofoils.* Journal of Fluids & Structures, 2014. pp. 170-185. ISSN 08899746.

[4] ANDRO, J. & JACQUIN L. *Frequency Effects on the Aerodynamic Mechanisms of a Heaving Airfoil in a Forward Flight Configuration.* Aerospace Science & Technology, 2009, vol. 13, no. 1. pp. 71-80. ISSN 12709638.

[5] AURELI, M. & BASARAN M.E. & PORFIRI M. *Nonlinear Finite Amplitude Vibrations of Sharp-Edged Beams in Viscous Fluids.* Journal of Sound & Vibration, 2012, vol. 331, no. 7. pp. 1624-1654. ISSN 0022460X.

[6] BANERJEE, J. *Explicit Frequency Equation and Mode Shapes of a Cantilever Beam Coupled in Bending and Torsion.* Journal of Sound and Vibration, 1999, vol. 224, no. 2. pp. 267-281. ISSN 0022460X.

[7] BENAOUICHA, M. & ASTOLFI J. *Analysis of Added Mass in Cavitating Flow.* Journal of Fluids & Structures, 2012. pp. 30-48. ISSN 08899746.

[8] BERCIN, A. & TANAKA M. *Coupled Flexural-Torsional Vibrations of Timoshenko Beams.* Journal of Sound and Vibration, 1997, vol. 207, no. 1. pp. 47-59. ISSN 0022460X.

[9] BESCH, P.K. & LIU Y. *Flutter and Divergence Characteristics of Four Low Mass Ratio Hydrofoils.* Naval Ship Research and Development Center, Washington D.C., 1971. Report 3410.

[10] BISPLINGHOFF, R.L. & ASHLEY, H. & HALFMAN, R.L. *Aeroelasticity.* Dover Publications Inc., New York, 1996. ISBN 978-0-486-69189-3.

[11] BLEVINS, R.D. *Formulas for Natural Frequency and Mode Shape.* Van Nostrand Reinhold, New York, 1979. ISBN 0-442-20710-7.

[12] CARCATERRA, A. & DESSI D. & MASTRODDI F. *Hydrofoil Vibration Induced by a Random Flow: A Stochastic Perturbation Approach.* Journal of Sound & Vibration, 2005, vol. 283, no. 1. pp. 401-432. ISSN 0022460X.

[13] CHAE, E.J. & AKCABAY D.T. & YOUNG Y.L. *Dynamic Response and Stability of a Flapping Foil in a Dense and Viscous Fluid.* Physics of Fluids, 2013, vol. 25, no. 10. pp. 104106. ISSN 10706631.

[14] COOK, R.D. et al. *Concepts and Applications of Finite Element Analysis.* John Wiley & Sons Inc., fourth edition, 2002.

[15] DE JONG J.H. *A Framework for Energy Saving Device (ESD) Decision Making.* International Conference on Ship Efficiency, Hamburg, Germany, 2011 [cited 27.05.2016]. Available from: http://www.ship-efficiency.org/2011/programme.html

[16] DSME. *Energy Saving Devices.* 2008 [cited 27.05.2016]. Available from: http://legacy.sname.org/sections/greece/DSME%20Energy%20Saving%20Device%20for%20GreeceSNAME(4distribution).pdf

[17] Ducoin A. & YOUNG Y.L. *Hydroelastic Response and Stability of a Hydrofoil in Viscous Flow.* Journal of Fluids and Structures, 2013, vol. 38. pp. 40-57. ISSN 08899746; 10958622.

[18] FACCI, A.L. & PORTIFI M. *Analysis of Three-Dimensional Effects in Oscillating Cantilevers Immersed in Viscous Fluids.* Journal of Fluids & Structures, 2013. pp. 205-222. ISSN 08899746.

[19] HAN, S.M. & BENAROYA H. & WEI T. *Dynamics of Transversely Vibrating Beams using Four Engineering Theories.* Journal of Sound and Vibration, 1999, vol. 225, no. 5. pp. 935-988. ISSN 0022460X.

[20] HOFFMANN J.A. & WERTHEIMER T. *Cantilever Beam Vibration.* Journal of Sound and Vibration, 2000, vol. 229, no. 5. pp. 1269-1276. ISSN 0022460X.

[21] HOLLENBACH U. & REINHOLZ O. *Hydrodynamic Trends in Optimizing Propulsion.* Proceedings of the Second International Symposium on Marine Propulsors smp'11, Hamburg, Germany, 2011 [cited 27.05.2016]. Available from: http://www.marinepropulsors.com/proceedings-2011.php

[22] INMAN, D.J. *Engineering Vibrations.* Pearson Education International, third edition, 2009.

[23] KATZ, J. & PLOTKIN, A. *Low-Speed Aerodynamics.* McGraw-Hill Inc., 1991. ISBN 0-07-100876-4.

[24] LA MANTIA, M. & DABNICHKI P. *Added Mass Effect on Flapping Foil.* Engineering Analysis with Boundary Elements, 2012, vol. 36, no. 4. pp. 579-590. ISSN 09557997.

[25] LA MANTIA, M. & DABNICHKI P. *Structural Response of Oscillating Foil in Water.* Engineering Analysis with Boundary Elements, 2013, vol. 37, no. 6. pp. 957-966. ISSN 09557997.

[26] LIANG, C. et al. *The Free Vibration Analysis of Submerged Cantilever Plates.* Ocean Engineering, 2001, vol. 28, no. 9. pp. 1225-1245. ISSN 00298018.

[27] MCCROSKEY, W.J. *Unsteady Airfoils.* Annual Review of Fluid Mechanics, 1982, vol. 14, no. 1. pp. 285-311. ISSN 0066-4189.

[28] NEWMAN, J.N. *Marine Hydrodynamics.* Cambridge (MA): MIT Press, 1977. ISBN 0-262-14026-8.

[29] OTTOSEN, N.S. & PETERSSON H. *An Introduction to the Finite Element Method.* Prentice Hall, 1992. ISBN 978-0-13-473877-2.

[30] PARNES, R. *Solid Mechanics in Engineering.* Chichester: Wiley, 2001. ISBN 0-471-49300-7.

[31] REDDY, J.N. & LEE, K.H. & WANG, C.M. *Shear Deformable Beams and Plates : Relationships with Classical Solutions.* Elsevier Science & Technology, New York, 2000.

[32] SAPOUNTZAKIS, E.J. & DOURAKOPOULOS J.A. *Shear Deformation Effect in Flexural-Torsional Vibrations of Composite Beams by Boundary Element Method (BEM).* Journal of Vibration & Control, 2010, vol. 16, no. 12. pp. 1763-1789. ISSN 10775463.

[33] SHUBOV, M.A. *Mathematical Modeling and Analysis of Flutter in Bending-Torsion Coupled Beams, Rotating Blades, and Hard Disk Drives.* Journal of Aerospace Engineering, 2004, vol. 17, no. 2. pp. 56-69. ISSN 08931321.

[34] TANAKA, M. & BERCIN A.N. *Finite Element Modelling of the Coupled Bending and Torsional Free Vibration of Uniform Beams with an Arbitrary Cross-Section.* Applied Mathematical Modelling, 1997, vol. 21, no. 6. pp. 339-344. ISSN 0307904X.

[35] TIMOSHENKO, S. *Vibration Problems in Engineering.* Van Nostrand, New York, second edition, 1937.

[36] TONG, X. & TABARROK B. & YEH K.Y. *Vibration Analysis of Timoshenko Beams with Non-Homogeneity and Varying Cross-Section.* Journal of Sound and Vibration, 1995, vol. 186, no. 5. pp. 821-835. ISSN 0022460X.

[37] TORRE, D.L. et al. *Experimental Investigation of Added Mass Effects on a Hydrofoil Under Cavitation Conditions.* Journal of Fluids & Structures, 2013. pp. 173-187. ISSN 08899746.

[38] WEAVER, W.JR. & TIMOSHENKO S. & YOUNG D.H. *Vibration Problems in Engineering.* Wiley, fifth edition, 1990.

[39] YADYKIN, Y. & TENETOV V. & LEVIN D. *The Added Mass of a Flexible Plate Oscillating in a Fluid.* Journal of Fluids & Structures, 2003, vol. 17, no. 1. pp. 115-123. ISSN 08899746.

[40] YAO, Z. et al. *Effect of Trailing Edge Shape on Hydrodynamic Damping for a Hydrofoil.* Journal of Fluids & Structures, 2014. pp. 189-198. ISSN 08899746.

[41] YUCEL S.B. & SAHIN M. & Unal M.F. *Strong Transient Effects of the Flow Around a Harmonically Plunging NACA0012 Airfoil at Low Reynolds Numbers.* Theoretical & Computational Fluid Dynamics, 2015, vol. 29, no. 5. pp. 391-412. ISSN 09354964.

[42] ZARRUK, G. et al. *Experimental Study of the Steady Fluid-Structure Interaction of Flexible Hydrofoils.* Journal of Fluids and Structures, 2014, vol. 51. pp. 326-343. ISSN 08899746.

[43] ZIENKIEWICZ, O.C. & TAYLOR R.L. *The Finite Element Method, Volume 1: The Basis.* Butterworth-Heinemann, fifth edition, 2000. ISBN 0-7506-5049-4.

[44] ZONDERVAN G. & HOLTROP J. & VAN TERWISGA T. *On the Design and Analysis of Pre-Swirl Stators for Single and Twin Screw Ships.* Proceedings of the Second International Symposium on Marine Propulsors smp'11, Hamburg, Germany, 2011. [cited 27.05.2016]. Available from: `http://www.marinepropulsors.com/proceedings-2011.php`

[45] *Chinese vessel reports second signal detected in search for missing MH370.* The Times, 07.04.2014. [cite 27.05.2016]. Available from: `http://www.thetimes.co.uk/tto/news/world/asia/article4055681.ece`

[46] *Energy Saving Devices - Design and Optimization.* HSVA Website. [cited 27.05.2016] Available from: `http://www.hsva.de/our-services/numerical-predictions/cfd-esd-design-optimisation.html`

[47] *Pass the sea-sick pills: The terrifying moment a cruise ship was slammed by giant Antarctic waves.* The Daily Mail, 10.12.2010. [cited 27.05.2016]. Available from: `http://www.dailymail.co.uk/news/article-1337062/Cruise-ship-slammed-enormous-Antarctic-waves.html`

Appendices

Appendix A

A Verification case results

The four different verification cases are shown in this Appendix. The first three are used to compare analytical and current results and the fourth is used to compare numerical and current results. The EOM used are without shear deformation, rotary inertia, coupling and added mass terms if not otherwise indicated.

The first case compares the five lowest natural frequencies and mode shapes of a uniform cantilever beam in bending obtained with an analytical formula, in Figure A.1, and the current approach, in Figure A.2.

The second case compares the five lowest natural frequencies and mode shapes of a uniform cantilever beam in torsion obtained with an analytical formula, in Figure A.3, and the current approach, in Figure A.4.

The third case shows the lowest natural frequencies and mode shapes of a linearly tapered cantilever beam in bending obtained with the current approach with different taper ratios in Figures A.5 - A.9.

The fourth case shows the five lowest natural frequencies and mode shapes of uniform NACA0012 cross-sectioned cantilever beam in bending obtained with the current approach. Figures A.10 and A.11 are calculated in a vacuum, meaning without the added mass term, without and with the coupling term, respectively. Figures A.12 and A.13 are calculated in water, meaning with the added mass term and without and with the coupling term, respectively. The EOM are used with shear deformation and rotary inertia terms.

The order of mode shape and corresponding natural frequency is shown above each of the graphs. The graphs show the bending shape with a dotted line and the torsion shape with a dashed line.

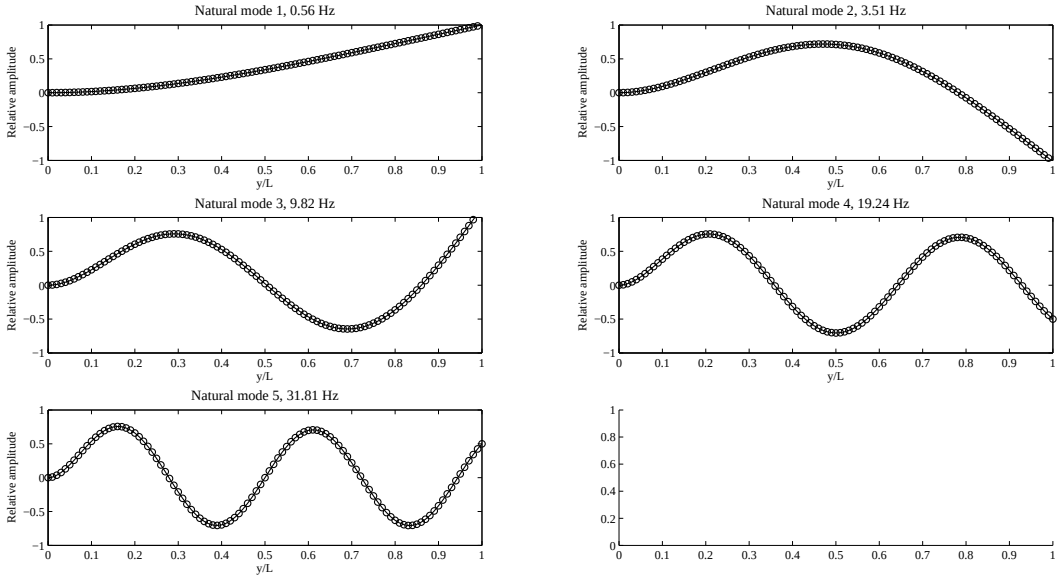

Figure A.1: Verification against analytical results: analytical mode shapes of uniform cantilever beam in bending without shear deformation, rotary inertia, coupling and added mass terms

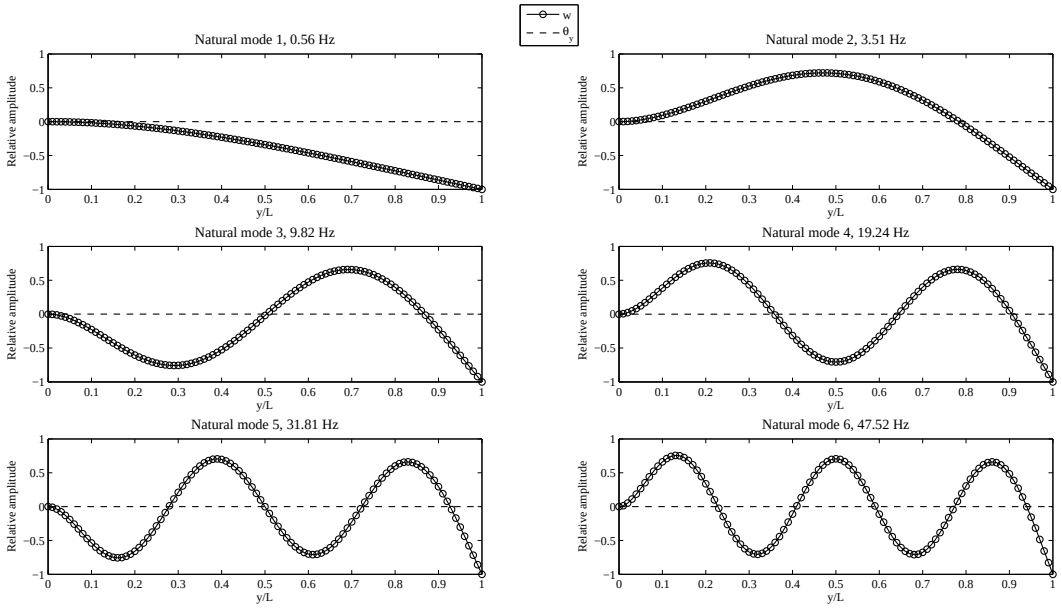

Figure A.2: Verification against analytical results: calculated mode shapes of uniform cantilever beam in bending without shear deformation, rotary inertia, coupling and added mass terms

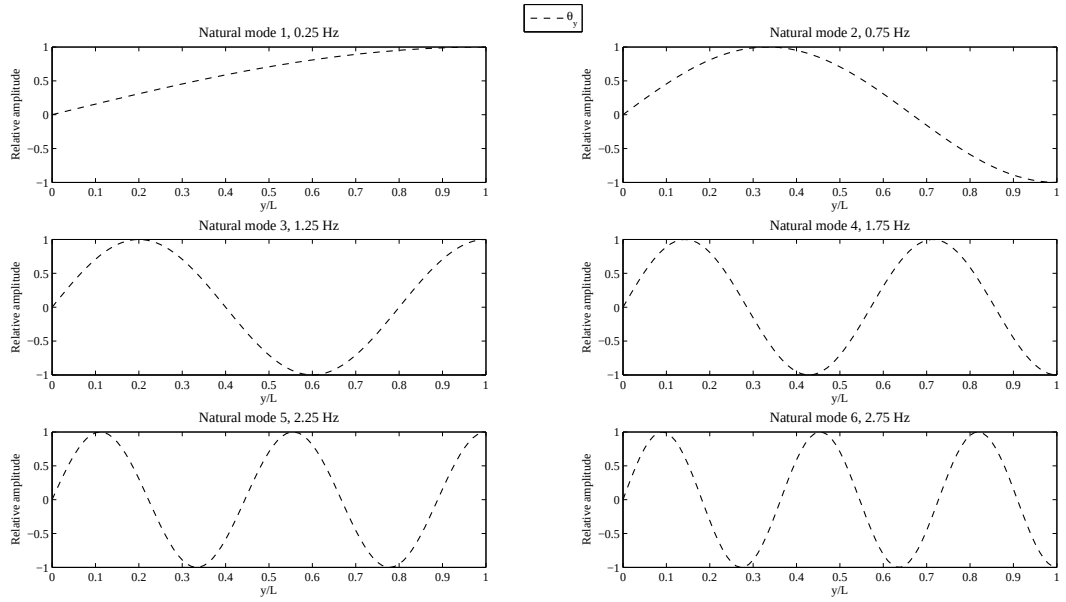

Figure A.3: Verification against analytical results: analytical mode shapes of uniform cantilever beam in torsion without shear deformation, rotary inertia, coupling and added mass terms

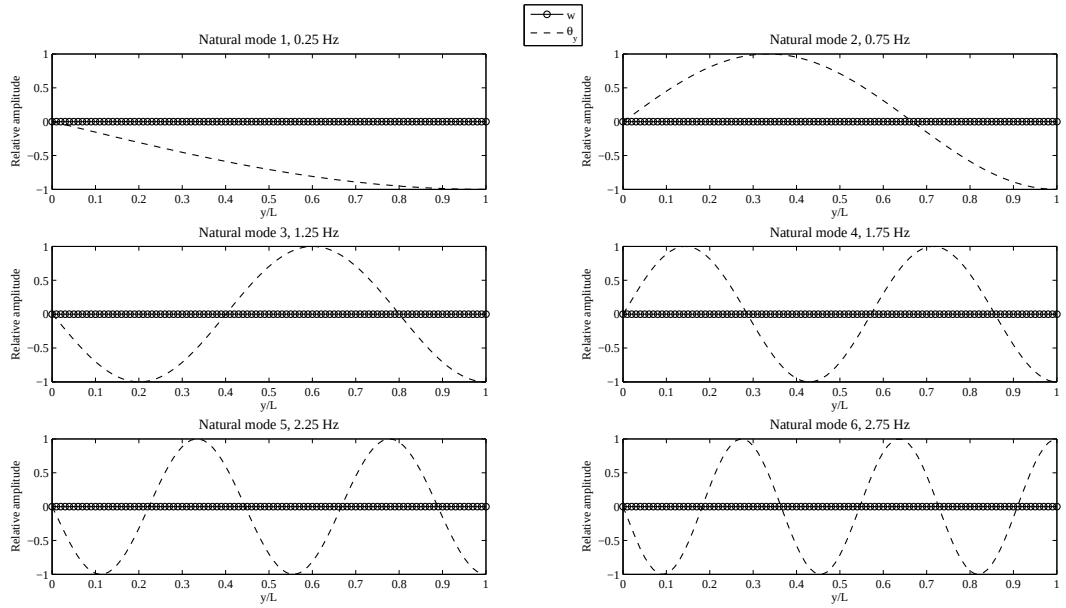

Figure A.4: Verification against analytical results: calculated mode shapes of uniform cantilever beam in torsion without shear deformation, rotary inertia, coupling and added mass terms

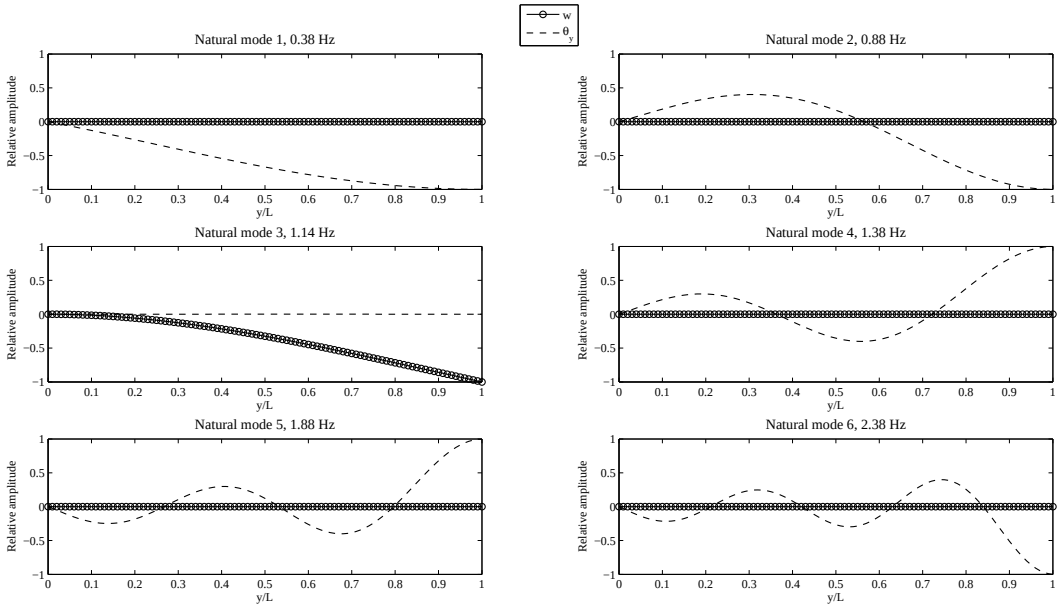

Figure A.5: Verification against analytical results: analytical mode shapes of linearly tapered (taper ratio 0) cantilever beam in bending without shear deformation, rotary inertia, coupling and added mass terms

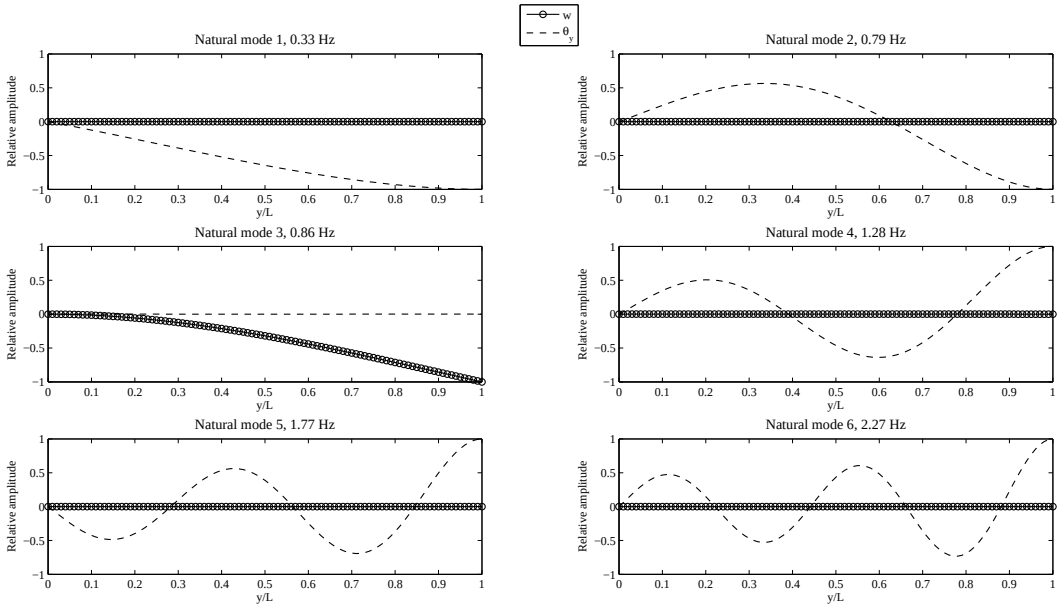

Figure A.6: Verification against analytical results: analytical mode shapes of linearly tapered (taper ratio 0.2) cantilever beam in bending without shear deformation, rotary inertia, coupling and added mass terms

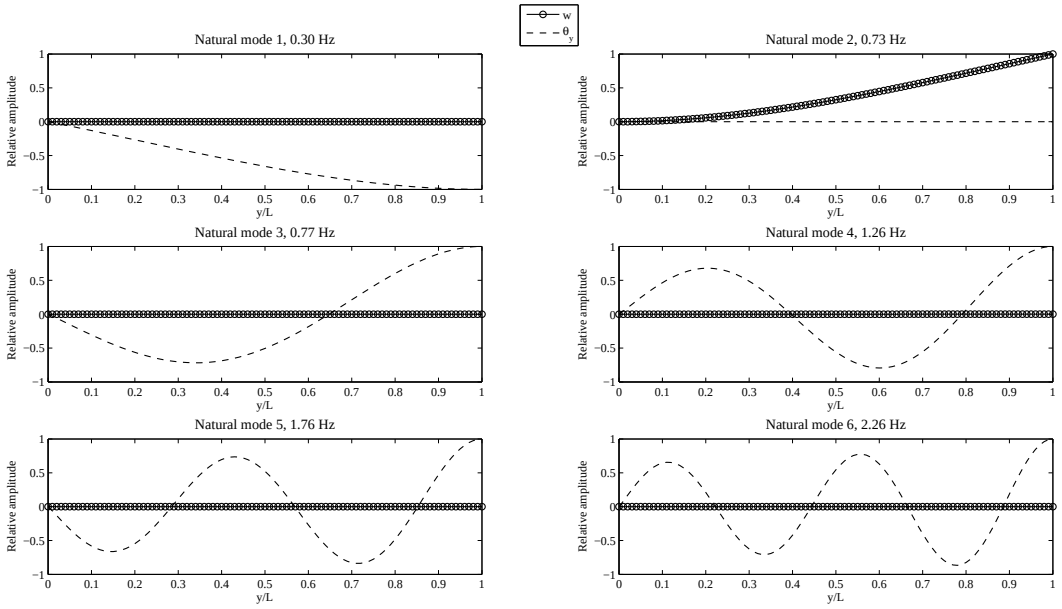

Figure A.7: Verification against analytical results: analytical mode shapes of linearly tapered (taper ratio 0.4) cantilever beam in bending without shear deformation, rotary inertia, coupling and added mass terms

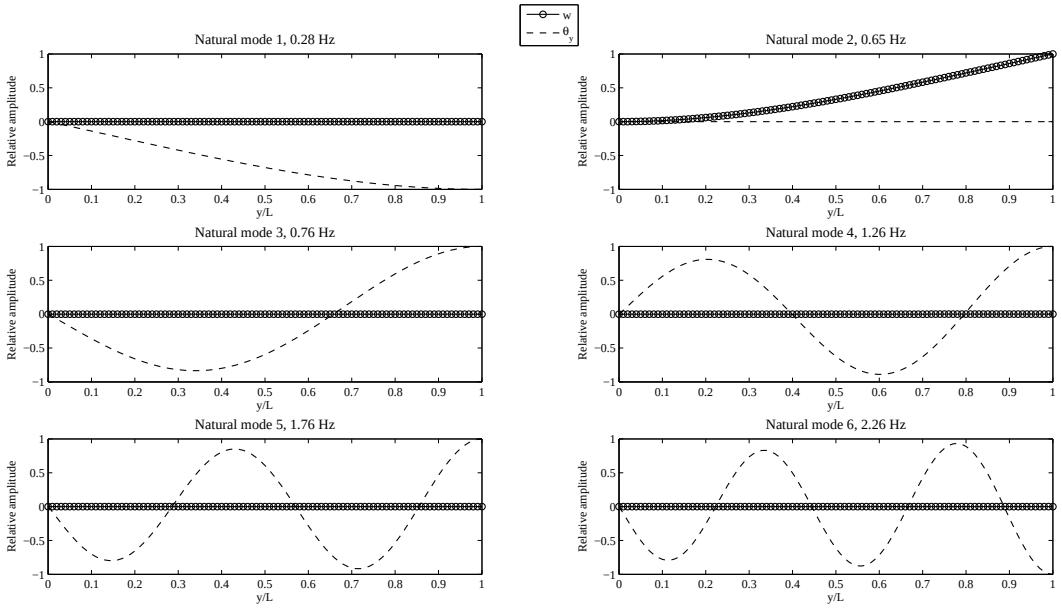

Figure A.8: Verification against analytical results: analytical mode shapes of linearly tapered (taper ratio 0.6) cantilever beam in bending without shear deformation, rotary inertia, coupling and added mass terms

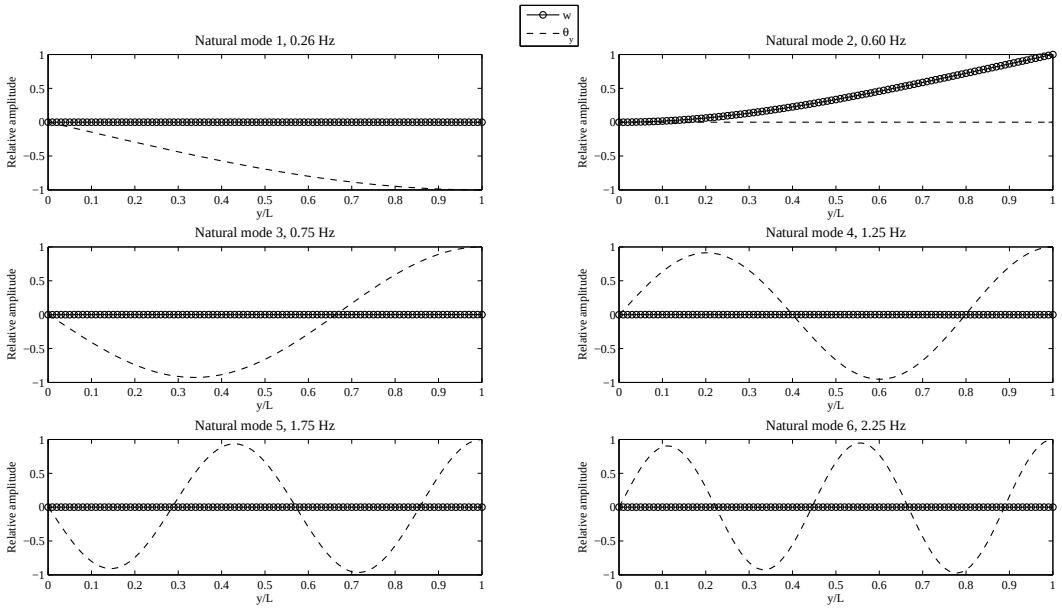

Figure A.9: Verification against analytical results: analytical mode shapes of linearly tapered (taper ratio 0.8) cantilever beam in bending without shear deformation, rotary inertia, coupling and added mass terms

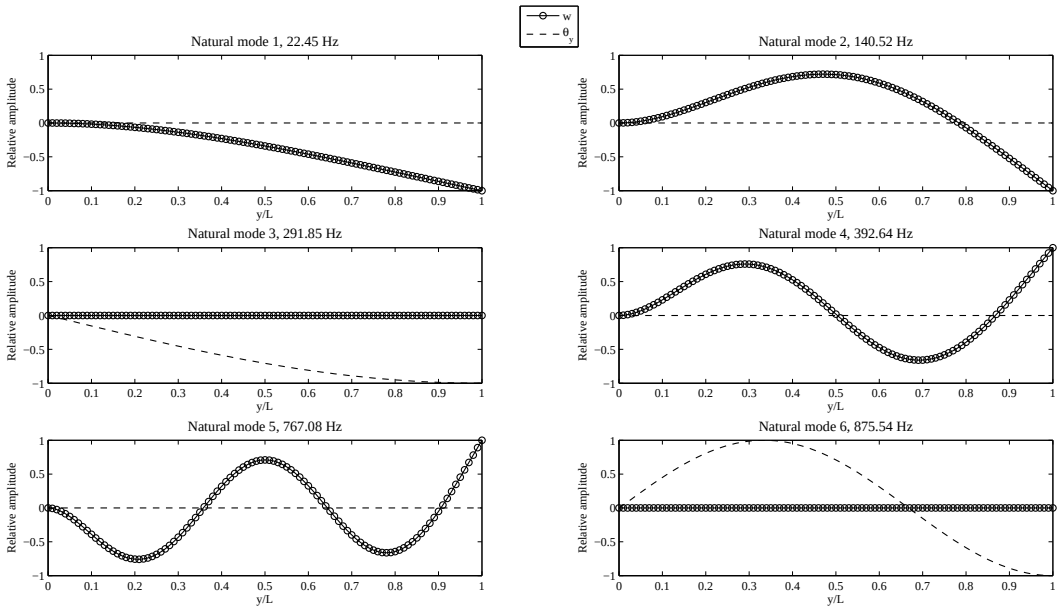

Figure A.10: Verification against numerical results: NACA0012 cantilever in vacuum without the coupling term

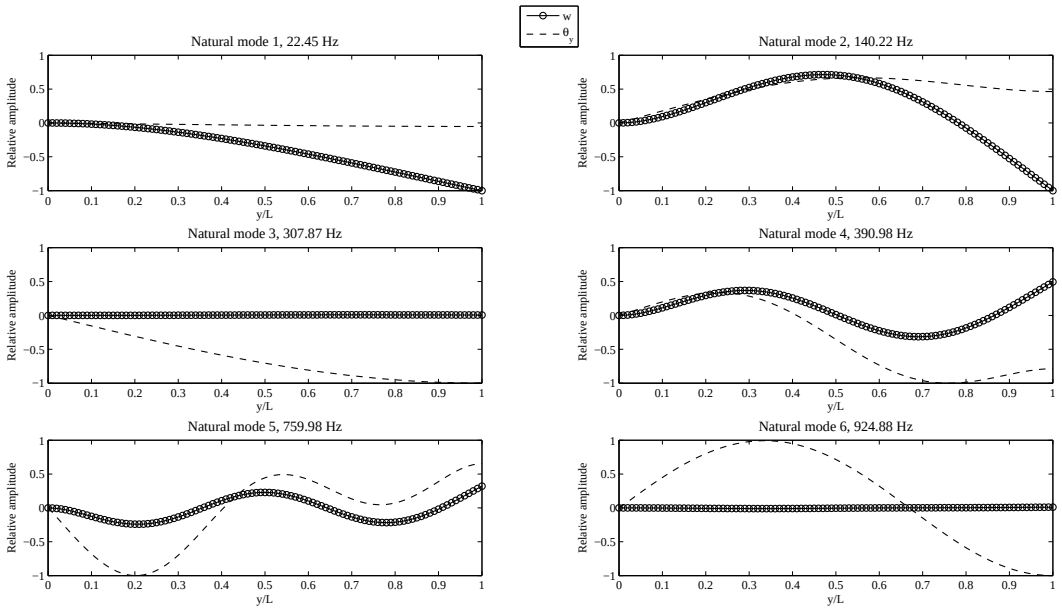

Figure A.11: Verification against numerical results: NACA0012 cantilever in vacuum with the coupling term

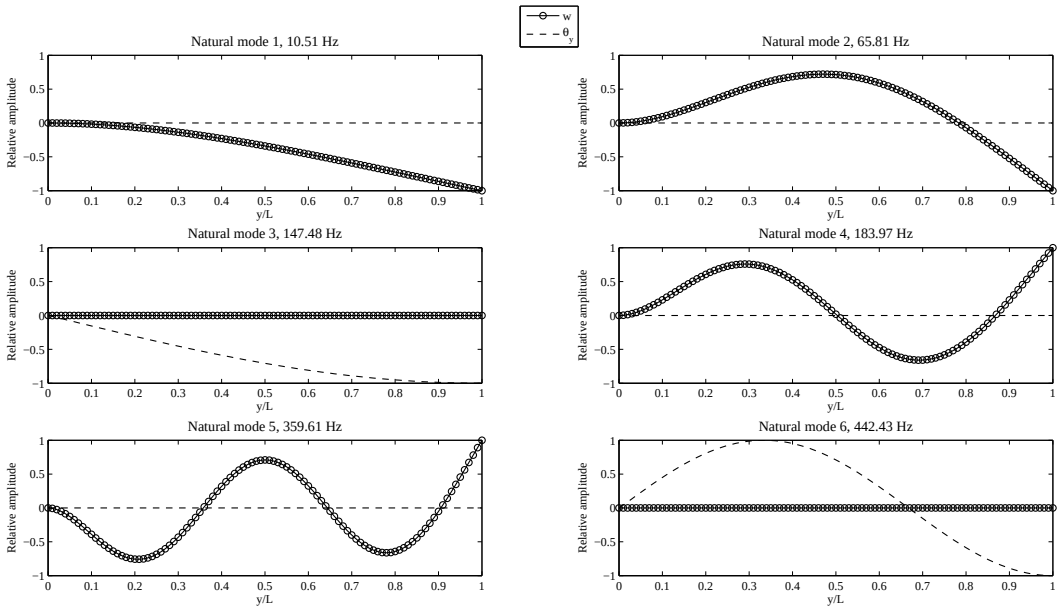

Figure A.12: Verification against numerical results: NACA0012 cantilever in water without the coupling term

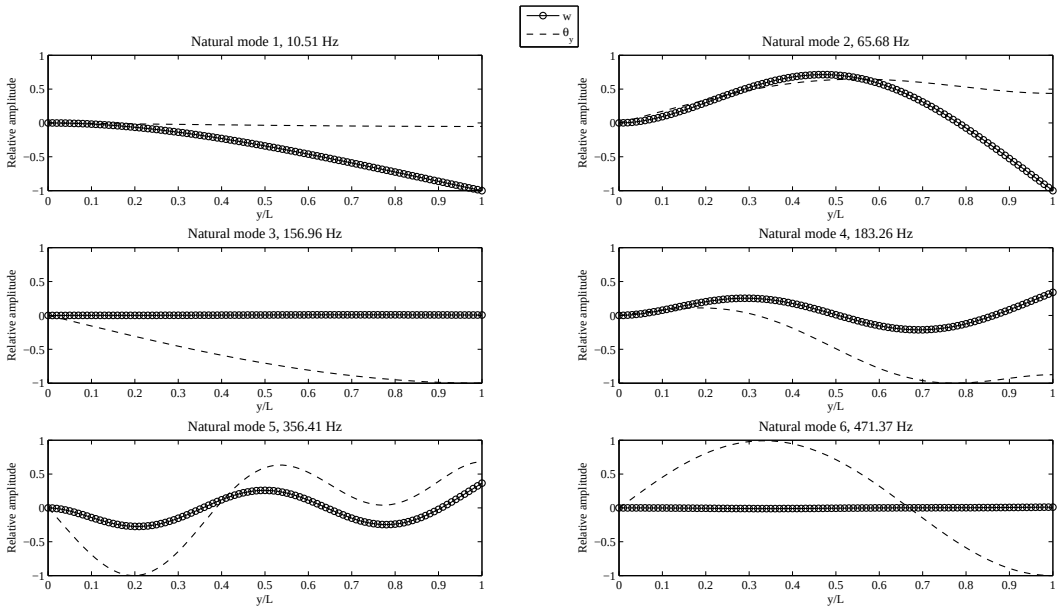

Figure A.13: Verification against numerical results: NACA0012 cantilever in water with the coupling term

Appendix B

B Validation case results

The natural frequencies and mode shapes of the four validation cases are calculated with the current approach and shown in this Appendix. The EOM used are with shear deformation, rotary inertia, coupling and added mass terms if not otherwise indicated.

Validation Case 1 is shown in Figures B.1 and B.2.

Validation Cases 2 and 3 are shown in the same Figures B.3 and B.4 because the current approach is not taking into account the difference of the cross-section shape between the cases.

Validation Case 4.1 is shown in Figures B.5 and B.6, while those of 4.2, 4.3 and 4.4 are shown in Figures B.7 and B.8, B.9 and B.10, and B.11 and B.12, respectively.

The order of mode shape and corresponding natural frequency is shown above each of the graphs. The graphs show the bending shape with a dotted line and the torsion shape with a dashed line.

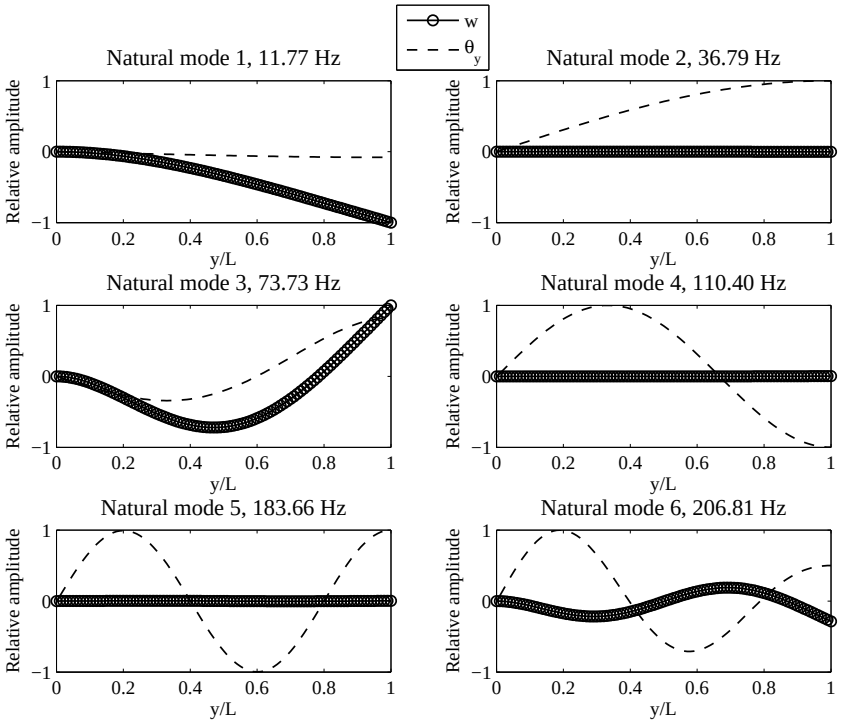

Figure B.1: Validation Case 1: in air

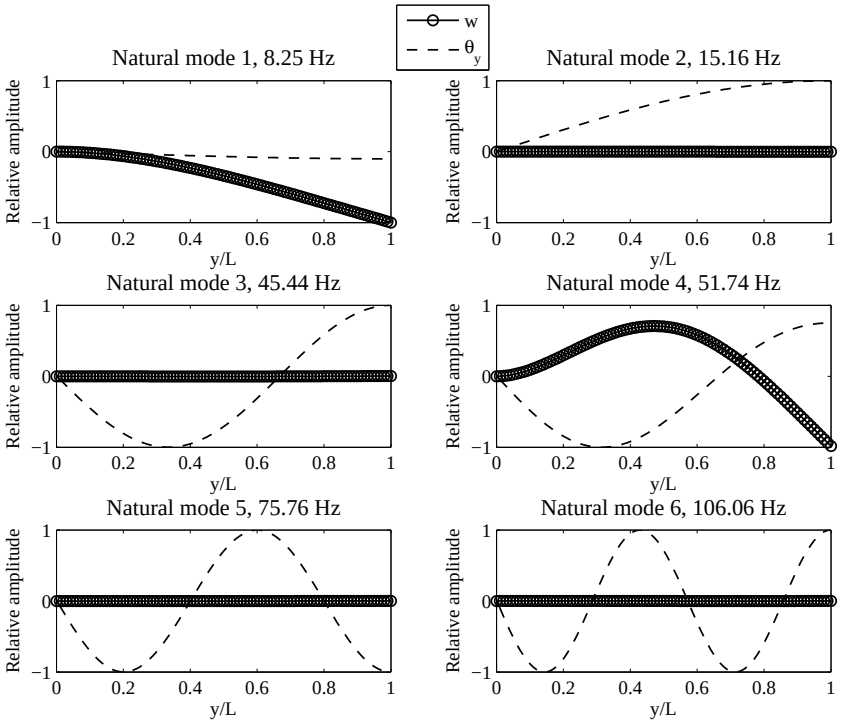

Figure B.2: Validation Case 1: in water

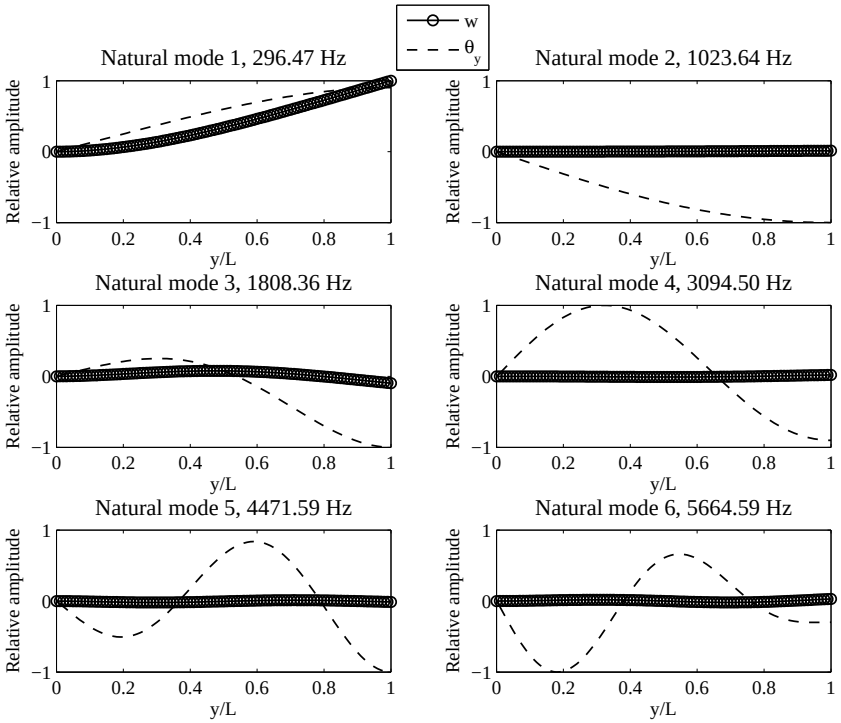

Figure B.3: Validation Cases 2 & 3: in air

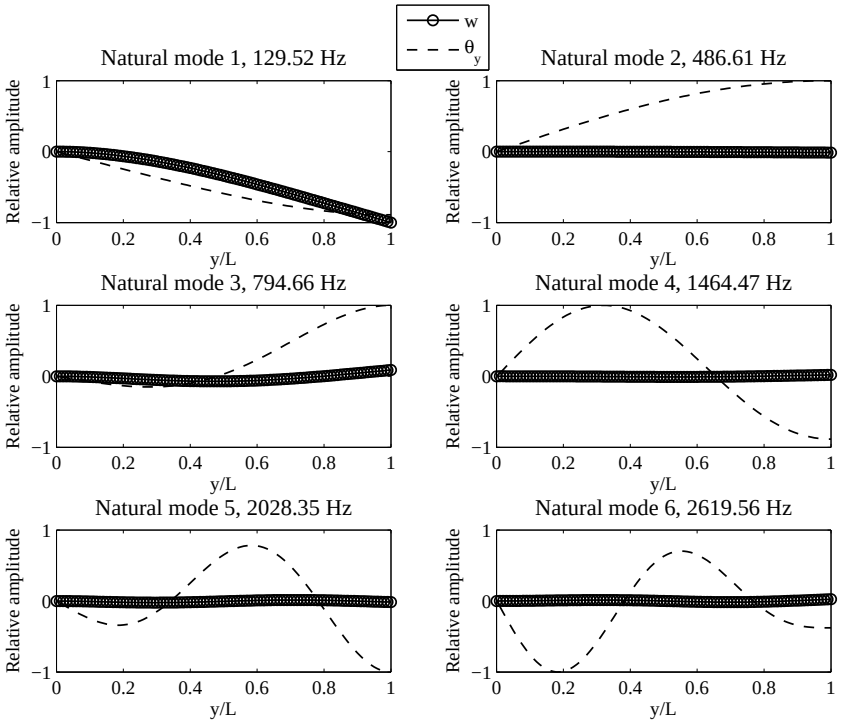

Figure B.4: Validation Cases 2 & 3: in water

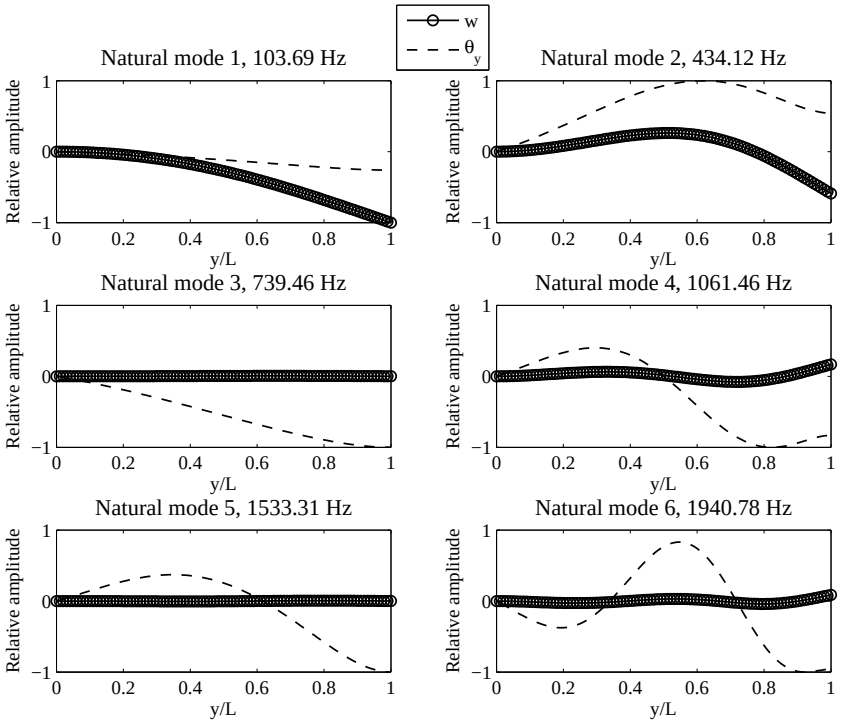

Figure B.5: Validation Case 4.1: in air

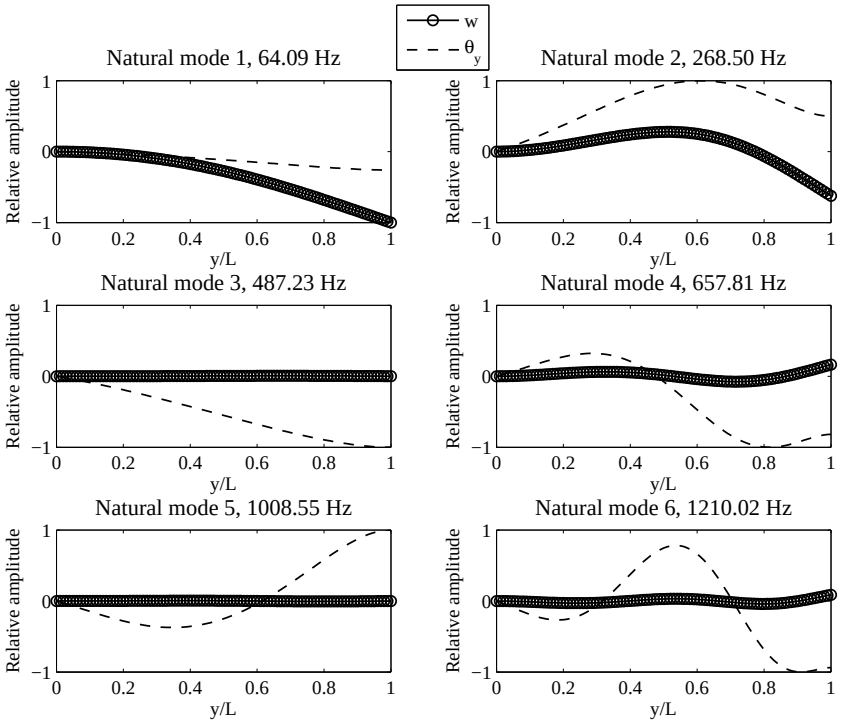

Figure B.6: Validation Case 4.1: in water

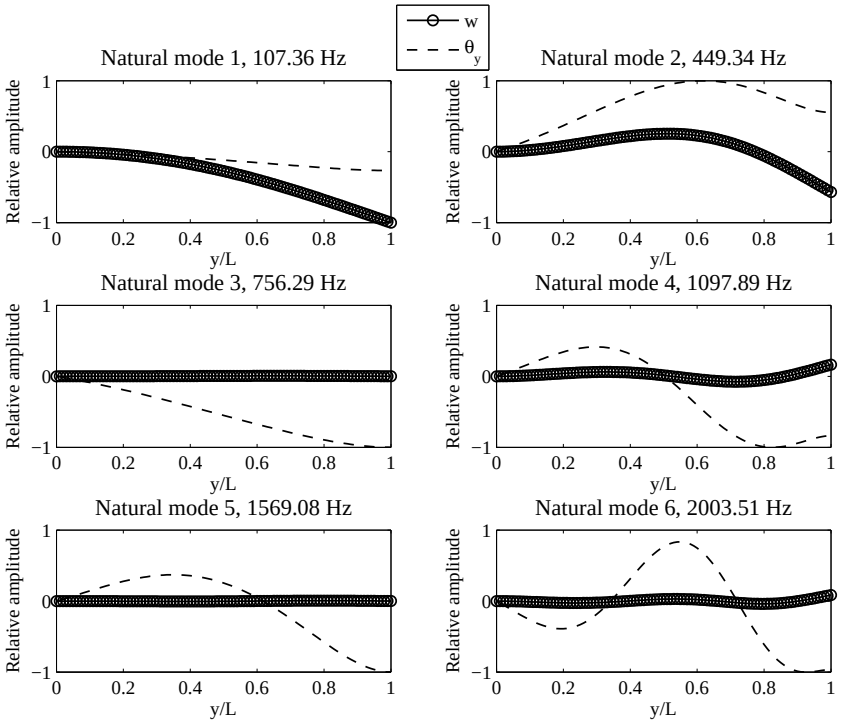

Figure B.7: Validation Case 4.2: in air

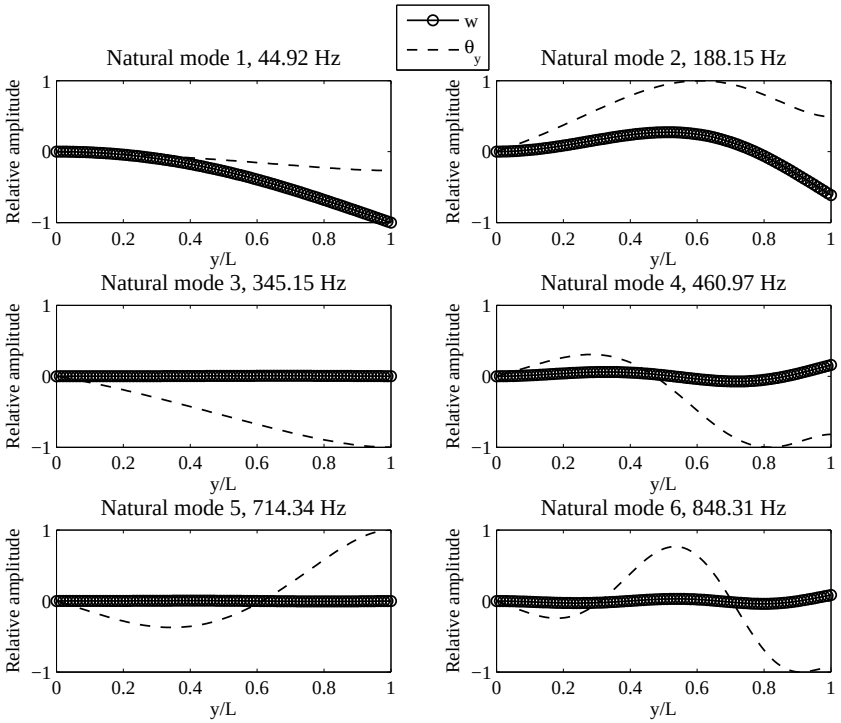

Figure B.8: Validation Case 4.2: in water

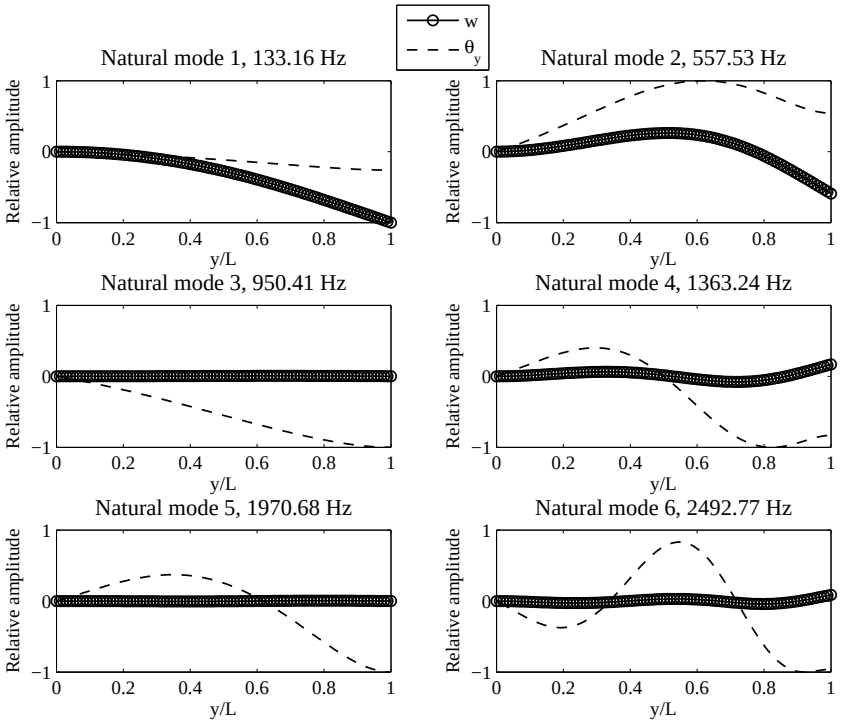

Figure B.9: Validation Case 4.3: in air

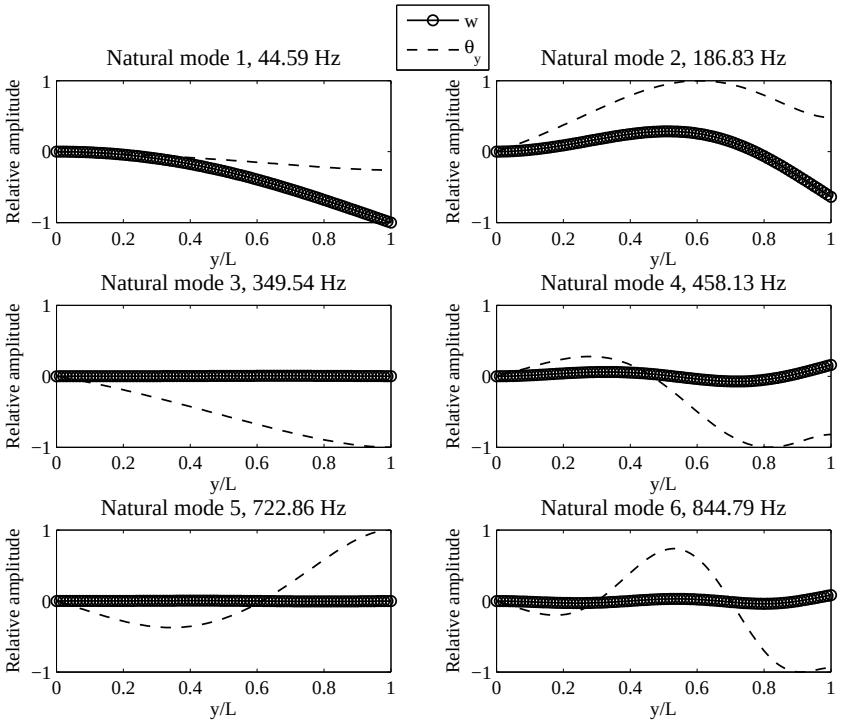

Figure B.10: Validation Case 4.3: in water

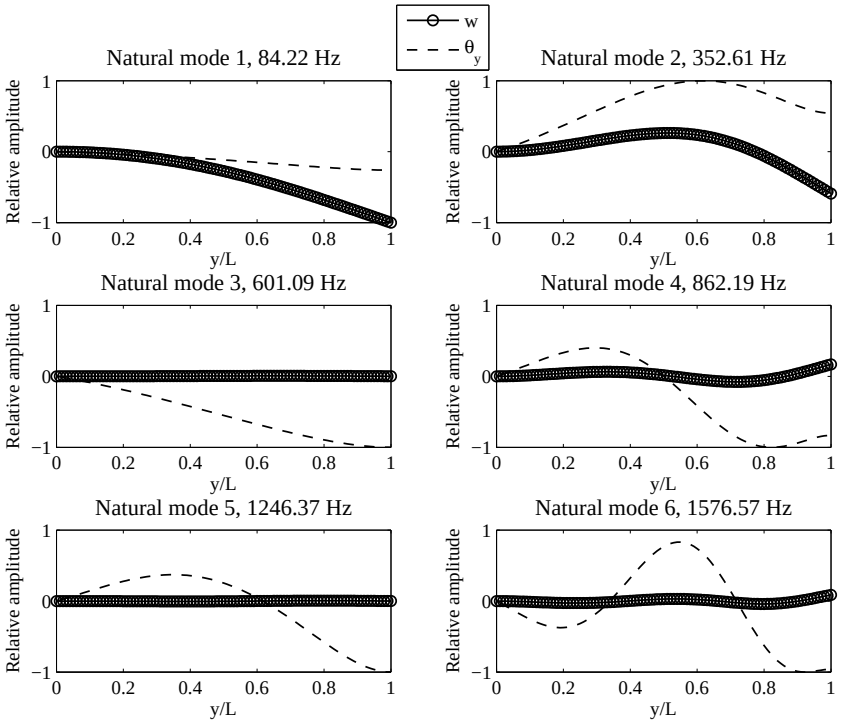

Figure B.11: Validation Case 4.4: in air

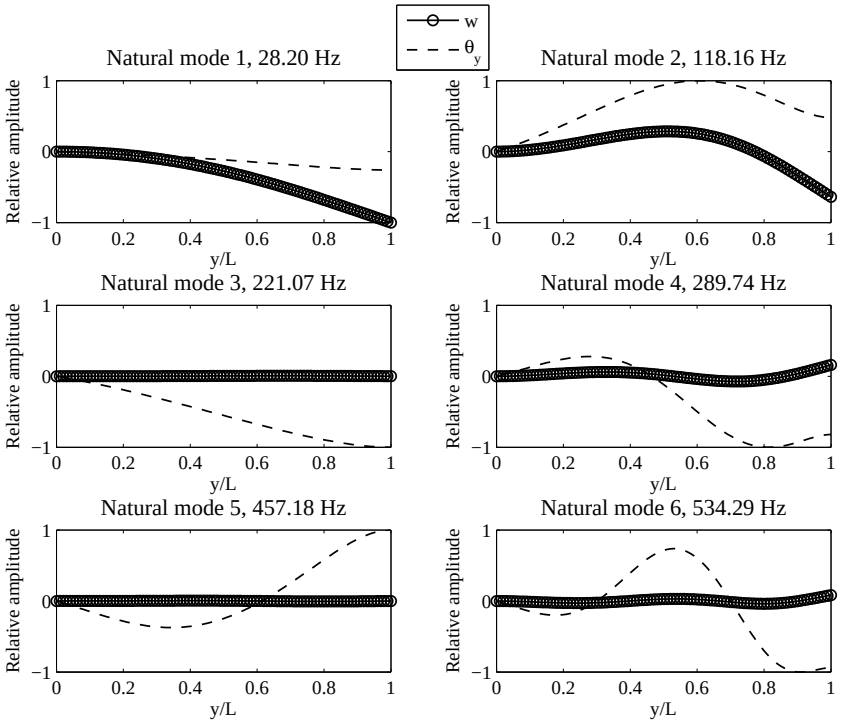

Figure B.12: Validation Case 4.4: in water

Appendix C

C Term significance study

The four different cases of the term significance study are shown in this Appendix. The first case studies the shear deformation term, the second the rotary inertia term, the third the coupling term and the fourth the added mass term. The five lowest natural frequencies are compared with and without the term studied. The graphs show the relative difference in per cent between the EOM with and without the studied term. The cases are shown in Figures C.1, C.2, C.3 and C.4, respectively.

The EOM used are without shear deformation, rotary inertia, coupling and added mass terms if not otherwise indicated. The cross-sectional properties are calculated with the approximative formulas given in Section 2.3. The beam is uniform and made of steel if not otherwise indicated.

In the graphs, the number in the legend indicates the type of the mode shape. Bending mode is indicated with number 1, torsion with number 2 and mixed mode with number 3. The type is defined as bending or torsion if the maximum relative amplitude of the respective mode shape is more than 5 times larger than another. Otherwise, the type is defined as a combination. Hyphens separate the results with and without the term studied, respectively. Commas separate the modes 1st, 2nd, 3rd, 4th and 5th, respectively.

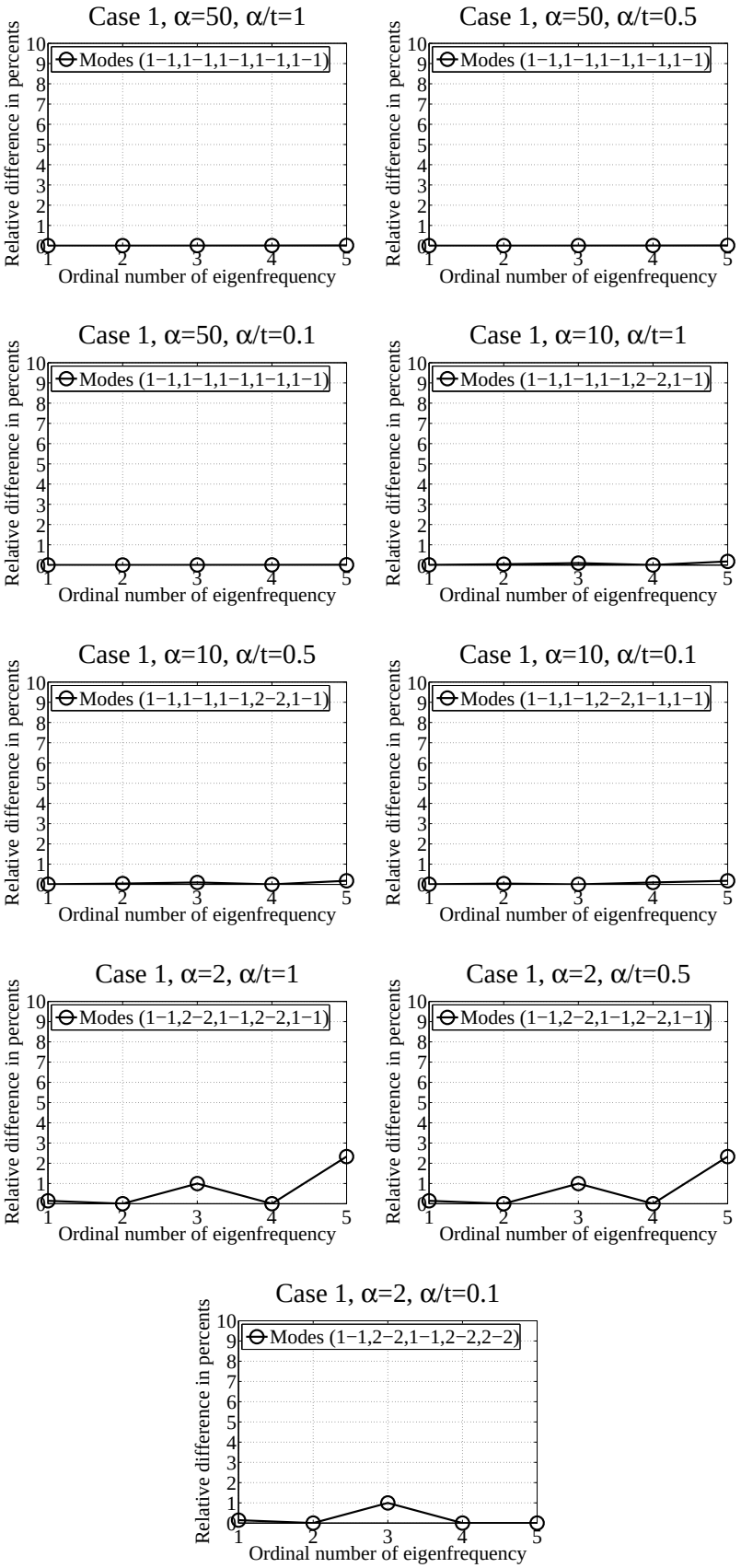

Figure C.1: Case 1 of term significance study: shear deformation term. The varying parameters are slenderness ratio α and ratio of slenderness ratio and thickness α/t.

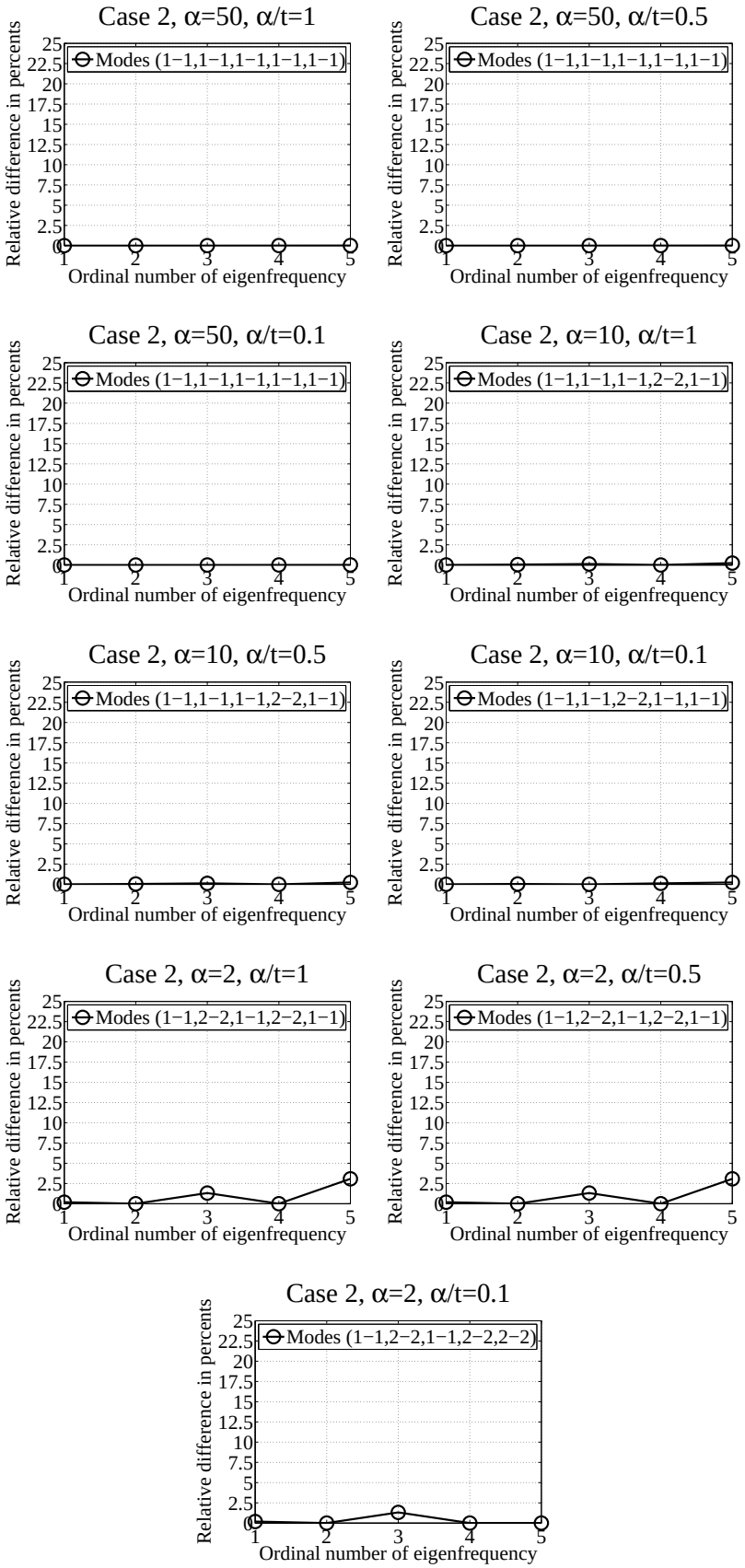

Figure C.2: Case 2 of term significance study: rotary inertia term. The varying parameters are slenderness ratio α and ratio of slenderness ratio and thickness α/t.

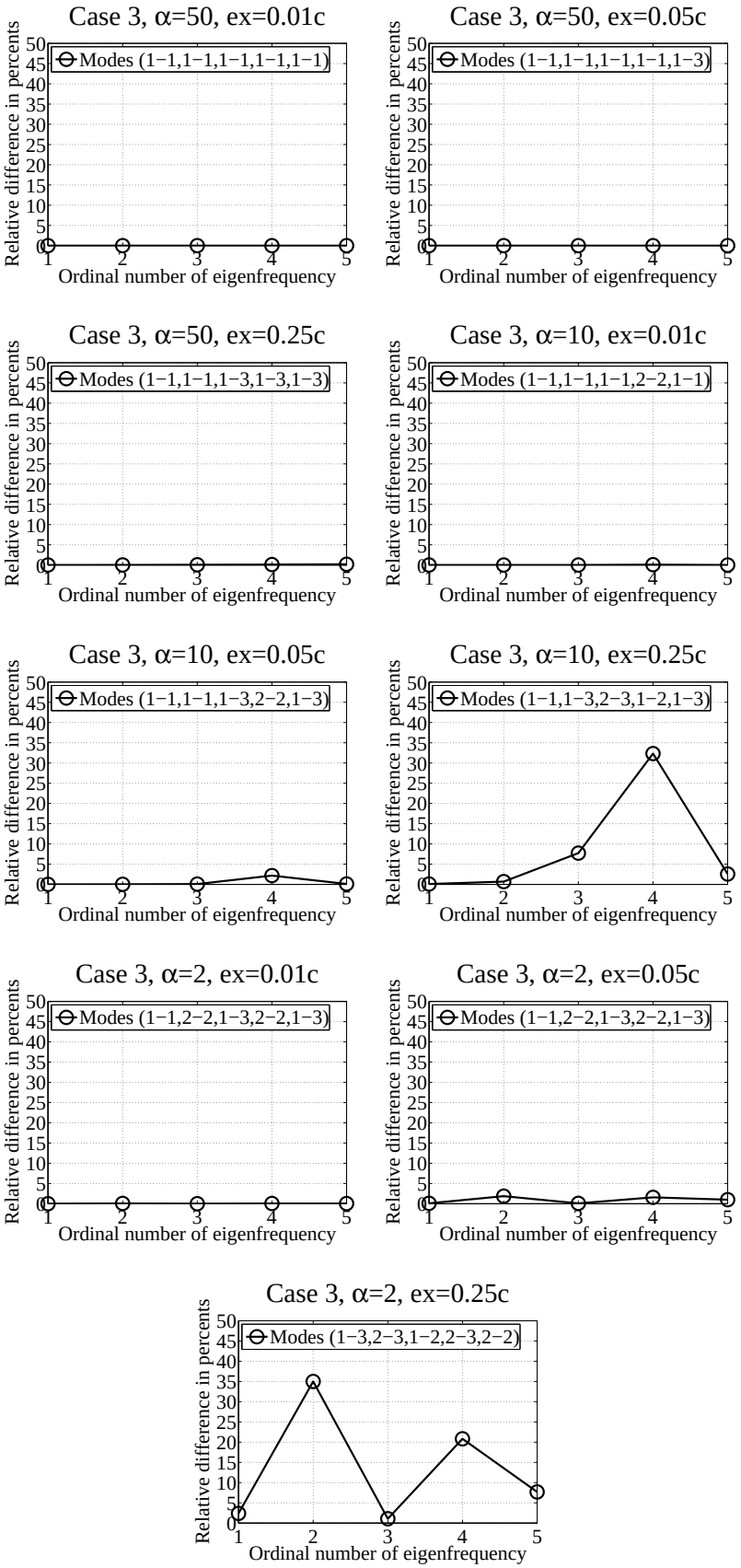

Figure C.3: Case 3 of term significance study: coupling term. The varying parameters are slenderness ratio α and distance between the SC and COG along the x-axis e_x.

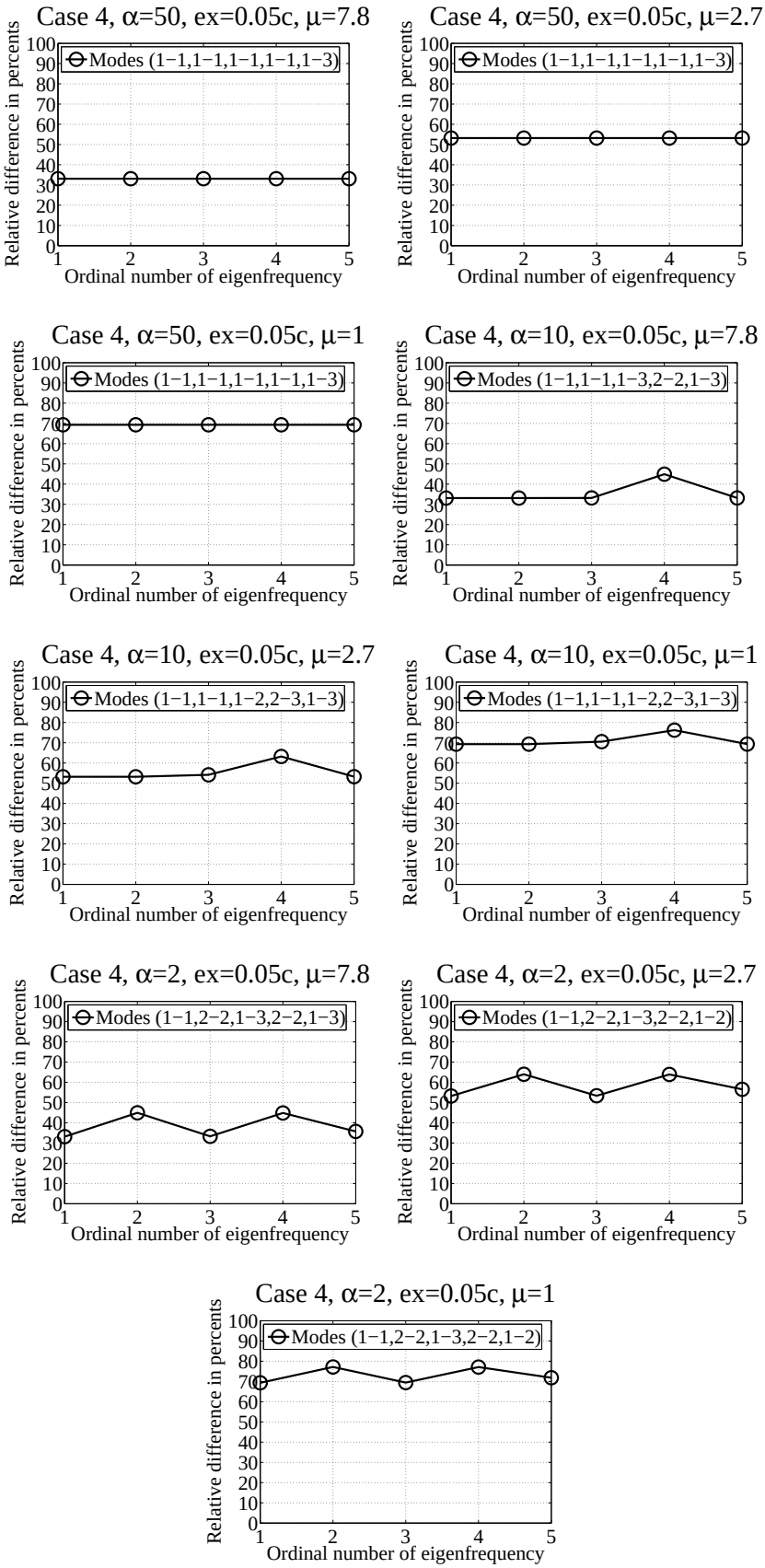

Figure C.4: Case 4 of term significance study: added mass term. The varying parameters are slenderness ratio α and density ratio μ. The distance between the SC and COG along the x-axis is $e_x = 0.05c$.

Appendix D

D Parameter dependency study

The ten cases of the parameter dependency study are shown in this Appendix. The cases are described in Table 3.15 and the parameter variations in Table 3.16. If not otherwise shown, the beam is uniform and made of steel. The surrounding fluid is water. The EOM used include shear deformation, rotary inertia and added mass terms. The cases 1-6 include the coupling term and the cases 7-10 do not. The cases are shown in Figures D.1, D.2, D.3, D.4, D.5, D.6, D.7, D.8, D.9 and D.10, respectively.

One graph shows one varied parameter. One figure includes all seven parameter graphs of the case. In the graphs, the five lowest natural frequencies are shown with different marker lines which are defined in the legend. The numbers inside brackets indicate the type of the mode shape. Bending mode is indicated with number 1, torsion with number 2 and mixed mode with number 3. The type is defined as bending or torsion if the maximum relative amplitude of the respective mode shape is more than 5 times larger than another. Otherwise, the type is defined as a combination.

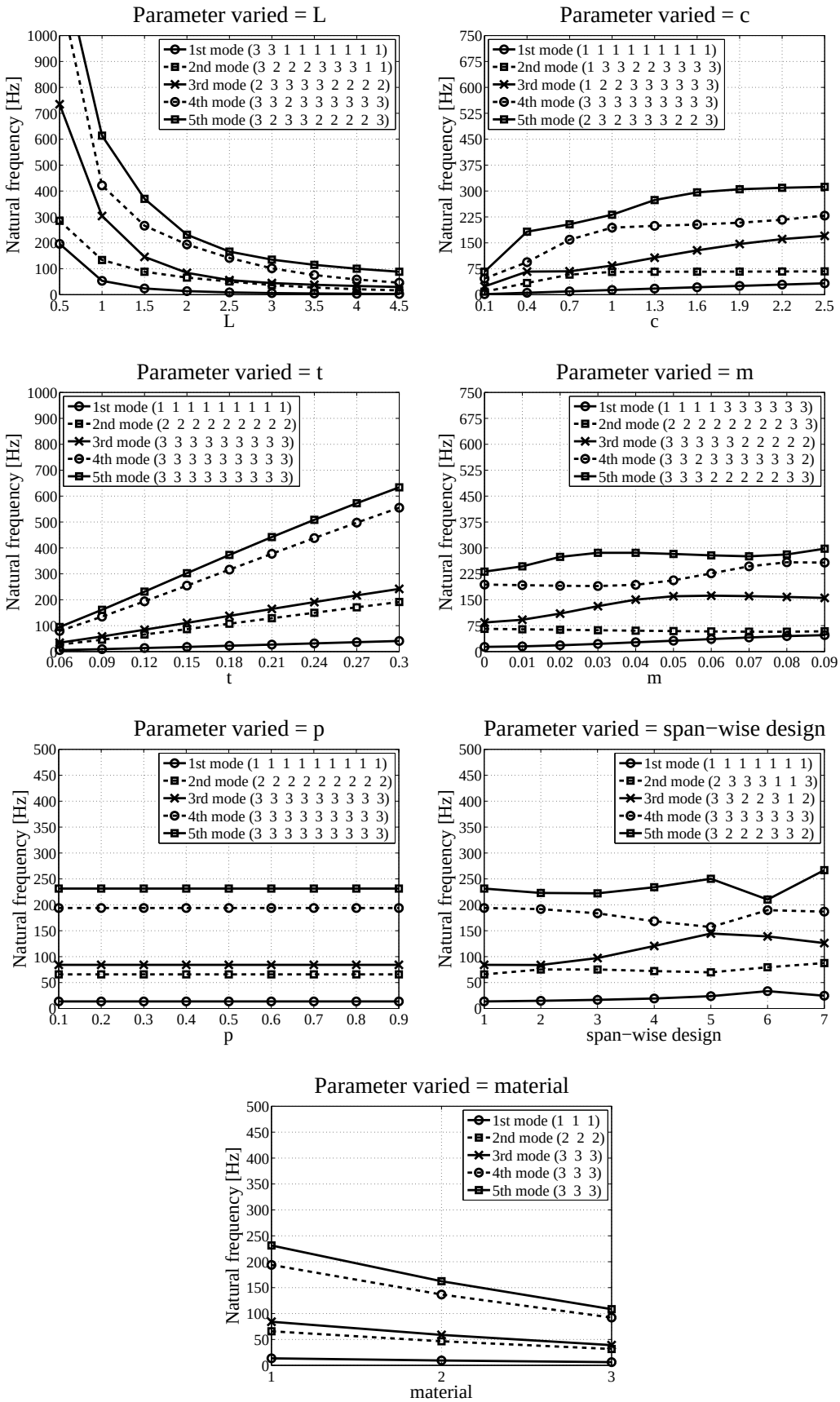

Figure D.1: Case 1 with coupled EOM and parameters $L = 2$ m, $c = 1$ m, $m = 0$ and $p = 0$.

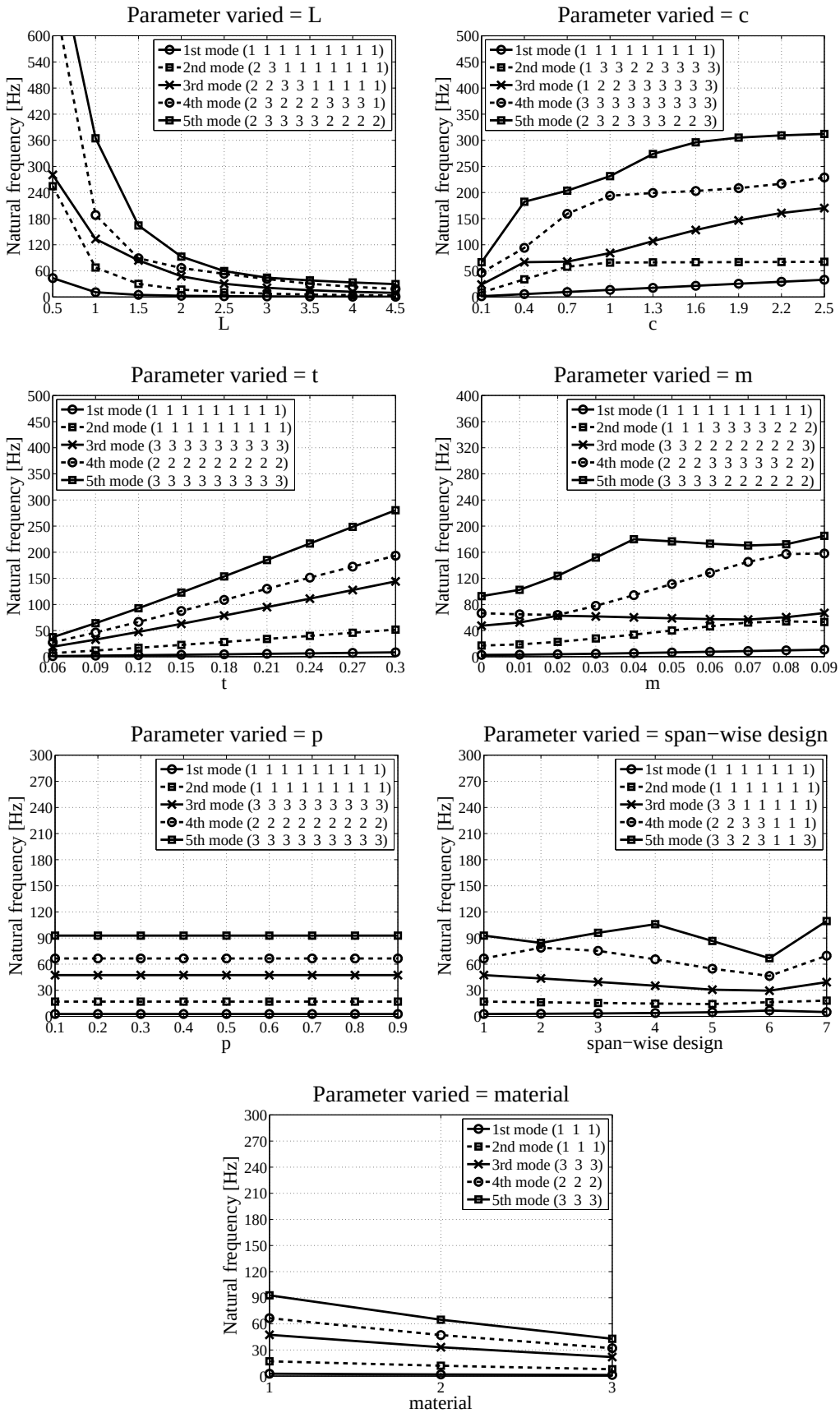

Figure D.2: Case 2 with coupled EOM and parameters $L = 2$ m, $c = 0.2$ m, $m = 0$ and $p = 0$.

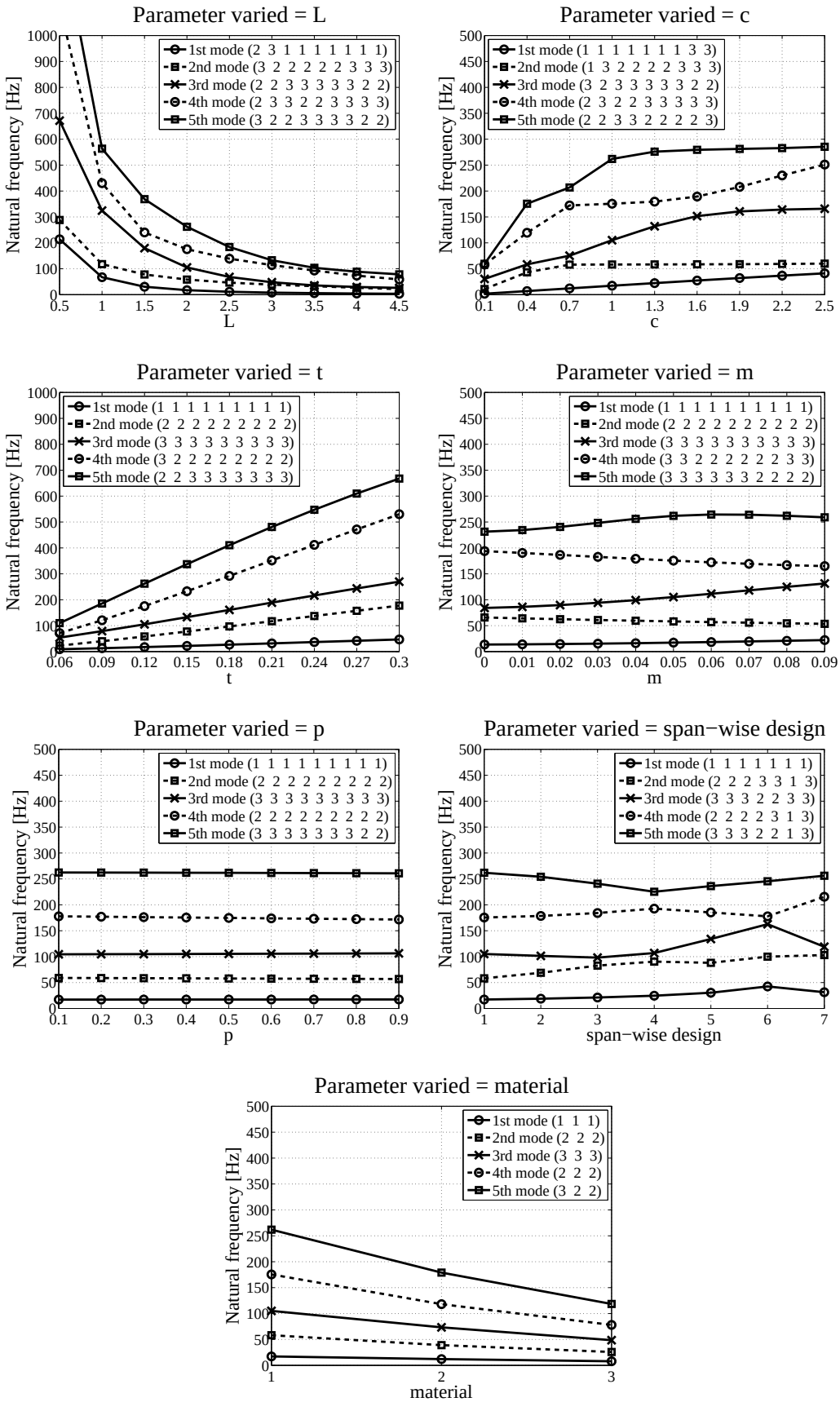

Figure D.3: Case 3 with coupled EOM and parameters $L = 2$ m, $c = 1$ m, $m = 0.05$ and $p = 0.4$.

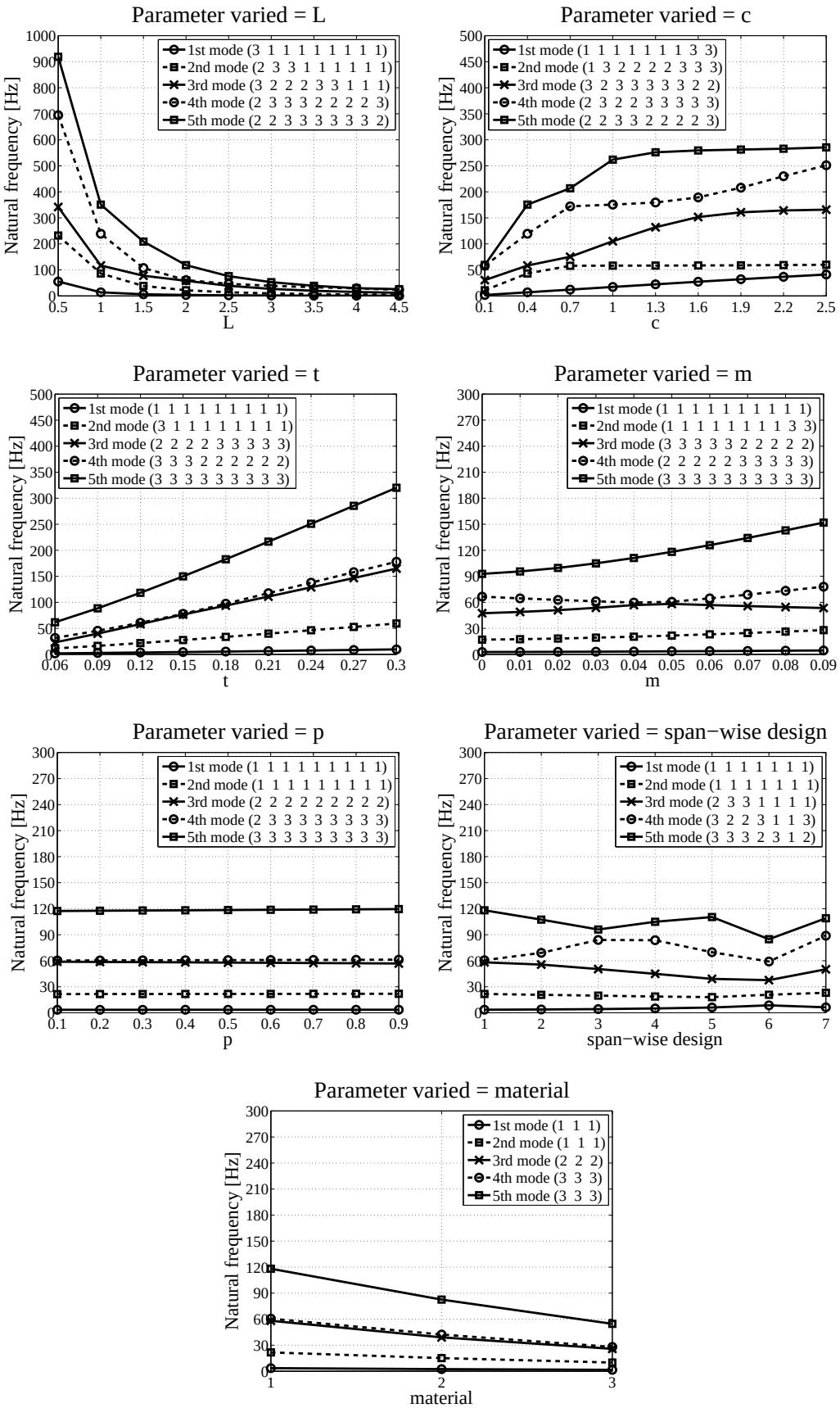

Figure D.4: Case 4 with coupled EOM and parameters $L = 2$ m, $c = 0.2$ m, $m = 0.05$ and $p = 0.4$.

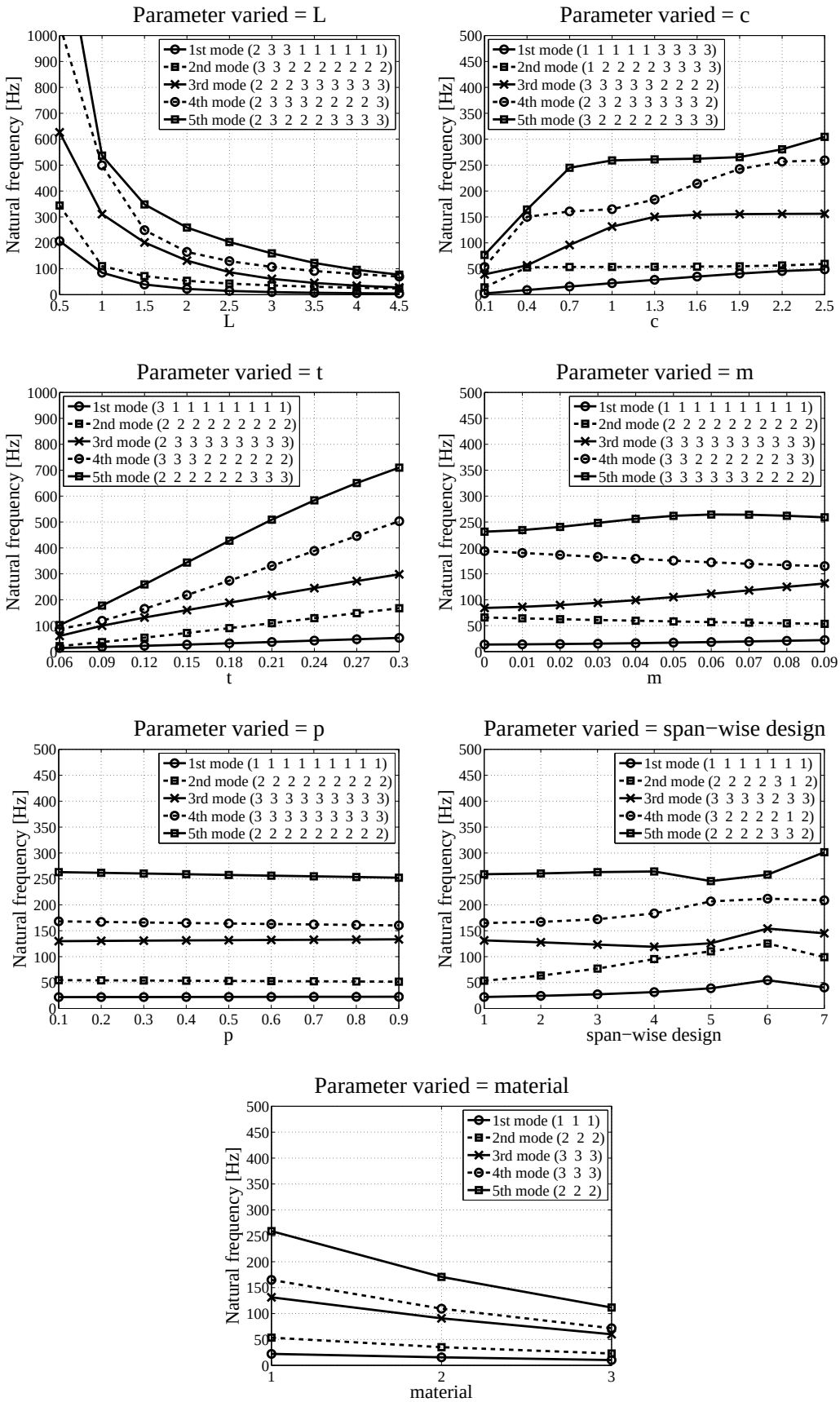

Figure D.5: Case 5 with coupled EOM and parameters $L = 2$ m, $c = 1$ m, $m = 0.09$ and $p = 0.4$.

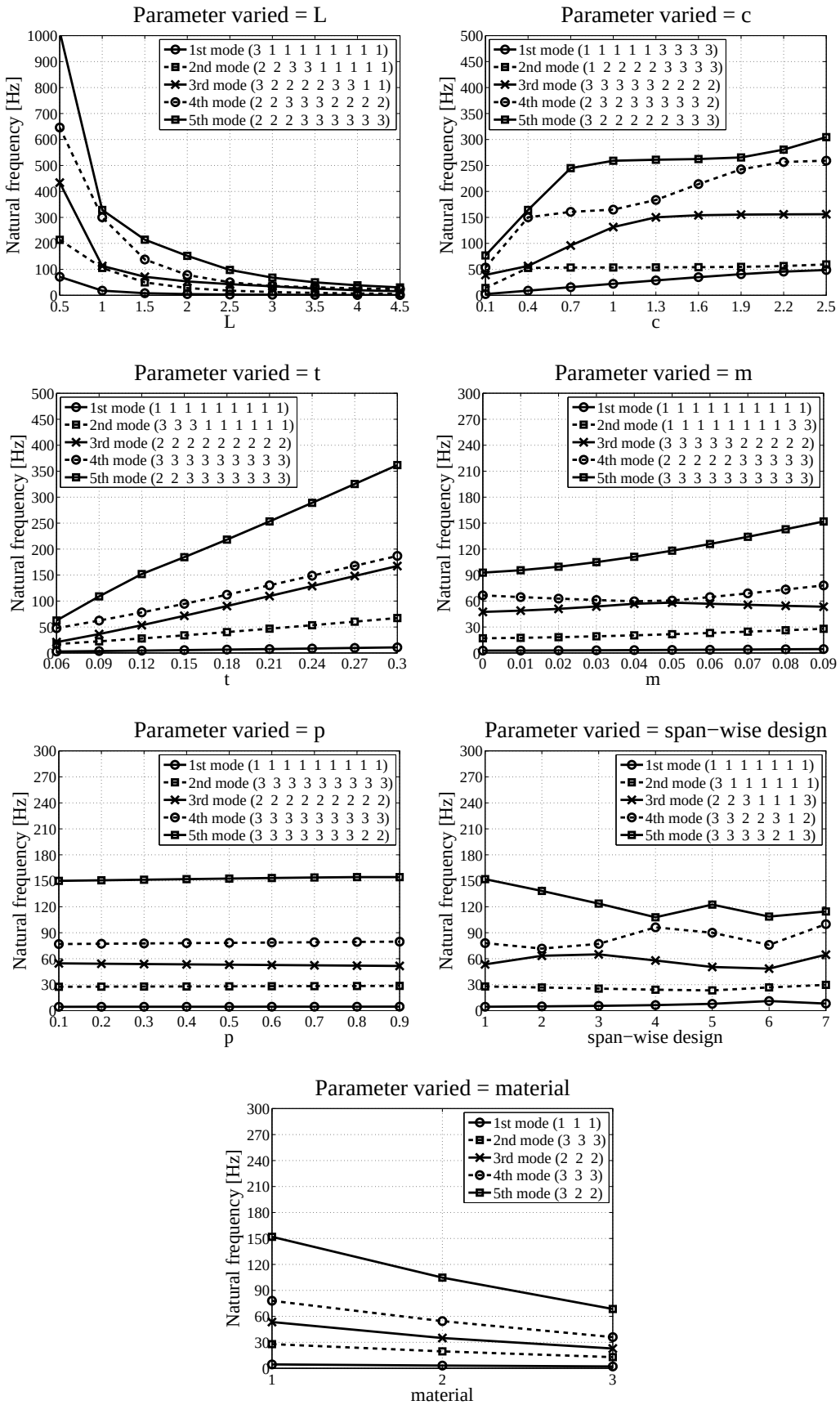

Figure D.6: Case 6 with coupled EOM and parameters $L = 2$ m, $c = 0.2$ m, $m = 0.09$ and $p = 0.4$.

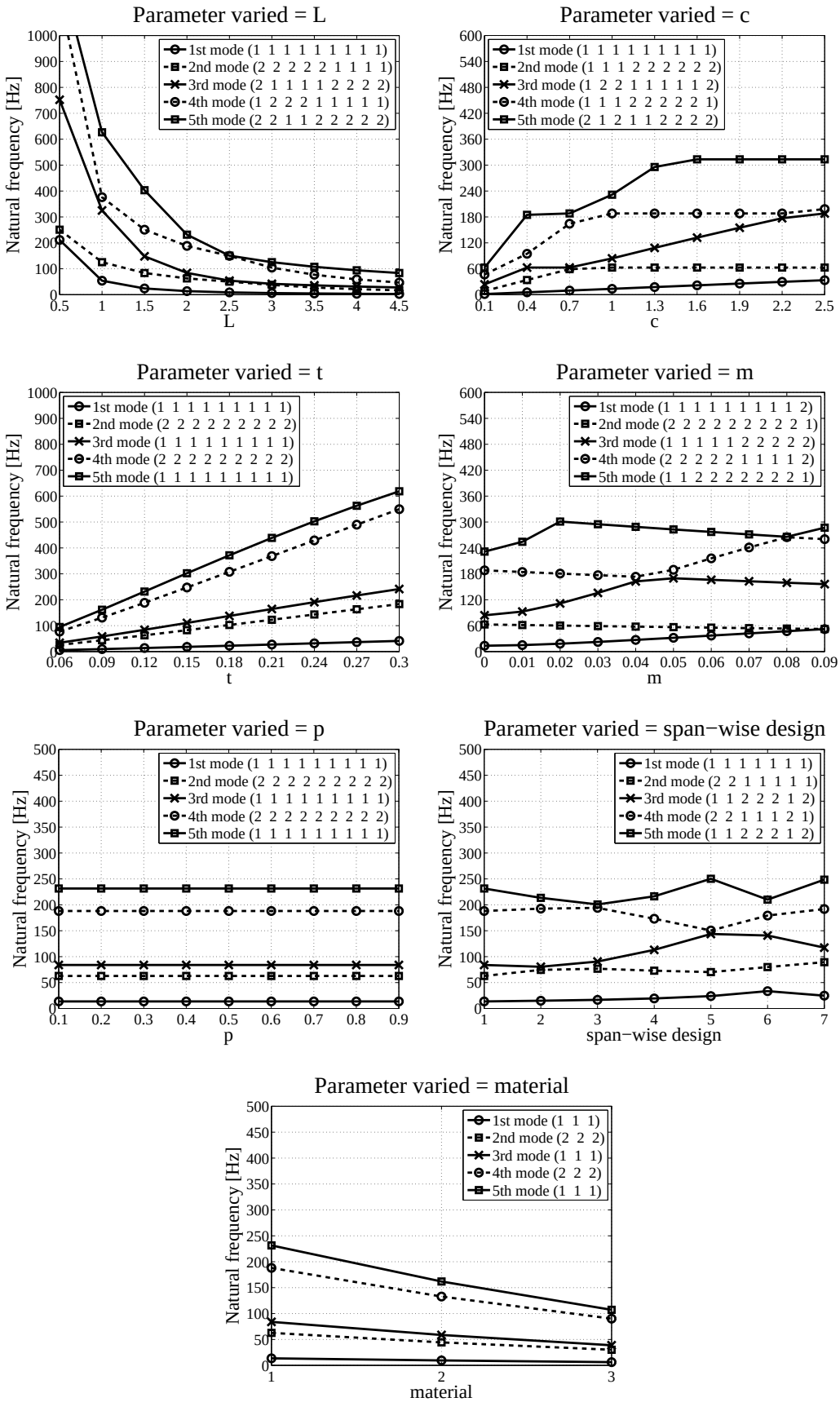

Figure D.7: Case 7 with uncoupled EOM and parameters $L = 2$ m, $c = 1$ m, $m = 0$ and $p = 0$.

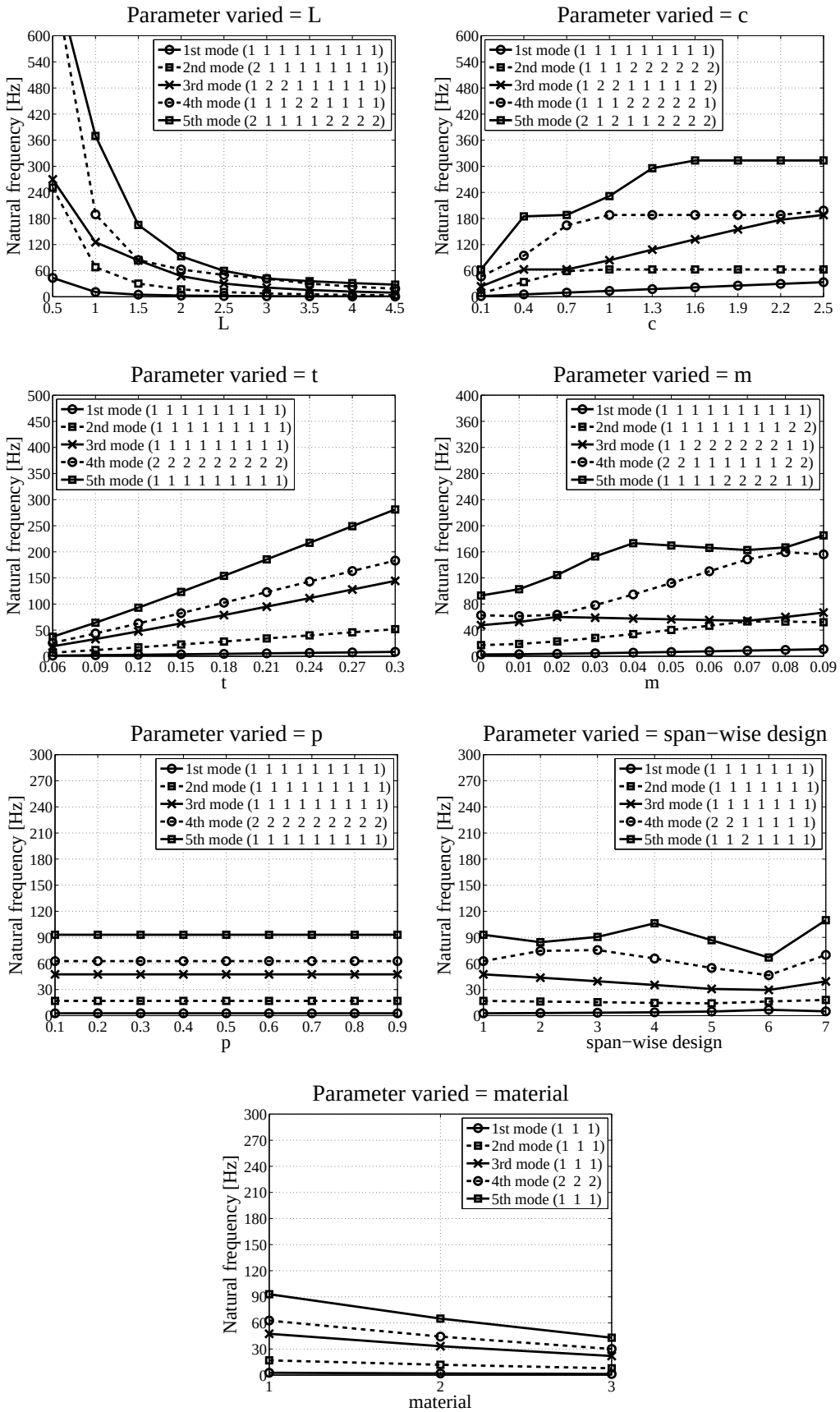

Figure D.8: Case 8 with uncoupled EOM and parameters $L = 2$ m, $c = 0.2$ m, $m = 0$ and $p = 0$.

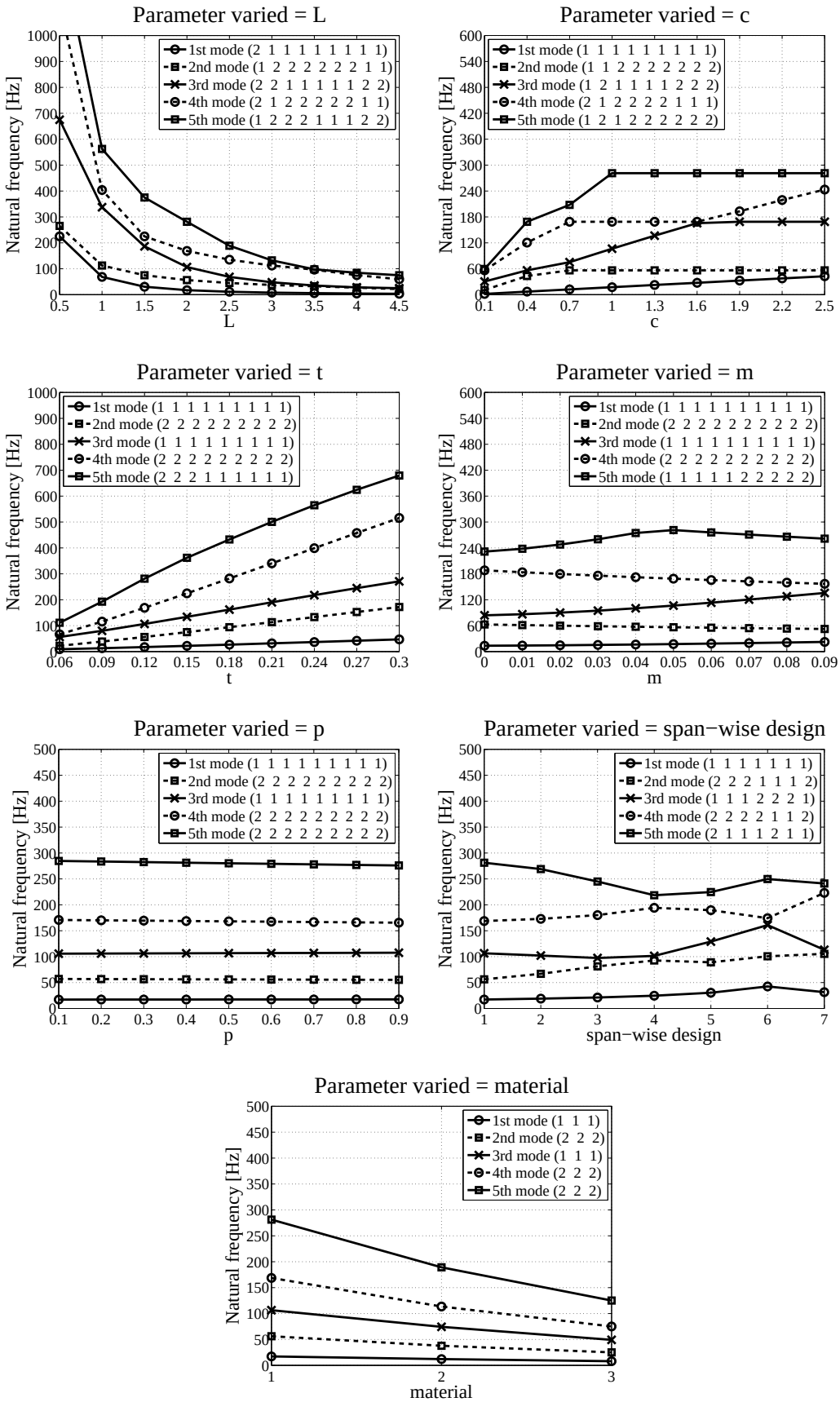

Figure D.9: Case 9 with uncoupled EOM and parameters $L = 2$ m, $c = 1$ m, $m = 0.05$ and $p = 0.4$.

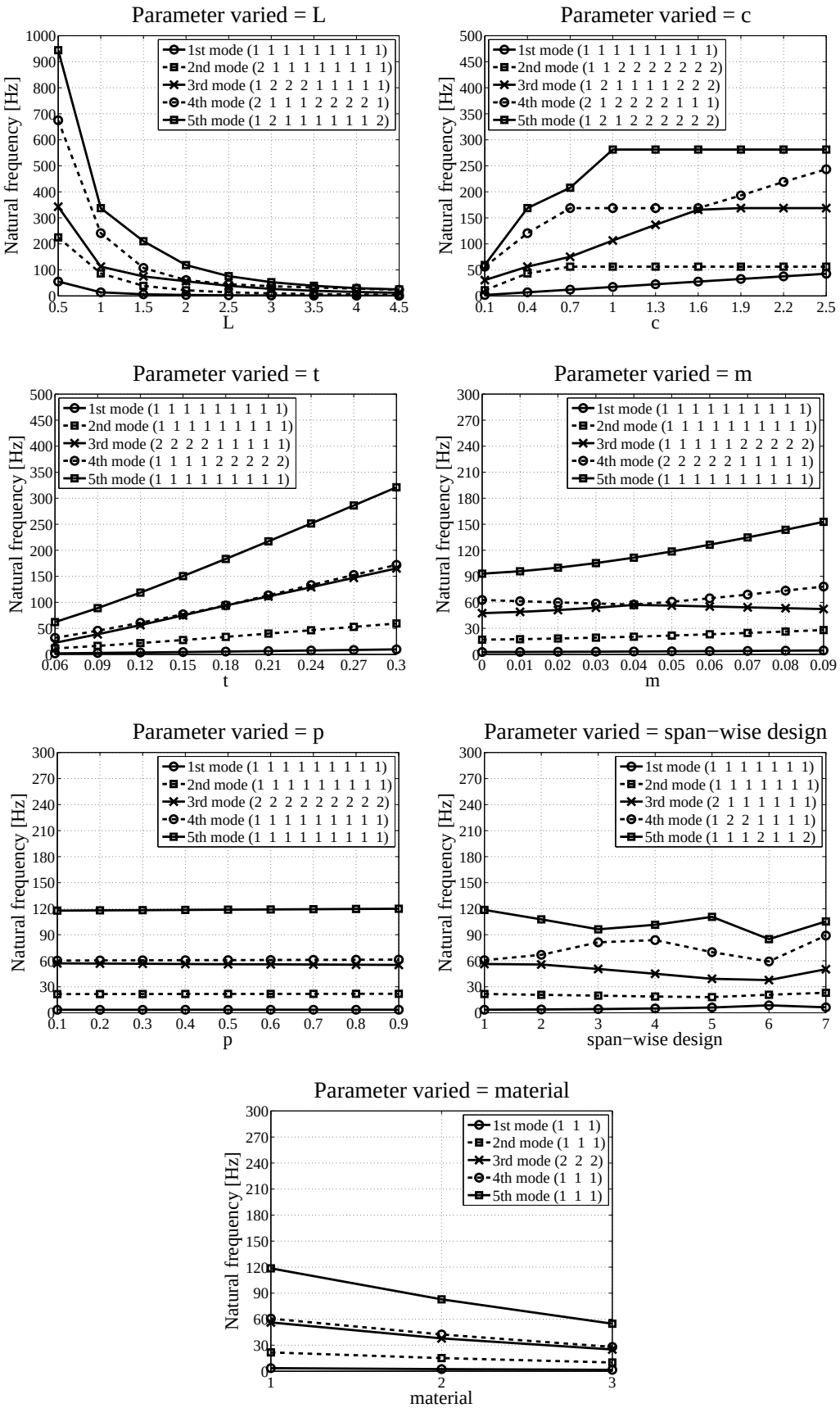

Figure D.10: Case 10 with uncoupled EOM and parameters $L = 2$ m, $c = 0.2$ m, $m = 0.05$ and $p = 0.4$.

Appendix E

E Design graph group example

The example of the design graph group is shown in this Appendix. The parameters used and their ranges are shown in Table 3.21. The graphs show the first natural frequencies of fins with varying parameters. The parameters varying inside the graphs are chord length and camber. The parameters varying between the graphs in the figures are different depending on the presentation alternative. The four different presentation alternatives are shown in Figures E.1, E.2, E.3 and E.4. In the first figure, the length and thickness are varied between graphs. In the second, the span-wise variation and material are varied between graphs. In the third, the span-wise variation and thickness are varied between graphs. In the fourth, the span-wise variation and length are varied between graphs.

Figures E.5 - E.10 show the whole design group of 54 graphs and 6 figures in total. The length and thickness are varied between the 9 graphs in the same figure. The span-wise variation and material are varied between the 6 figures.

The EOM used include shear deformation, rotary inertia, coupling and added mass terms. The surrounding fluid is water. The parameter values used are shown above each of the graphs. Uniform means the span-wise variation option 1 in Table 3.21, linear means option 2 and poly means option 3. S means the material option 1 in Table 3.21 and AL means option 2. They are steel and aluminium, respectively. The first natural frequencies are shown in contours with a step size of 5 Hertz. The colorbar on the right side of each graph shows the contour levels of the frequency in Hertz.

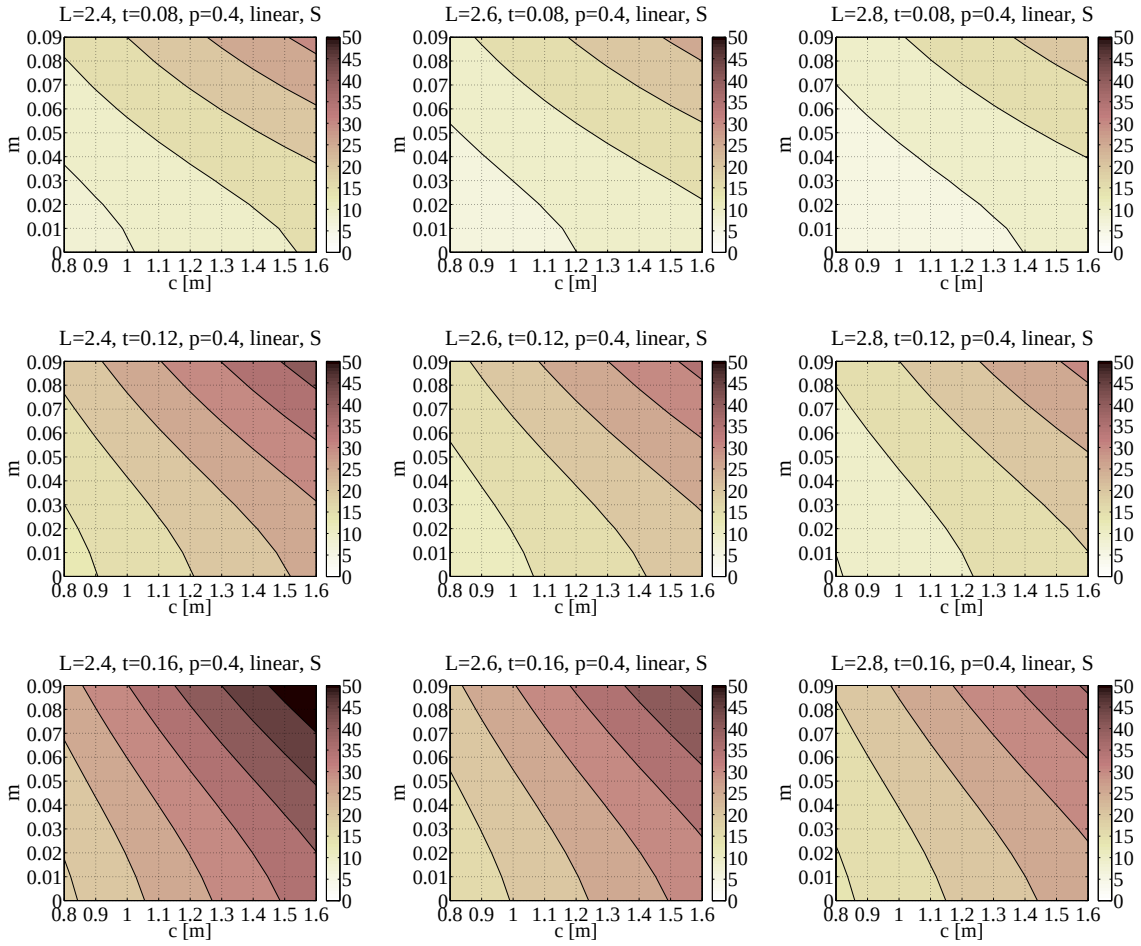

Figure E.1: The presentation alternative 1 in which the length and thickness are varied between graphs on the same figure.

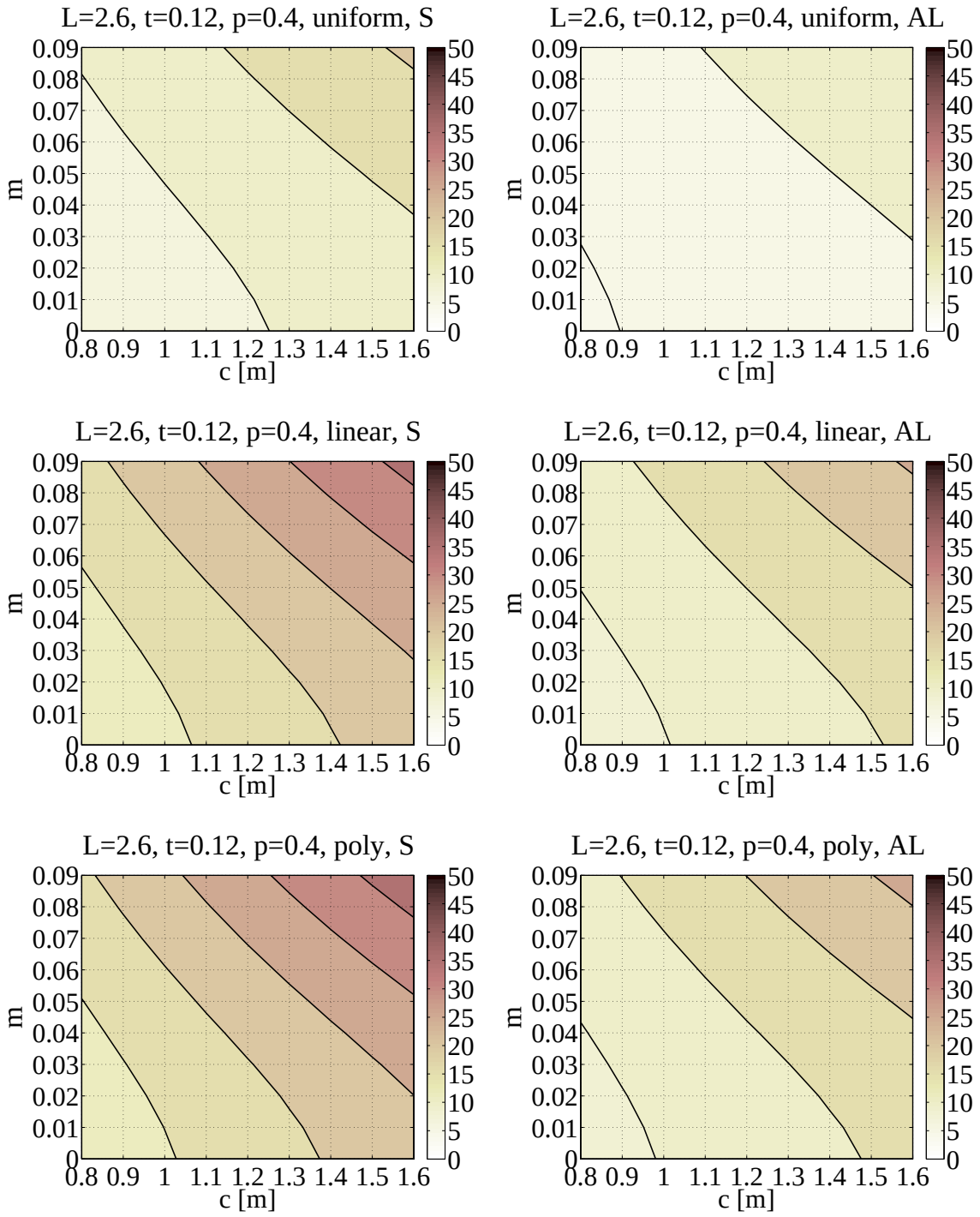

Figure E.2: The presentation alternative 2 in which the span-wise variation and material are varied between graphs on the same figure.

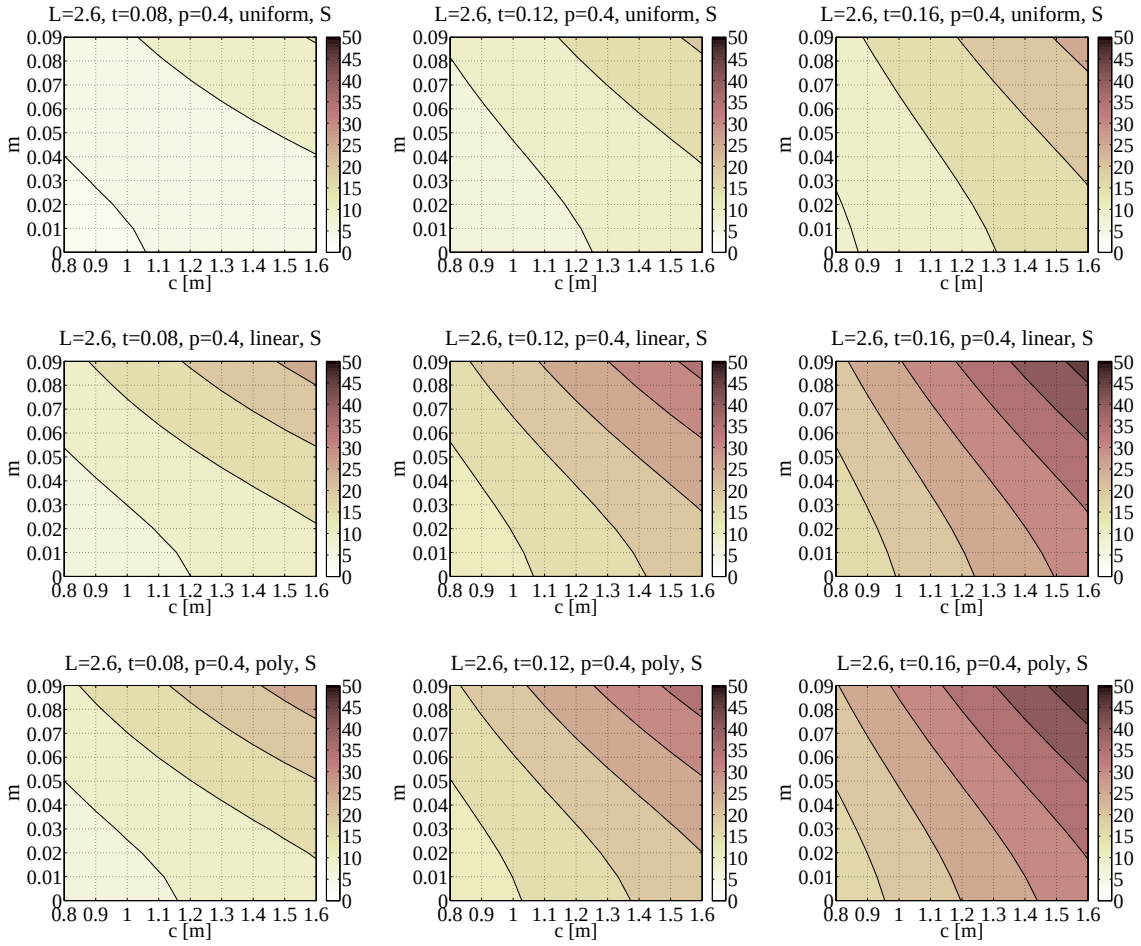

Figure E.3: The presentation alternative 3 in which the span-wise variation and thickness are varied between graphs on the same figure.

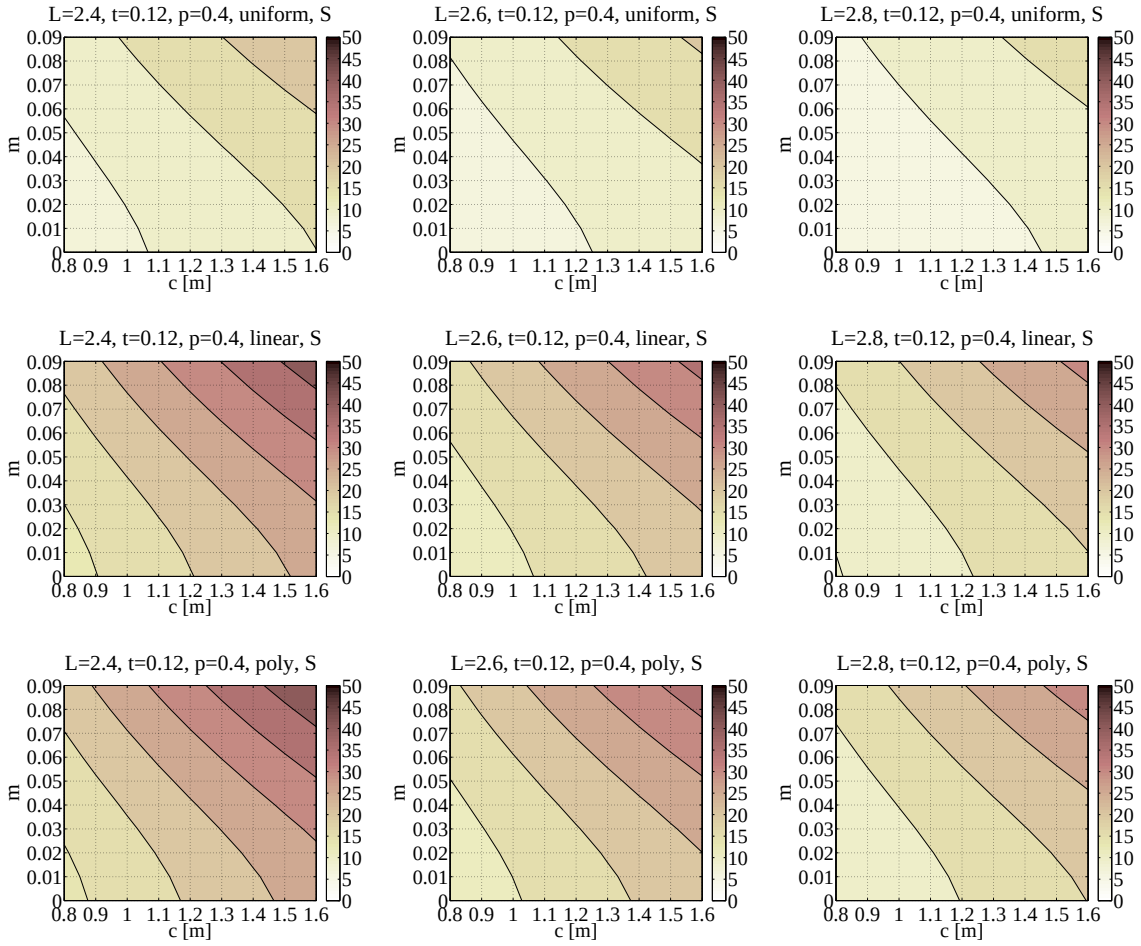

Figure E.4: The presentation alternative 4 in which the span-wise variation and length are varied between graphs on the same figure.

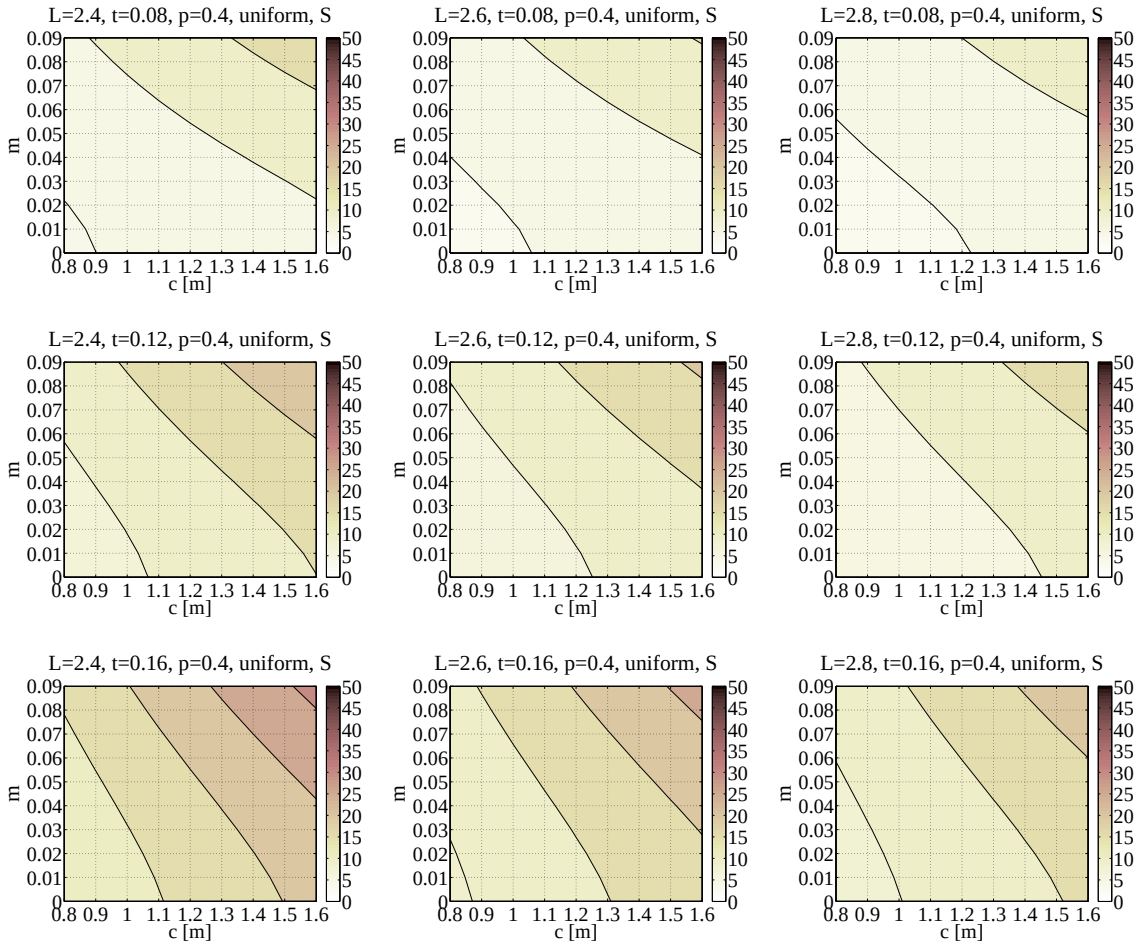

Figure E.5: The whole design group shows 54 graphs and 6 figures in total. The length and thickness are varied between the 9 graphs in the same figure. The spanwise variation and material are varied between the 6 figures.

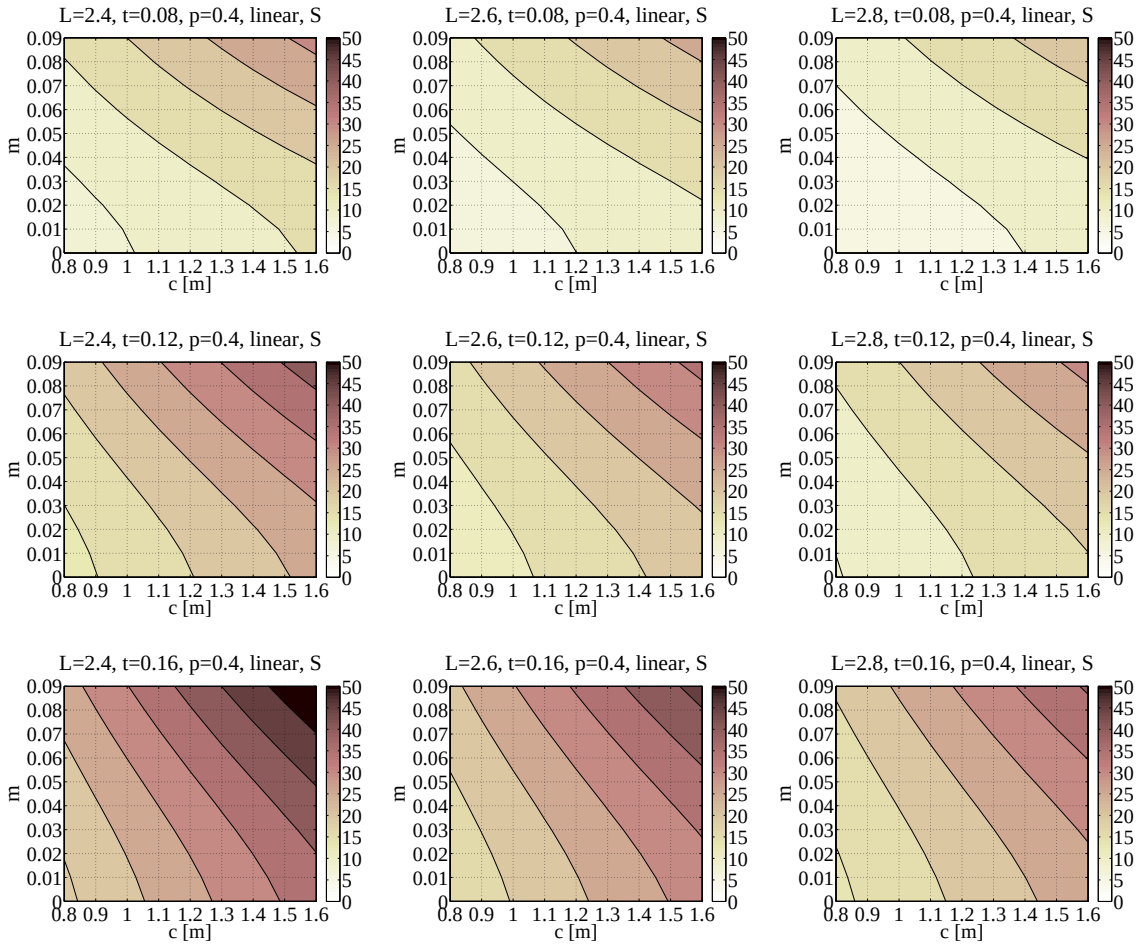

Figure E.6: The whole design group shows 54 graphs and 6 figures in total. The length and thickness are varied between the 9 graphs in the same figure. The spanwise variation and material are varied between the 6 figures.

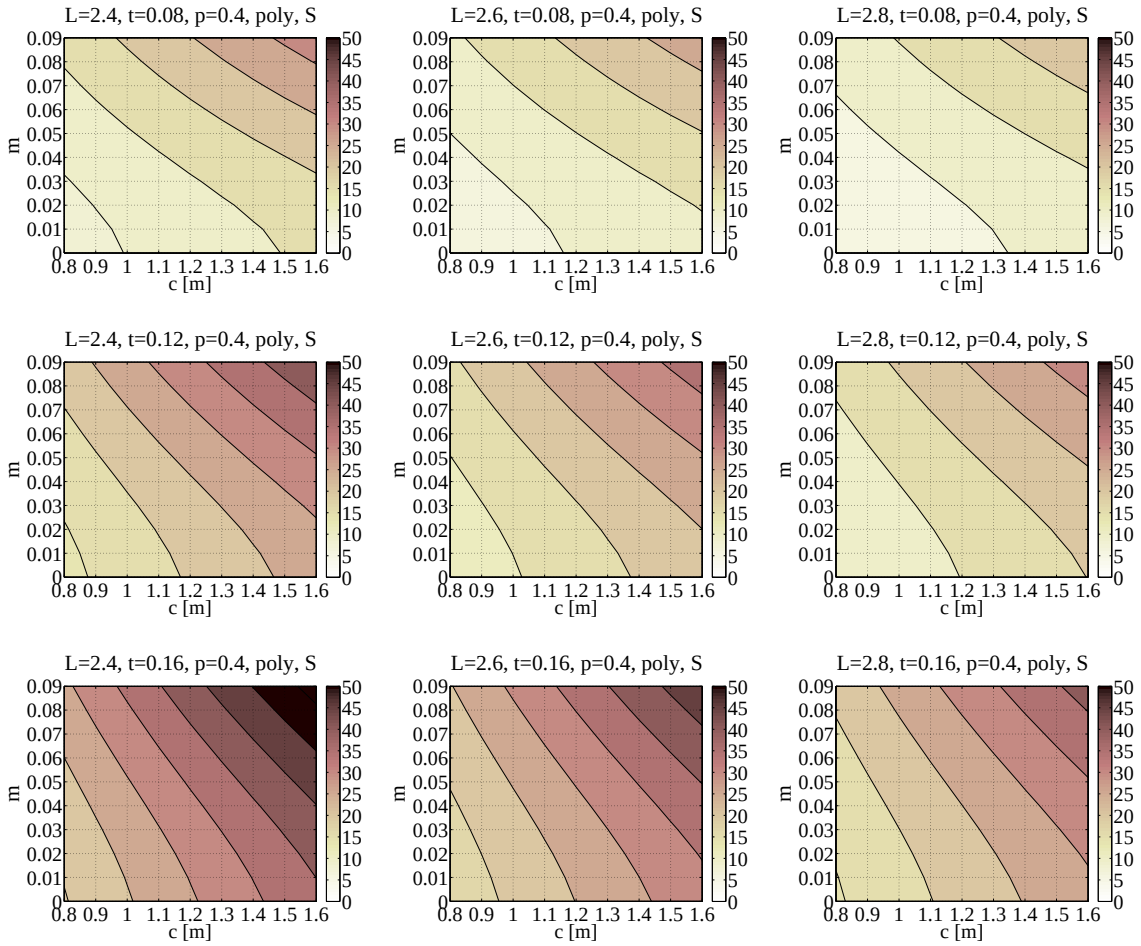

Figure E.7: The whole design group shows 54 graphs and 6 figures in total. The length and thickness are varied between the 9 graphs in the same figure. The spanwise variation and material are varied between the 6 figures.

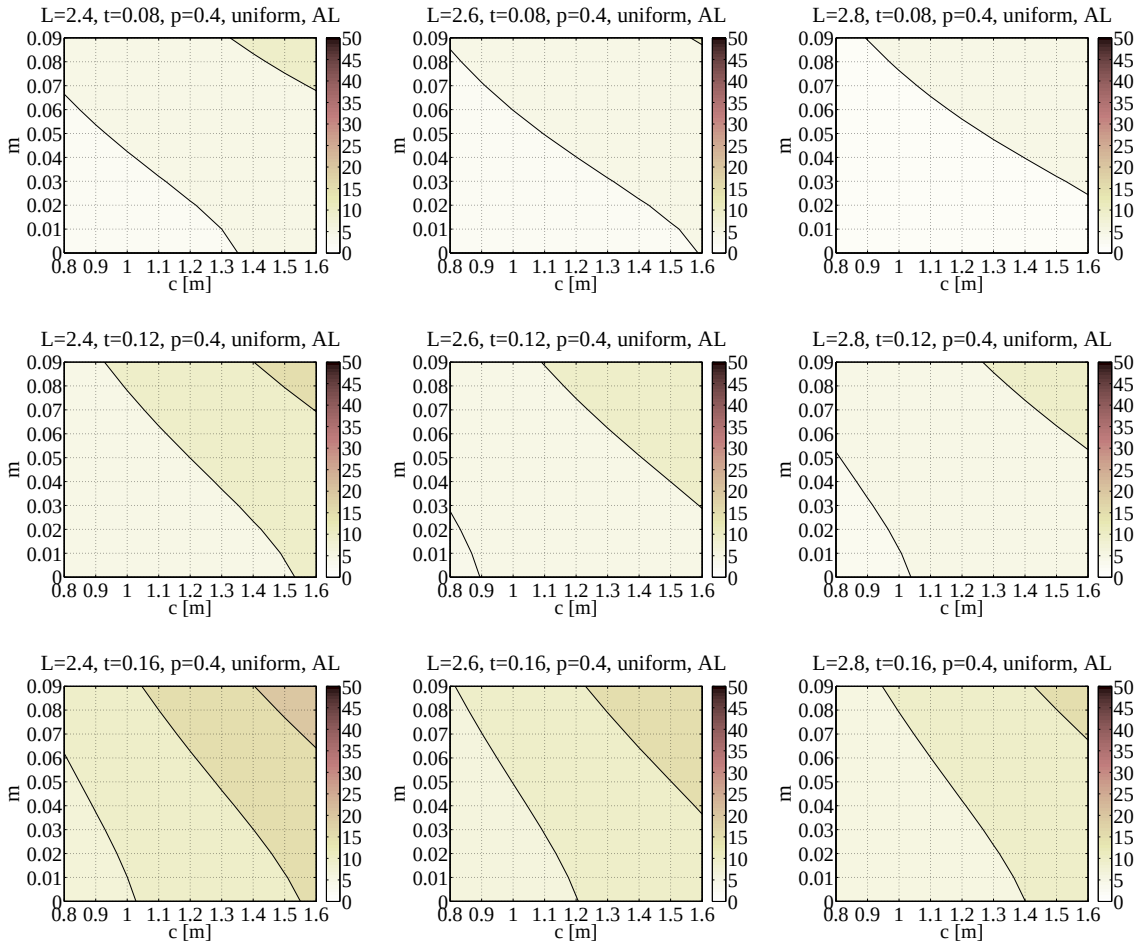

Figure E.8: The whole design group shows 54 graphs and 6 figures in total. The length and thickness are varied between the 9 graphs in the same figure. The spanwise variation and material are varied between the 6 figures.

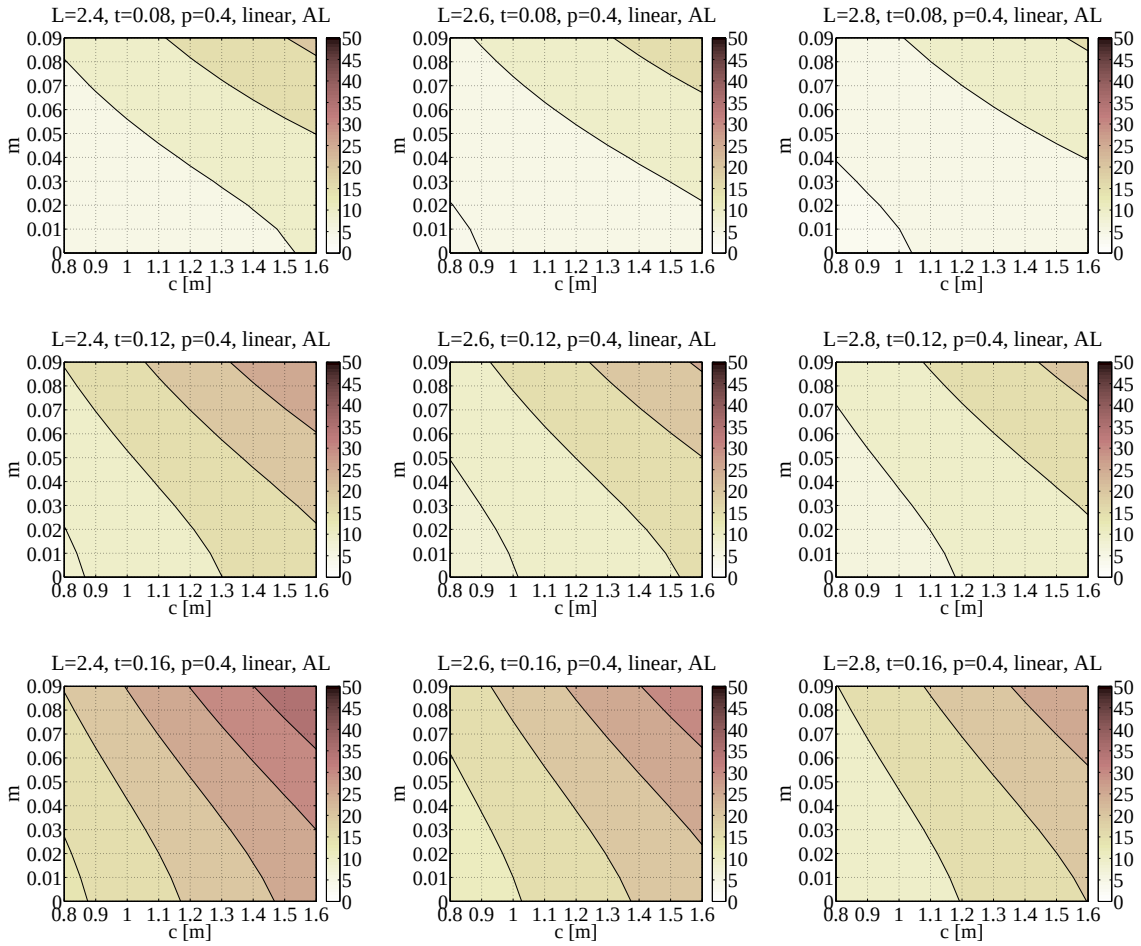

Figure E.9: The whole design group shows 54 graphs and 6 figures in total. The length and thickness are varied between the 9 graphs in the same figure. The spanwise variation and material are varied between the 6 figures.

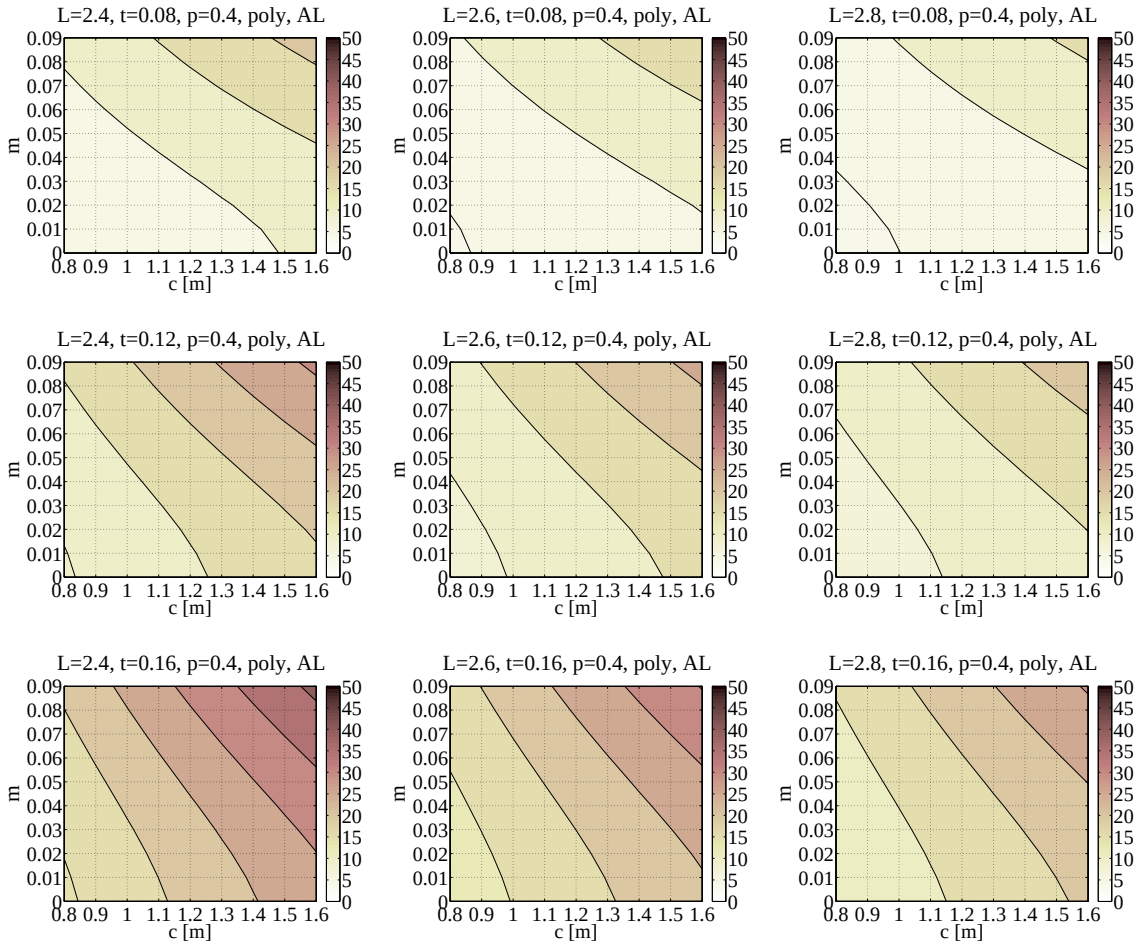

Figure E.10: The whole design group shows 54 graphs and 6 figures in total. The length and thickness are varied between the 9 graphs in the same figure. The span-wise variation and material are varied between the 6 figures.